Development of Conductive Sodium Alginate-Polyacrylamide Hydrogels for Biomedical Applications

By

Shahin Torki

A Thesis submitted to the Faculty of Graduate Studies of

The University of Manitoba

in partial fulfilment of the requirements of the degree of

MASTER OF SCIENCE

Department of Biosystems Engineering

University of Manitoba

Winnipeg

Table of Contents

Abstract

Hydrogels, known for their 3D crosslinked networks that retain significant water, have garnered substantial attention due to their potential in various biomedical fields including tissue engineering, wound dressings, and wearable electronics. To enhance the functionality of hydrogels with both robust mechanical property and excellent conductivity, this work investigates the development of novel conductive hydrogels composed of sodium alginate (SA), polyacrylamide (PAM), and polypyrrole (Ppy). The developed hydrogels are promising for at biomedical applications such as biosensors and drug delivery. The primary focus of this study is to enhance the mechanical robustness and electrical conductivity of these hydrogels to suit potential applications in non-invasive biosensing devices for continuous health monitoring.

The work explores the synergistic effects of integrating conductive polymers and double-network structures, where SA and PAM create a robust matrix through chemical and physical crosslinks, $CaCl_2$ (Ca^{2+}) creates ionic bonds with SA. The Ppy is also incorporated for its conductivity and biocompatibility. Fourier Transform Infrared Spectroscopy (FTIR) confirmed successful synthesis with key functional groups indicating robust formation. Mechanical testing across weight ratios of 1:10, 1:15, and 1:20 for SA-PAM with $CaCl_2$ concentrations of 5wt%, 10wt%, and 20wt% demonstrated the optimal mechanical strength at a 1:10 (weight) ratio with 10wt% $CaCl_2$ with modulus of 385 KPa and peak stress of 61.5 KPa. Similarly, conductivity tests revealed peak conductivity levels of 0.2847 S/cm for positive currents and 0.2748 S/cm for negative currents at the same hydrogel composition (1:10 PAM-SA, 10wt% CaCl2), suggesting excellent potential

for biosensor devices designed for continuous health monitoring. The integration of Ppy not only enhanced the conductivity but also contributed to the hydrogels' biocompatibility and mechanical resilience, making them promising candidates for next-generation medical devices. In addition, rheological studies affirmed the structural integrity under dynamic stresses, indicating the hydrogels' potential in various biomedical fields including tissue engineering, drug delivery, and wearable electronics. Enhanced crosslinking within the hydrogel matrix ensures improved mechanical properties, enabling broader applications in medical diagnostics and therapeutics, and paving the way for more effective and adaptable hydrogel-based systems in the medical field.

Keywords: hydrogels, PAM-SA, $CaCl_2$, Ppy, mechanical strength, conductivity

Acknowledgment

I would like to express my deepest gratitude to my supervisor Dr. Wen Zhong, for her expert guidance and valuable insights, which have been fundamental to my personal and professional growth throughout the research and writing journey. Her unwavering support, patience, and encouragement have inspired me and shaped my academic path profoundly. Thank you for being a tremendous mentor and for the significant impact you have had on my life. I am also thankful to my committee members Dr. Malcom Xing and Dr. Ramanathan Sri Ranjan for their constructive critiques and suggestions that significantly shaped this thesis.

I owe a great deal of appreciation profoundly to my family, Friend, and my beloved partner Darya Nematisouldaragh for their love, encouragement, and sacrifices, which have been my cornerstone throughout my academic journey.

I would like to extend my gratitude to my peers and colleagues in the lab especially Dr. Yuqing Liu, whose camaraderie and collaborative spirit have enriched my graduate experience. Also, I extend my thanks to Natural Sciences and Engineering Research Council of Canada (NSERC), whose financial support made my research possible.

Last but not least, I would like to acknowledge my own perseverance through this challenging process. The countless hours dedicated to studying, the sacrifices made to balance work and research, and the unwavering determination to complete this master's

degree are achievements I proudly recognize. I am grateful to myself for staying committed to my goals and reaching this significant milestone.

List of Figures

List of Tables

Chapter I: Introduction

1.1 Overview

Hydrogels, characterized by their unique three-dimensional (3D) crosslinked polymer networks that retain a significant amount of water, have emerged as highly promising materials for diverse biomedical applications, including drug delivery vehicles, tissue engineering scaffolds, wound dressings, and wearable electronic devices(1–4). Recent advancements have focused on enhancing the properties of hydrogels to make them highly elastic, tough, flexible, conductive, and responsive to environmental stimuli, thereby enabling their utilization in biosensors, particularly for glucose monitoring in diabetic patients(5,6). Continuous monitoring of blood glucose levels is essential for effective health management, and hydrogel-based glucose sensors offer the potential for soft, wearable biosensors that seamlessly integrate with the skin(7,8).

Moreover, since the traditional metal sensors face challenges in attaching to the skin and detecting strains, the development of attachable and wearable biosensors has garnered significant attention(9). It is because of their ability to provide convenient real-time health monitoring(7). Ideal electronic devices should possess high sensitivity, efficiency, reliability, cost-effectiveness, and adaptability to various geometries and sizes(10). An alternative approach involves combining polymers with conductive nanoparticles to create flexible biosensors. For example, blending poly(dimethylsiloxane) (PDMS) with polyacrylamide and sodium alginate yields a stretchable, conductive biosensor with high sensitivity and rapid response(11). Additionally, conductive polymers such as polypyrrole (Ppy) and polyaniline (PANI) offer excellent conductivity and biocompatibility but lack

mechanical strength(12–14). Despite the ongoing research, these hydrogels still provide weak mechanical strength and network which impacts the significance of the application especially at clinical level. To address this concern, researchers are exploring double-network hydrogels composed of both chemical and physical crosslinking reinforced with conductive nanocomponents to achieve robustness and toughness(15,16). Moreover, they are looking for higher swelling ratio with competent elasticity compared to natural tissues(17). The exploration of hybrid double-network hydrogels has ignited pioneering research interest, aiming to integrate them with conductive nano components. This incorporation of conductive materials, such as Ppy, graphene, and carbon nanotubes (CNT), into the hydrogel composite contributes to enhancing its elasticity and flexibility to achieve higher grades(18,19). Furthermore, integrating 3D printing technology enables the fabrication of hydrogel-based biosensors with intricate architectures, opening new avenues for advanced sensing applications(20). In addition, hydrogels can be further developed into microneedles for theragnostic devices that provides a combination of diagnosis and therapy such as drug delivery(21,22).

1.2 Problem statement

The development of hydrogels has often been constrained by a trade-off between mechanical robustness and functionality. Traditional single-network hydrogels, while beneficial in terms of biocompatibility and inherent hydrophilicity, typically suffer from poor mechanical properties, such as low tensile strength and susceptibility to rapid degradation under physiological conditions(23). These limitations severely restrict their practical

applications, particularly in dynamic environments where robust mechanical behavior is crucial.

To address these deficiencies, the design of hybrid, double-network hydrogels, such as those combining polyacrylamide (PAM), sodium alginate (SA), and calcium chloride ($CaCl_2$), offers a promising pathway. In these systems, the dual-network structure leverages the distinct mechanical contributions of each component: the PAM provides elastic resilience, while the ionic crosslinking of SA with $CaCl_2$ enhances the overall toughness and structural integrity(24). This synergistic combination results in a hydrogel that not only withstands mechanical stress more effectively but also maintains the desirable properties of each individual polymer network. However, these hydrogels inherently lack sufficient conductivity for electronic applications. The integration of conductive polymers such as polypyrrole (Ppy) into PAM-SA hydrogels represents a strategic innovation aimed at bridging this gap. Ppy, known for its conductivity and biocompatibility, could potentially endow the hydrogel with the requisite electronic properties without compromising its mechanical integrity(25). The challenge, however, lies in ensuring that the incorporation of Ppy does not adversely affect the hydrogel's structural properties. Achieving a homogeneous distribution of Ppy within the hydrogel matrix is crucial, as it maintains the balance between enhancing conductivity and preserving the mechanical characteristics essential for practical applications. Successfully combining these elements could lead to a new class of multifunctional hydrogels, capable of meeting the demanding requirements of modern technological applications.

1.3 Objective

The objective of this research is to develop 3D printable multifunctional hydrogels composed of polyacrylamide and sodium alginate with superior toughness and conductivity that may potentially use in biosensors. These hydrogels are designed based on hybrid double-network polymeric crosslinking systems and incorporated with conductive material polypyrrole.

Chapter II: Literature Review

This chapter introduces the basics of hydrogels, covering the nature of the materials and their application in different fields. Moving forward, it explores the functional hydrogels with self-healing and conductivity and their applications in biosensors and microneedles for drug delivery.

2.1 Basics of Hydrogels

Hydrogels represent hydrophilic polymer 3D mesh networks crosslinked via chemical and/or physical bonds(26). In recent years, there has been significant research and development focused on enhancing hydrogel's response to various environmental stimuli such as light, pressure, temperature, and chemicals/pH values(5). These advanced features, particularly the reversible property changes in response to environmental cues, enable the utilization of conductive hydrogels in biosensors, including glucose biosensors, facilitating real-time monitoring of blood glucose levels. Such monitoring is paramount for diabetic patients to manage their health effectively(27). Glucose biosensors typically measure changes in blood glucose levels using enzymes such as glucose oxidase, which catalyze the reaction of glucose with oxygen to produce hydrogen peroxide(27,28). The adoption of hydrogel-based glucose sensors is anticipated to drive the transition from bulky devices to soft, wearable biosensors that seamlessly integrate with and mimic the skin(29). In addition, hydrogels have comprehensive application in field of biomedical engineering, industry water filtration, tissue engineering and cosmetic products such as contact lenses(30–32).

Moreover, Hydrogels can be designed into the microneedles. Hydrogel microneedles signify a ground-breaking leap in biomedical science, blending the advantages of hydrogel materials with the precision of microneedle delivery systems(21,33). These minute needles, usually measuring less than a millimeter in length, are crafted from hydrogel materials, and engineered to effortlessly penetrate the skin's surface. This inventive method provides a minimally invasive avenue for drug delivery and biosensing, transforming a multitude of biomedical applications(33).

2.2 Hydrogel classification

The categorization of hydrogel can be extended into source of the materials which include natural and synthetic polymers, crosslinking methods, and network types.

2.2.1 Natural polymers for hydrogels

Hydrogels based on natural polymers, such as cellulose, chitosan, sodium alginate, collagen, pectin, or their combinations, have found extensive applications in biomedicine, drug delivery, and biosensing(2). Their biocompatibility and minimal toxicity make them highly desirable materials in these fields(34).

Chitosan, a common natural polysaccharide derived from chitin found in crustacean exoskeletons and fungal cell walls, is biodegradable, biocompatible, and possesses antibacterial and antifungal properties(35–37). It is extensively used in various fields including biotechnology, medicine, food science, drug delivery, and biosensing(37,38). Chitosan hydrogels have been developed for biomedical applications such as wound

dressings, tissue scaffolds, and controlled drug release systems(39). However, their mechanical strength is often insufficient, necessitating physical and chemical crosslinking for reinforcement(37,40).

Cellulose, another natural polymer, primarily consists of β-linked D-glucose and can be obtained from plant cell walls(41). Known for its high thermal expansion, stability, biocompatibility, and tensile strength, cellulose can be further processed into nanocellulose through mechanical, chemical, enzymatic treatments, or a combination of these methods(41,42). Nanocellulose exhibits high stiffness and strength-to-weight ratio, making it an excellent sustainable alternative to plastics(42). Nanocellulose hydrogels, fabricated using physical and chemical crosslinking, possess high surface area, excellent mechanical properties, and biodegradability, rendering them promising for various biomedical applications including wound care, wearable biosensors, tissue engineering, and drug delivery(43–45). However, due to its hydrophilic nature, cellulose requires chemical modification to impart hydrophobicity for certain biosensor applications(46). Hydrophobic cellulose biosensors can also measure changes in hydrophobicity of the medium(46).

These hydrophobic biosensors can be designed to detect various biomolecules or environmental parameters, making them valuable tools in medical diagnostics, environmental monitoring, and other fields(47). The hydrophobicity of cellulose can be engineered to control the interactions between the sensor surface and target molecules. Utilizing the hydrophobic cellulose hydrogel in glucose biosensors protects the enzyme

from degradation and the hydrophilicity nature of cellulose hydrogel enhances the sensor's selectivity and sensitivity(47). To be more specific, the modified cellulose hydrogels with hydrophobic groups provide a proper environment for immobilizing glucose-specific recognition elements(48,49). These recognition elements can include enzymes such as glucose oxidase (GOx) or glucose dehydrogenase (GDH)(50).

Originating from brown algae, alginate is a naturally occurring polymer known for its high solubility in water(51). Sodium alginate, a derivative of alginate, exhibits unique properties such as viscosity and biodegradability, making it a popular choice as an industrial thickening agent in products like toothpaste, salad dressing, pharmaceuticals, and bioprinting(52). When exposed to divalent cations, notably calcium ions (Ca^2+), sodium alginate readily forms a three-dimensional mesh network, resulting in the formation of mechanical robust, sodium alginate-calcium hydrogels(53,54). These hydrogels possess excellent water absorption and biocompatibility, making them suitable for various applications including wound dressing, drug delivery, and biosensors(53). To be more specific, in enzymatic biosensors, GOx enzymes within sodium alginate hydrogels undergo oxidation in the presence of glucose(50,55). Biosensors with ion-selective electrodes detect ions like potassium and calcium(54). The hydrogel structure acts as a barrier in biosensor applications, preventing interference from assay reactants and immobilizing biological components. Glucose and essential enzymes permeate the hydrogel barrier, facilitating glucose sensor functionality, while blocking interference from other molecules(56). Additionally, the hydrogel protects enzymes from degradation, ensuring sustained activity. Analytes like glucose can react within the hydrogel's free

volume matrix in biosensor applications(57). Recent studies have shown increased interest in the applications of sodium alginate, driven by its potential to enhance biosensor sensitivity and selectivity, thereby improving biosensor accuracy(51,56).

2.2.2 Synthetic Polymers for Hydrogels

Synthetic polymer hydrogels are materials have been composed of artificial polymers such as polyacrylic acid (PAA), polyvinyl alcohol (PVA) and polyacrylamide (PAM), that have been crosslinked to form a three-dimensional network capable of retaining large amounts of water. The synthesis of synthetic polymer hydrogels allows for precise control over their structure, and properties, making them mechanically sturdy and adaptable to specific application requirements.

Polyacrylic acid (PAA) is a synthetic polymer derived from acrylic acid monomers, commonly utilized in applications ranging from superabsorbent polymers to drug delivery systems and water treatment(58). It exhibits water-solubility and can form hydrogels when crosslinked, providing versatility in its applications(59). Polyacrylic acid hydrogel, synthesized from PAA polymer chains, displays high water absorption due to its hydrophilic nature, making it suitable for drug delivery and wound healing applications(60). Additionally, its pH-responsive behavior enables it to swell under acidic conditions and collapse under basic conditions, offering potential in sensing and tissue engineering applications(61,62). Modifications in the composition (adding functional groups), and crosslinking density of PAA hydrogels allow for the customization of their

properties, enhancing their suitability for specific biomedical, environmental, and industrial purposes(59,63).

Polyvinyl alcohol (PVA) is a water-soluble synthetic polymer widely used in hydrogels, particularly in the biomedical field(64). These hydrogels can be produced by crosslinking with other agents such as chitosan, starch and glutaraldehyde to enhance their biocompatibility and water retention properties according to specific applications(65,66). Notably, their capacity to promote cell growth makes them valuable for tissue engineering purposes(67). PVA hydrogels are known for their mechanical strength, high water retention capability, and compatibility with conductive materials, rendering them suitable for use in biosensors(68). Importantly, they exhibit biocompatibility and can be utilized internally or externally on the skin(69).

Polyacrylamide (PAM) hydrogels are formed through mixing of acrylamide monomers along with a crosslinking agent. These hydrogels possess high water retention capacity and find widespread usage across multiple industries(70). One significant application involves their use in drug delivery systems, where the control of crosslinking density and porosity can regulate the duration of drug release(71). Additionally, the distinct properties of PAM hydrogels make them well-suited for biosensor applications(72). Their high-water content facilitates strong binding between biological components and molecules, enabling their adaptation for various biosensors, including those for glucose and toxin monitoring(73). Compared to other synthetic polymer hydrogels, PAM hydrogels offer advantages such as faster preparation, enhanced toughness, and lower toxicity, making

them valuable for applications in biosensors, tissue engineering, and industrial settings(74,75).

2.2.3. Physical and Chemical Crosslinked Hydrogels

Hydrogels are composed of networks formed through crosslinking, which can involve chemical crosslinking, physical crosslinking, or a combination of both methods. These crosslinking techniques are crucial in the design of hydrogels, allowing for control over properties such as swelling ratio, mechanical strength and elasticity(76,77).Chemical crosslinking involves the formation of irreversible covalent bonds between or within polymers using multifunctional compounds. This process results in mechanically solid hydrogels with high stability and durability. However, the catalysts employed in these reactions may possess toxicity, leading to reduced biocompatibility. Additionally, covalently crosslinked hydrogels exhibit lower sensitivity to environmental stimuli such as pH changes and are less suitable for applications in biosensors(77,78).

On the other hand, physically crosslinked hydrogels are formed through reversible physical interactions such as ionic, van der Waals, or hydrogen bonds. These interactions make them uncomplicated to prepare and manipulate, without the need for catalysts(77). As a result, these hydrogels are often less toxic and more biocompatible. Additionally, incorporating pH responsive metal ions or polyelectrolytes as crosslinker allows hydrogels with induce sensitivity to specific pH ranges, allowing them to respond to acidic or basic environments(79). However, compared to chemically crosslinked hydrogels, physically crosslinked hydrogels may exhibit weaker mechanical strength and lower stability. They

are also more sensitive to environmental changes, which can impact their functionality. Despite these limitations, physically crosslinked hydrogels find applications in drug delivery(77).

In recent studies, researchers have developed hydrogels with double networks comprising both chemical and physical crosslinks. These hybrid hydrogels exhibit high mechanical robustness and biocompatibility, making them promise for biomedical applications, including biosensors(80).

2.2.4 Single and Double Network Hydrogels

The network structures of hydrogels play a crucial role in determining their physical and mechanical properties. Hydrogels can be organized into single networks (SN) or interpenetrating networks (IPN)(2). Single network hydrogels consist of a single crosslinked polymer network, which can be either covalently or ionically crosslinked(2). While SN hydrogels exhibit high water absorption capacity, their limited mechanical strength may restrict their functionality in their applications(81). Additionally, SN hydrogels may lack chemical stability and degradability, being more susceptible to environmental factors like pH and temperature changes(82).

On the other hand, interpenetrating network (IPN) hydrogels consist of two or more interpenetrating crosslinked networks(2,81). The most common type of IPN hydrogel is the double network (DN) hydrogel, comprising two different types of polymers. Typically, one polymer network provides toughness and mechanical strength, while the other offers

high water storage capacity and flexibility(83). These two networks are crosslinked either physically or chemically, creating a unique interconnected structure. In addition. By adjusting the (weight) ratio of these polymers and employing both chemical and physical crosslinking, hybrid double network hydrogel (hDN) can be tailored(81,82).

Specifically, hDN hydrogels are characterized by a dual-network structure, combining two interpenetrating polymer networks(84). They offer superior mechanical properties, including high strength, toughness, and flexibility, making them ideal for tissue engineering and biomedical applications(83,84). These hydrogels can be tailored to specific requirements by adjusting their composition and fabrication methods(84). They are biocompatible and have versatile applications in drug delivery, biosensors. In this matter, Hong *et al.* designed a hDN hydrogel employing reversible crosslinking of the chemical crosslinked SA and physical crosslinked polyethylene glycol (PEG) which illustrated significant mechanical robust(85).

2.3 Conductive Components incorporated in Hydrogels

Conductive materials are pivotal components to endow hydrogels conductivity offering a wealth of possibilities for transformative applications(86). Carbon-based nanomaterials, including carbon nanotubes (CNTs), graphene, and graphene oxide (GO), stand out for their remarkable electrical conductivity, high surface area, and mechanical strength(87,88). These materials can be integrated into hydrogel matrices to enhancing their electrical properties while retaining their biocompatibility(89). Peng *et al.*(90) designed a B-PVA-KCL-GO hydrogel with ionic conductivity and self-healing ability.

Subsequently, Feng *et al.*(91) designed rGO/cellulose hydrogel with great conductivity which was utilized in a supercapacitor, the ion channels exhibited exceptional capacitance, maintaining high level of performance.

Additionally, conductive polymers such as Ppy, polyaniline (PANI), and poly(3,4-ethylenedioxythiophene) (PEDOT) contribute to the conductivity of hydrogels(92). These polymers offer unique advantages such as flexibility, tunable conductivity, and biocompatibility, making them suitable for a wide range of biomedical applications(92,93). Polypyrrole stands out as an exceptional conductive polymer crafted through oxidative polymerization. This method entails the interaction of pyrrole monomers with oxidizing agents like iron (III) chloride ($FeCl_3$) or ammonium persulfate (APS), forging covalent bonds among them(25,94). Ppy offers numerous advantages, including high electrical conductivity, chemical stability, and compatibility with flexible substrates. Additionally, through careful chemical modifications, it can be suitable for a wide range of applications, including biocompatible sensors and actuators(94,95). However, it also has limitations. Ppy tends to be brittle and lacks mechanical strength, making it less suitable for applications requiring high mechanical integrity(94,96). Additionally, processing challenges may arise due to its tendency to form non-uniform structures. While Ppy is generally chemically stable, concerns about its long-term biocompatibility and doping dependency also exist, requiring careful consideration in biomedical and sensor applications(96). Despite these limitations, Ppy remains a valuable material with diverse potential applications.

Moreover, Polymers like polyaniline are synthesized in a manner akin to Ppy, involving the reaction of aniline monomers with oxidizing agents like $FeCl_3$ via oxidation(92). PANI exhibits remarkable characteristics, including high conductivity and stability, rendering it well-suited for biosensor applications(12). Nevertheless, it's essential to note its susceptibility to environmental variations such as temperature and pH fluctuations. Despite these considerations, PANI remains a promising polymer with vast potential across diverse fields, especially upon requisite modifications(97).

Carbon nanomaterials such as carbon nanotubes (CNT) and graphene have also been used as conductive agents for conductive hydrogels recently (87,88). These materials have high surface area-to-volume ratios, exceptional interaction with sensing materials, and offer high sensitivity for biosensors(18). Graphene, comprising a single layer of carbon atoms in a hexagonal lattice, exhibits remarkable conductivity, stability, and crucially, thermal conductivity(98). Its versatility extends to various industries, with applications ranging from touch screens to biomedicine, thanks to its high electrical conductivity, transparency, and mechanical strength(98). Similarly, CNTs possess specific electrocatalytic surface areas and excellent conductivity, making them ideal for glucose biosensor applications. Recent studies utilizing CNTs in combination with modified immobilized glucose oxidase (GOx) have demonstrated enhanced conductivity(99). Due to their extensive surface area, CNTs facilitate improved electron transfer, resulting in highly sensitive and stable glucose detection. For instance, research conducted by Xia *et al.*(100) showcased a glucose biosensor employing horseradish peroxidase with immobilized enzyme techniques, achieving a sensitivity of 270 ± 10 μA Cm−2 mM−1,

surpassing other enzymes and methodologies. These findings underscore the potential of CNTs as excellent candidates for biosensors.

Furthermore, hybrid materials combining different conductive elements offer synergistic benefits, combining the strengths of each component to create multifunctional hydrogel composites. These hybrid materials can be tailored to meet specific requirements, offering enhanced conductivity, mechanical strength, and biocompatibility for diverse applications. In biosensing, conductive hydrogels enable the development of sensitive and selective sensors for detecting biomolecules such as glucose, proteins, and DNA. In wearable biosensors, they facilitate the creation of flexible and stretchable devices that conform to the body's contours while maintaining electrical functionality. In tissue engineering, conductive hydrogels provide cues for cell growth and differentiation, promoting tissue regeneration and repair

2.4 Self-healing Hydrogel

Self-healing hydrogels are fascinating materials with the ability to repair themselves after experiencing damage or deformation. This property is particularly advantageous in applications where mechanical integrity is crucial, such as wearable sensors, and soft robotics(101). The self-healing mechanism of these hydrogels relies on dynamic chemical bonds, physical interactions, or supramolecular structures within the polymer network. One common approach to achieving self-healing in hydrogels is through dynamic covalent chemistry, where reversible chemical reactions enable the broken bonds to reform and heal the material(102,103). Examples of dynamic covalent bonds include

disulfide bonds, imine bonds, and Diels-Alder reactions. When the hydrogel is damaged, these reversible reactions are triggered, allowing the material to repair itself over time(104). In addition to the healing mechanisms, the kinetics and efficiency of self-healing in hydrogels can be influenced by factors such as temperature, pH, and the presence of specific catalysts or stimuli(105). Researchers continue to explore novel materials and strategies to enhance the self-healing capabilities of hydrogels, aiming to develop materials with improved mechanical strength, rapid healing kinetics, and broad applicability in diverse fields(103,105).

Darabi *et al.*(106) introduced a self-healing hydrogel combining physical and chemical crosslinking bonds for enhanced strength and conductivity. The incorporation of acrylic acid (AA) polymerization within the hydrogel matrix resulted in a double network, with PAA and conductive material (pyrrole) bonds responsible for mechanical strength. Berger *et al.*(107) similarly reinforced chitosan hydrogel with covalent crosslinking (PAA and PVA), enhancing structure and functionality. However, Darabi's hydrogel biosensor faced challenges in rapid synthesis due to toxicity concerns in the absence of covalent bonds, prompting Li *et al.*(108) to develop a self-healing hydrogel with dynamic imine linkage for sensor applications. Despite spontaneous healing, Darabi et al.'s hydrogel required two minutes for compression healing, with incomplete conductivity recovery, possibly due to material concentration variations(106). Park *et al.*(109) explored alternative hydrogel materials like NIPAM and B-cyclodextrin polymers, improving self-healing management. In addition, Liang *et al.* developed a chitosan-based self-healing glucose biosensor with CeO_2/MnO_2, demonstrating rapid response and promising longevity over a month(110).

2.5 Biosensors

Biosensors, mainly wearable ones, are increasingly important for non-invasive health monitoring and managing chronic conditions. Over recent decades, there has been significant research into hydrogel-based biosensors. Some detect substances like glucose or cholesterol using specific enzymes such as glucose oxidase or cholesterol oxidase(27,111). In addition, hydrogel biosensors can be designed to detect specific protein or nucleic acids for diagnosing specific physiological condition or genetic disorders(112,113). Mechanical sensors are also widely used in wearable devices including robotics and smart farming(114,115). PH-sensitive sensors have biomedical applications, and multifunctional biosensors combine various sensing capabilities(116). For instance, combining glucose biosensors with pH-sensitive materials enables glucose level monitoring under different pH conditions(117). Features like pre-programmability and self-healing capacity are also being developed(118,119). However, a major challenge is designing thin, fast-response sensors that are highly compatible with the human body. Thus, further research is needed to enhance sensor performance for biomedical applications(120).

2.5.1 Non-invasive Hydrogel Biosensors

Advancements in medical technology have brought forth non-invasive hydrogel biosensors, revolutionizing how to monitor the vital signs without resorting to invasive methods like blood extraction. These biosensors, integrating into hydrogel materials known for their biocompatibility, can adapt to body contours, ensuring comfort and ease of wear(121,122). By embedding sensing components within the hydrogel structure, such

as enzymes indicator, they can detect different biomarkers such as tears, sweat, and urine(123). The nature of these biosensors makes them ideal candidate for continues health monitoring a in the medical applications such as diabetes. The ongoing research endeavors to enhance the sensitivity of these sensors(123).

To be more specific, Blood glucose monitoring is crucial for diagnosing and managing diabetes(124). Traditional methods involve using glucose meters and test strips, which necessitate frequent finger pricking and pose infection risks due to open wounds(27). Minimally invasive glucose sensors alleviate discomfort and infection risks by penetrating the skin's outer layer to access interstitial fluid for glucose measurement(27). Non-invasive glucose sensors offer a pain-free experience without skin penetration, yet they may be influenced by environmental factors like skin conditions(122). Zhai *et al.* engineered a biosensor using platinum nanoparticles/polyaniline (PtNP/PANI) hydrogels. Featuring a 3D porous nanostructure, this hydrogel biosensor enhances the catalytic oxidation of glucose, thereby minimizing the diffusion distance for glucose molecules. Consequently, the biosensor achieves ultra-sensitivity, exhibiting a rapid response time of 3 seconds and a low detection limit of 0.7 μM(125).

2.5.2 Enzymatic and Non-enzymatic Biosensors

Enzymatic hydrogel biosensors employ enzymes embedded inside the hydrogel matrix to detect specific molecule such as glucose(126). The application of these sensors is based on the catalytic activity of the enzymes which provide measurable response to the

specific bioreceptor. Additionally, the 3D matrix of the hydrogel provides adequate protection for the enzyme, enhancing the activity and sensitivity of the biosensor(126).

On the other hand, Enzyme-free glucose sensors employ alternative methods to accurately measure glucose levels, offering reliability and precision(127). These sensors can adopt electrochemical mechanisms, leveraging materials like carbon nanotubes for direct glucose interaction and electrical signal detection(127). Alternatively, optical techniques utilize light-glucose molecule interactions, employing methods such as plasmon resonance and fluorescence for glucose level determination. Microfluidic sensors utilize microfluidic channels to analyze glucose concentration via refractive index measurements(128). Notably, non-enzymatic sensors are a great alternative to enzyme-based sensors as they can provide precise measurements without the need for enzyme protection from degradation and other unwanted molecules such as smaller proteins(129).

2.6 Microneedles

Microneedles (MNs) are composed of flexible micro-sized needles that are able to penetrate the skin to deliver drugs or other substances(130,131). To be more specific, they can bypass the outer layer of the skin, known as the stratum corneum, creating micropores that enhance the skin's permeability for drug delivery and other biomedical applications(131). Moreover, the skin comprises three layers: the epidermis, dermis, and hypodermis(132). The use of hypodermic needles in the hypodermis layer can cause swelling and pain. However, the top layer, the epidermis, which is approximately 1500 μm

thick, lacks nerve endings, allowing for the passage of lightweight molecules. Thus, Microneedles penetrate this layer, facilitating substance delivery(133). With advancements in microfabrication techniques, MNs have gained popularity in scientific and industrial domains. Furthermore, MNs offer cost-friendly, safe, controlled release, and compatibility with biodegradable materials(131). One of the applications of the MNs is delivering the substances such as glucose into the skin for control and measurement purposes(134). It is essential to mention that MNs provide higher benefits than traditional needles, including painlessness with minimum skin injury and lower sensitivity. Overall, MNs improve patient compliance, enhance drug delivery efficiency, and contribute to patient safety during procedures(131).

Based on their materials, microneedles can be classified into solid, coated, hollow and dissolved MN. This allows for a wide range of application including diagnostic(135). Solid MNs are mainly designed from a single piece of metal, facilitating their application by poking and passing through the stratum corneum (136). These MNs boast enhanced robustness, sharpness, and longevity, attributed to their solid construction. Additionally, they can be created from polymers, metals (gold particles) and silicone through such fabrication methods as micro-molding(135). Solid MNs penetrate the skin by creating micropores on the skin for the drugs to be delivered into the body in a controlled environment. Their shorter length makes them suitable for skin analysis and monitoring changes resulting from drug effects over time(136). Furthermore, Solid MNs are simpler to design compared to hollow types because of the lack of hollow channels which also, decrease the risk of clogging(136).

Hollow microneedles feature a chamber capable of storing larger drug volumes compared to another variant. They are specifically suitable for delivering fluids and can deliver in a range of nanoliters to microliters to the epidermis(137). Hollow MNs have applications in drug delivery, vaccine, and cosmetics(138,139). By controlling drug release, they accommodate heavier medications and offer extended-release durations, lasting up to several weeks(139). Moreover, hollow MNs can be designed through diverse techniques such as electroforming and micro-injecting molding from polymers, metals, silicon, and glass(140). It's crucial to note that this specific type of MNs can deliver substances precisely to targeted locations within the skin by overcoming the stratum corneum barrier. However, their less robust structure and higher maintenance requirements make them less practical for industrial use compared to solid microneedles(137,141). Despite their precision, they are prone to issues such as leakage and clogging, especially when dealing with viscous substances(137).

Coated MNs can be consist of either solid or hollow microneedles fabricated to have the drug or substance coated on the surface or within the coating layer. They can be designed to dissolve or release the medicine upon administration, depending on the composition of the coating material(142). To be more specific, these microneedles are crafted from diverse materials including polymers, sugar, and sometimes lipids, influencing their drug capacity and release characteristics. Moreover, it is excelled in releasing the drug rapidly and can passing the smaller materials(135). However, the study done by Dang *et al.*(143) indicates that the performance of coated microneedles for vaccine delivery parallels that

of intradermal methods. In this concern, their performance is highly impacted by the properties of the substance being delivered and the coating material.

Dissolved microneedle leverages the specific properties of the drugs they carry(138). These microneedles are designed to release the drug payload as the needle tip dissolves upon insertion into the skin. One of their notable advantages lies in their versatility concerning size and composition, as they can be crafted from biodegradable materials(141). Specifically, they are typically composed of water-soluble materials like polyvinylpyrrolidone (PVP) and sugar, which augment their ability to regulate drug delivery compared to other microneedle variants(144). For instance, in a study by Zhan *et al.*(145) dissolving cellulose microneedles containing lidocaine were showcased. These microneedles demonstrated significantly higher anesthesia rates compared to traditional methods, albeit with a duration of effectiveness lasting only 16 minutes. This highlights the potential of such dissolving microneedles in providing rapid and localized drug delivery with enhanced efficacy.

2.7 Conclusion

To put it in a nutshell, hydrogels provide unique 3D structure that enhances their utility in biomedical applications, particularly in biosensors. Their adjustable nature allows for further innovation and progress, promising boundless potential in the future. However, substantial research is needed to bridge existing gaps in hydrogel-based biosensors. Some of the challenges include the biocompatibility of various hydrogel materials, and complete self-healing ability. Addressing these obstacles is crucial for integrating

hydrogels into clinical settings effectively. Therefore, it is essential for future experiments and applications to design a hydrogels and biosensors that overcome the barriers such as response time, size, chemical and toxicity while maintaining the self-healing ability, which allows for greater sensitivity and usability.

Thus, PAM-SA hydrogel with $CaCl_2$ have been used for this study for the exceptional combination of flexibility and toughness afforded by the hybrid double-network structure. This hydrogel composition leverages the viscoelastic properties of polyacrylamide (PAM) and the strong ionic crosslinking provided by the interaction between sodium alginate (SA) and calcium chloride ($CaCl_2$). The result is a robust matrix that not only maintains structural integrity under mechanical stress but also supports diverse biomedical applications where durability and biocompatibility are paramount. This makes it an ideal candidate for further functional enhancements, such as the incorporation of conductive polymers for bioelectronic applications.

Chapter III: Materials and methods

3.1 Introduction

In this research, we engineered a novel hybrid double network hydrogel that combines advantageous properties of both natural and synthetic materials, resulting in remarkable improvements in mechanical strength and elasticity. As illustrated in Figure 1. the process commenced with the formation of a non-conductive hydrogel by mixing sodium alginate (SA) and acrylamide (AM) with aluminum persulfate (APS) and Tetramethylethylendiamine (TEMED). This mixture was then crosslinked with N,N' methylenebiacrylamide (MBA) and poured into specific molds to shape the desired hydrogel based on the experiment's requirements. Subsequently, various concentration of Calcium chloride ($CaCl_2$) was introduced to the hydrogel. The penetration of calcium ions into the hydrogel initiated ionotropic gelation between calcium ions (Ca^{2+}) and sodium alginate polymers, resulting in the formation of calcium alginate through crosslinking with carboxylate groups (COO-). The final SA-PAM-Ca^{2+} was used in our experiments. Additionally, to augment mechanical strength and introduce conductivity, we further modified this hydrogel with Ppy. The Ppy nanoparticles were prepared separately, and then mixed with the hydrogel precursor before gelation. The resultant Ppy-SA-PAM-Ca^{2+} hydrogel demonstrates promising applications in biosensors, owing to its enhanced properties.

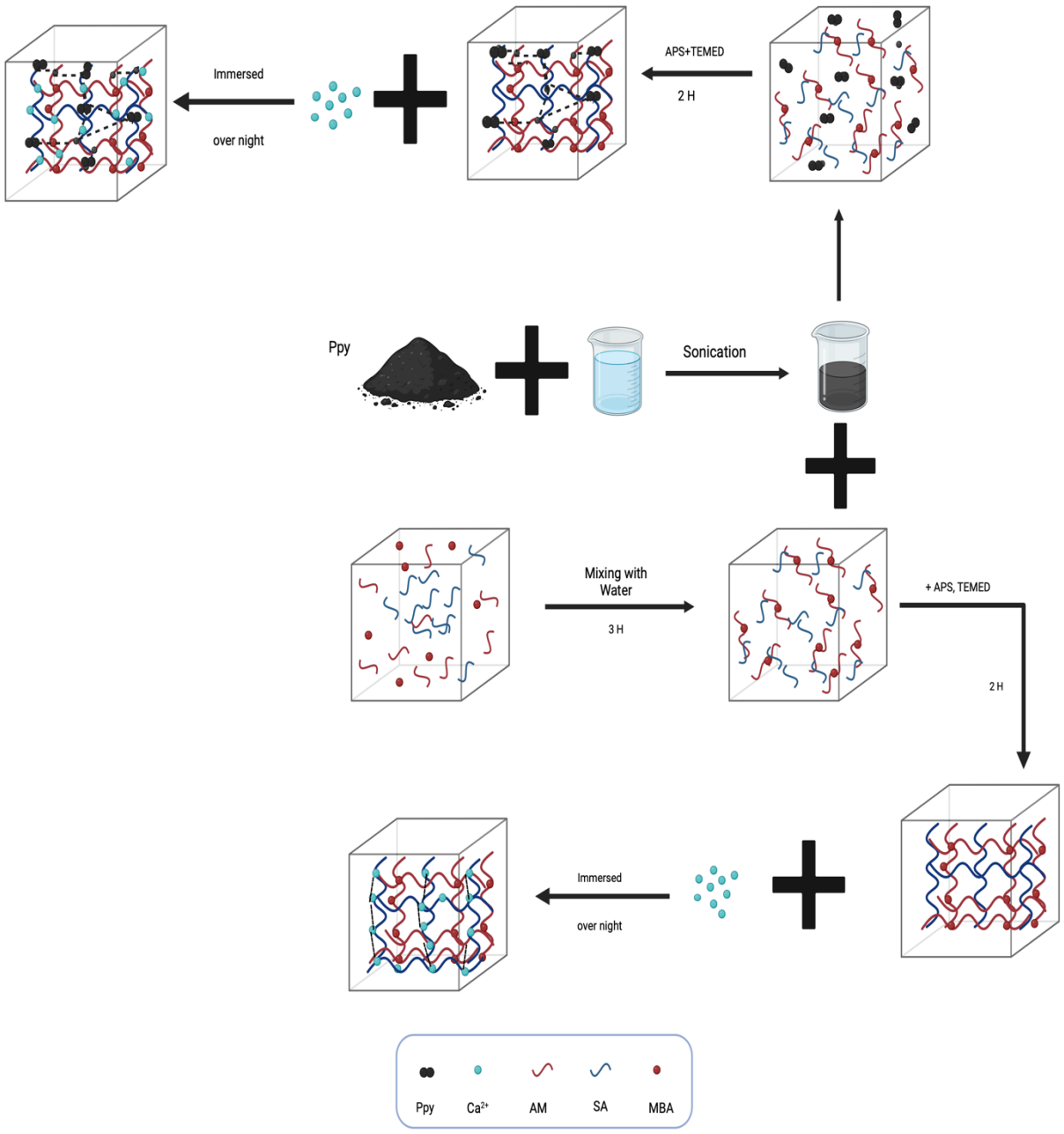

Figure 1. Schematic picture of the methods. The Ppy nanoparticles were mixed with DI water with sonication and added to the SA-PAM mixture to form conductive hydrogel with help of APS, MBA and TEMED. On the lower part the non-conductive hydrogel was mad

3.2 Materials

Acrylamide (AM), sodium alginate (SA), N,N' methylenebiacrylamide (MBA), Tetramethylethylendiamine (TEMED), Aluminum persulfate (APS) were purchased from Sigma-Aldrich, Canada. All materials were employed as received unless otherwise specified.

3.3 Preparation of hydrogels

3.3.1 Preparation of $CaCl_2$ Solutions

Various solutions of $CaCl_2$ were prepared, including concentrations of 5wt% (0.05 M), 10wt% (0.1 M) and 20wt% (0.2 M). Each hydrogel sample prepared as described in the next step would be immersed fully into these solutions.

3.3.2 Preparation of SA-PAM-Ca^{2+} Hydrogel

The SA-PAM-Ca^{2+} hydrogels were prepared with various ratios of SA and PAM as shown in table 1. While the amount of PAM remained constant at 4 g, varying amounts of SA were used, including 0.2 g, 0.27 g, and 0.4 g for weight ratios of 1:20, 1:15, and 1:10 respectively. DI water was added to reach a total mass of 20 g. The mixture was subsequently combined with 0.2% (wt%) MBA, 10% TEMED, and 10% APS in room temperature. The duration was 5 hours for each hydrogel to form. Each resulting hydrogel was then immersed into $CaCl_2$ solutions with various concentrations as stated in the previous section. Following immersion, the desired hydrogels were removed from $CaCl_2$

and washed the next day to prepare them for further procedures. It is important to note that, the MBA is the crosslinker and TEMED and APS help further with crosslinking.

Table 1. List of specific ratio and concertation of material in support of designing the desirable hydrogel.

Sodium Alginate (g)	Acrylamide (g)	Water (mL)	Ratio
0.2	4	15.8	1:20
0.27	4	15.73	1:15
0.4	4	15.6	1:10

3.3.3 Preparation of Ppy-SA-PAM-Ca^{2+} Hydrogel

In order to prepare Ppy, 0.2 g of pyrrole monomers were mixed with 20 mg SA which in here serves as stabilizing medium for the reaction. Subsequently, 0.1 M APS was added to the solution, which was then placed on ice (0-2 □C) with low speed stirring overnight to facilitate oxidation polymerization. The following day, the Ppy nanoparticles were filtered, washed, and dried. After that the nanoparticles were dissolve in water through sonication. A total of 0.208 mL of this solution was then mixed with the SA-PAM precursor. The hydrogels were fabricated similarly to the method described earlier, utilizing three different weight ratios of 1:20, 1:15, and 1:10, with varying concentrations of 5wt%, 10wt%, and 20wt% $CaCl_2$ separately.

3.3.4 Sonication

The Ppy solution was prepared using a sonicator SK92-INN, operating with interval cycle of 2 seconds on and 4 seconds off for a total duration of 60 minutes. In order to ensure the protection, samples were placed in plastic tubes in cold bath at 2°C.

3.3.5 Microneedles

To fabricate microneedles, a mold with 4 mm needles was produced using 3D printing. The hydrogel material was then poured into a designated medium, and the mold was applied with downward pressure for 5 hours at room temperature, forming the desired microneedles.

3.4 Characterizations

3.4.1 Fourier-Transformation Infrared (FTIR)

The FTIR spectroscopy analysis was conducted using a Bruker IFS 66v/s spectrometer from Germany, equipped with attenuated total reflection (ATR) capability. This method allowed the examination of the functional groups present within the hydrogels across a range of 4500-500 cm^{-1}. Prior to analysis, each sample was freeze-dried and crushed to ensure uniformity and optimal performance under the sensor of the device.

3.4.2 Scanning Electron Microscopy (SEM)

The freeze-dried samples of hydrogels underwent a gold coating process which is used to enhance image quality and stability. It prevents charge buildup by providing conductivity(146), improves resolution by increasing secondary electron emission, and

protects delicate samples under vacuum conditions(147). This ensures high-quality SEM images. Subsequently, they were mounted onto the metal holder for morphological examination using SEM microscopy. The SEM model employed was the FED 650, operating at a voltage of 20eV. This examination encompassed both surface and cross-sectional imaging for comprehensive analysis of each hydrogel sample.

3.4.3 Swelling Ratio

The swelling ratio test was conducted on all hydrogel samples with varying concentrations, as listed in Table 1. Sample with a size of 2x2x2 cm^3 were immersed into excess water for 24 hours. Weight measurements were taken at intervals of 1, 5, 15, 30, 60, 120 minutes, as well as after 6 and 24 hours. The swelling ratio was calculated using Equation 1, where Wt represents the weight of the swollen hydrogel and Wd signifies the weight of the air-dried hydrogel.

$$\boldsymbol{SR = Wt - Wd} \quad (1)$$

3.5 Mechanical Tests

The mechanical properties of the hydrogels were assessed using the Instron 5965 testing machine, with each concentration (as listed in table 3 for both non-conductive and conductive) tested at least three times. Average values and standard deviations for each sample were computed and graphed using Microsoft Excel software. Additionally, the Young's modulus was calculated from the stress-strain curves obtained during the tests.

3.5.1 Tensile Test

Each hydrogel sample underwent a minimum of three tensile tests conducted at a crosshead speed of 10 mm/min and room temperature. Tensile strain (ε) was calculated using Equation 2, where L and L0 represent the new and original lengths, respectively. Tensile stress (σ) was determined by Equation 3, with F representing the load, W the width, and T the thickness of the samples. Fracture toughness was computed using the area under the stress-strain curve (Equation 4). The hydrogels were designed as samples with dimensions of 40 mm in Length, 17 mm in width and 7mm in thickness.

$$\boldsymbol{\varepsilon = \frac{(L - L0)}{L0}} \tag{2}$$

$$\boldsymbol{\sigma = \frac{F}{(L0 \times W)}} \tag{3}$$

$$\boldsymbol{U = \int \sigma \; d\varepsilon} \tag{4}$$

3.5.2. Compression Test

The compression test was conducted on hydrogel samples with dimensions of 15 mm in height and 8 mm in diameter. The tests were carried out at a speed of 20 mm/min with a maximum compression rate of 80%.

3.6 Rheology Test

Rheology testing was conducted using a TA DHR-2 rheometer equipped with sample cylinders measuring 8 mm in diameter. To ensure optimal results, hydrogel samples of various concentrations were prepared in molds with an 8 mm diameter and 1 mm thickness.

3.7 Conductivity

The resistivity of each sample was determined using an electrochemical workstation (Cs350, China). From that the conductivity was calculated by Equations 5 and 6, where σ represents conductivity, ρ represents resistivity and W and D represent thickness and shape respectively.

$$\boldsymbol{\sigma = \frac{1}{\rho}} \tag{5}$$

$$\boldsymbol{\rho = \rho 0 \times W \times D} \tag{6}$$

3.8 Statistical Analysis

In this thesis the two tailed T-test was done for our samples with equal variant of generally n=3. The two-tailed t-test assesses whether the means of two groups are statistically different without predicting the direction of the difference. It checks for significance in both

directions, assuming normal data distribution. A p-value less than 0.05 typically indicates significant differences, suggesting the results are unlikely due to chance, while a larger p-value supports the null hypothesis that differences are due to random variations.

Chapter IV: Result and Discussion

4.1 Hydrogel Characterization

In this section we looked at the FTIR and SEM results which provide proof regarding the assembly of the hydrogels, porosity, and the functional group within the samples.

4.1.1 FTIR

The hydrogel samples were made of PAM, SA and $CaCl_2$ which provides adequate mechanical strength and elasticity. The success of the reaction was determined by having the specific functional groups within the samples such having the amide group and carboxylic group int eh SA-PAM-Ca hydrogel. the FTIR test was done on the samples to verify the formation of the interaction between the functional groups. In the FTIR spectrum. As it is demonstrated in Figure 2a, the peak at 1635 cm^{-1} shows the characteristic stretching amide bond of the PAM. The broad peak at wavelength of 3182 cm^{-1} is responsible for OH and secondary amide bonds in sodium alginate and PAM, respectively. In addition, the wavelength at 2936 cm^{-1} is responsible for CH stretching vibration for methyl bond in SA. the wavelength of 1580 cm^{-1} and 1431 cm^{-1} are also responsible for symmetric and asymmetric carboxylic bonds in SA.(148–150). To further substantiate the presence of the SA bond, Figure 2b presents the FTIR spectrum for SA powder. Here, the peak at 3241 cm^{-1}, corresponding to the OH bond, is similar to the 3182 cm^{-1} peak in Figure 2a. Additionally, the wavelengths at 1579 cm^{-1} and 1393 cm^{-1} represent the asymmetrical and symmetrical stretching vibrations of the COOH groups, respectively. These peaks are aligned with the 1580 $cm^{-1}$and 1431 cm^{-1} peaks observed in the PAM-SA hydrogel. At the beginning of the spectrum, the peak at 1014 cm^{-1} indicates

the elongation of the C-O group (151). In Figure 2c, the symmetrical and asymmetrical vibrations of the COO- group are depicted at 1402 cm^{-1} and 1577 cm^{-1}, respectively. Additionally, the presence of the Amide bond is confirmed at 1650 cm^{-1}, indicating the inclusion of PAM in the hydrogel. Furthermore, the NH_2 bond is observed at a wavelength of 3168 cm^{-1} in Figure 2c.(149,150,152).

Furthermore, the FTIR spectrum of Ppy in Figure 2d is illustrating the NH bond at peak of 3168 cm^{-1}, and 1647 cm^{-1} for stretching and bending bonds respectively. In addition, the broad peak of 1110 cm^{-1} is responsible for CN amine group(150,153). By analyzing the Figure 2e, we determined the formation of the Ppy-PAM-SA hydrogel by having broader peak at 3161 cm^{-1} for overlapping NH and Oh groups of Ppy and SA which are steeper. Also, the sharper peak at 1103 cm^{-1} represents overlapping CN bonds for both Ppy and PAM verifying the formation of the bonds. Similar to non-conductive hydrogel the ionic bond between Sa and Ca^{2+} ions was formed by showing COO- groups at wavelength of 1655 cm^{-1}. Moreover, the peaks at 870 cm^{-1} represent the CH waging for Ppy, which is similar to the peak 1024 cm^{-1} on Ppy powder spectrum. Lastly the peak 2936 cm^{-1} in Figure 2 c,d and 2935 cm^{-1} at Figure 2e represent CH bond(149,150,152,153).

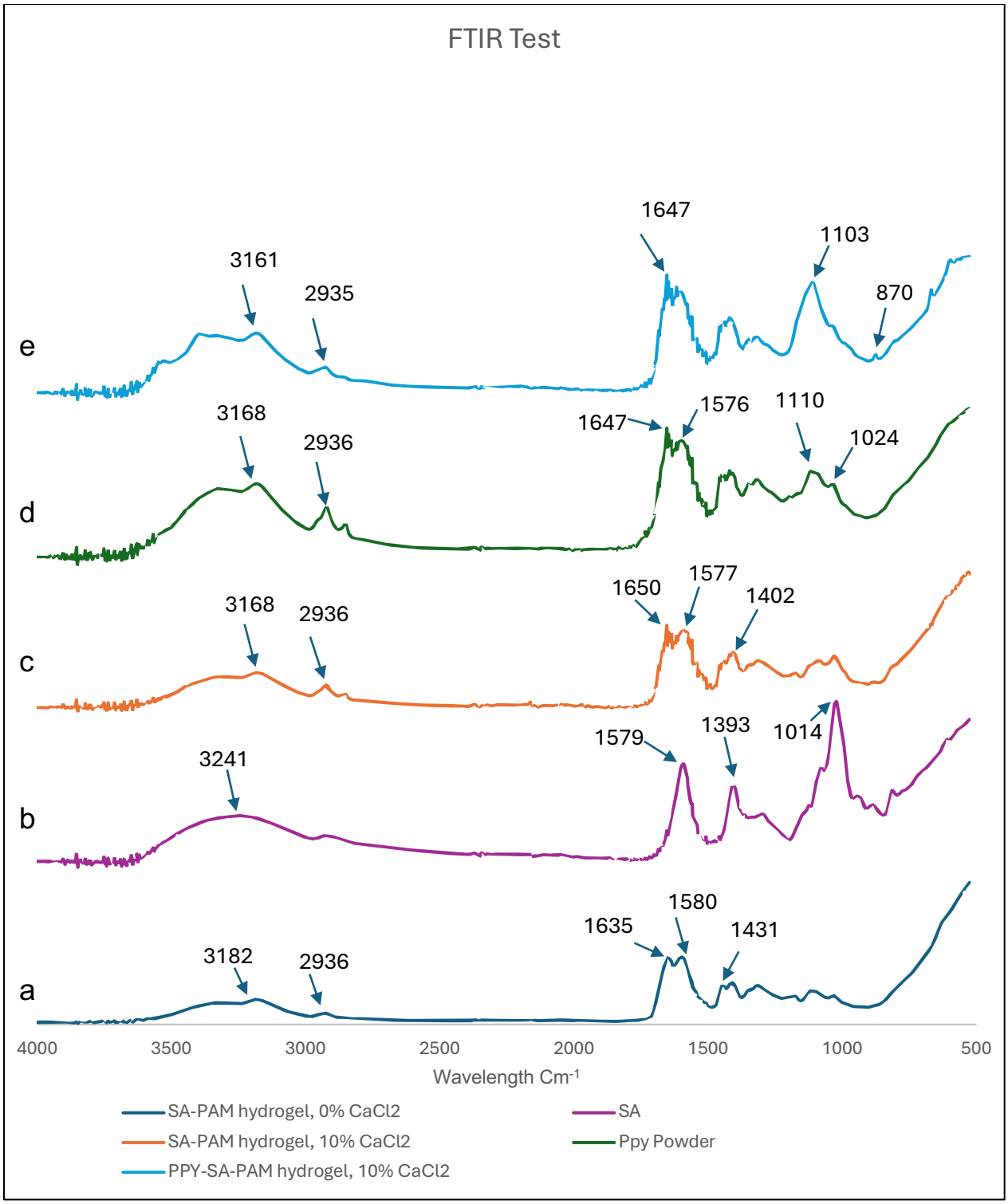

Figure 2. FTIR spectrum of samples. a) non-conductive SA-PAM hydrogel without $CaCl_2$, b) SA powder, c) SA-PAM hydrogel with addition of 10wt% $CaCl_2$, d) Ppy powder, e) PPY-SA-PAM conductive hydrogel with 10wt% $CaCl_2$

4.1.2 SEM Imaging

Similar to FTIR test, SEM imaging was performed to look into the formation of the hydrogels as well as the porosity. Figure 3 shows the PAM hydrogel without any additional material with 1000x magnification. From both surface and cross-sectional formation, we can see that the interior of the hydrogel is well-defined. Moreover, Figure 4 represents the surface and cross-sectional view of the SA-PAM hydrogel with 1:10 weight ratio and additional of 10wt% $CaCl_2$ in 1000x magnification. Although the controlling the porosity of the hydrogel is still a challenge, the smaller porosity of the hydrogels in figure 4 compared to Figure 3 verify the role of SA and Ca^{2+} in changing the hydrogel's interior design(153,154). By looking more closely, for the SA-PAM hydrogel, the surface view (Figure 3a) displays a porous, irregular texture, while the cross-sectional view (Figure 3b) shows a more uniform porous structure, suggesting a heterogeneous network with variable crosslink density. In contrast, the SA-PAM hydrogel with 10wt% $CaCl_2$ (Figure 4a and 4b) exhibits a significantly altered microstructure; both surface and cross-sectional views display more defined, uniform, and regular pore structures. The walls between pores are thinner, indicating a higher degree of crosslinking facilitated by the ionic interactions between alginate and calcium ions. This enhanced structure suggests a stronger and more stable network, likely contributing to improved mechanical properties suitable for applications in drug delivery, tissue engineering, and water treatment.

Furthermore, Figure 5, represents our sample with conductive material Ppy. Section a and b illustrates surface and cross-sectional view with 1000X magnification and from them the presence of Ppy on the hydrogel surface is shown. For better analyzation of the

surface of the sample, 2500x magnification was also captured to verify that Ppy polymers were perfectly cover the surface of the hydrogel. To be more specific, the rough surface verifies the existence of Ppy polymer inside the hydrogel, and Ppy powder is also shown for reference on Figure 5d. The distinct morphologies observed in these SEM images underline the importance of structural control in designing hydrogel composites. The integration of Ppy into hydrogels, as seen in the granularity and diverse particle sizes of Ppy, necessitates a careful balance between achieving desired conductivity and maintaining mechanical properties. For instance, uniform dispersion of Ppy within hydrogels can enhance electrical properties without compromising the gel’s physical integrity. Furthermore, the variation in hydrogel pore structures from these images indicates that tailoring the crosslinking density and pore architecture can significantly influence the hydrogel's suitability for specific applications, ranging from bioelectronics to scaffold-based tissue regeneration.

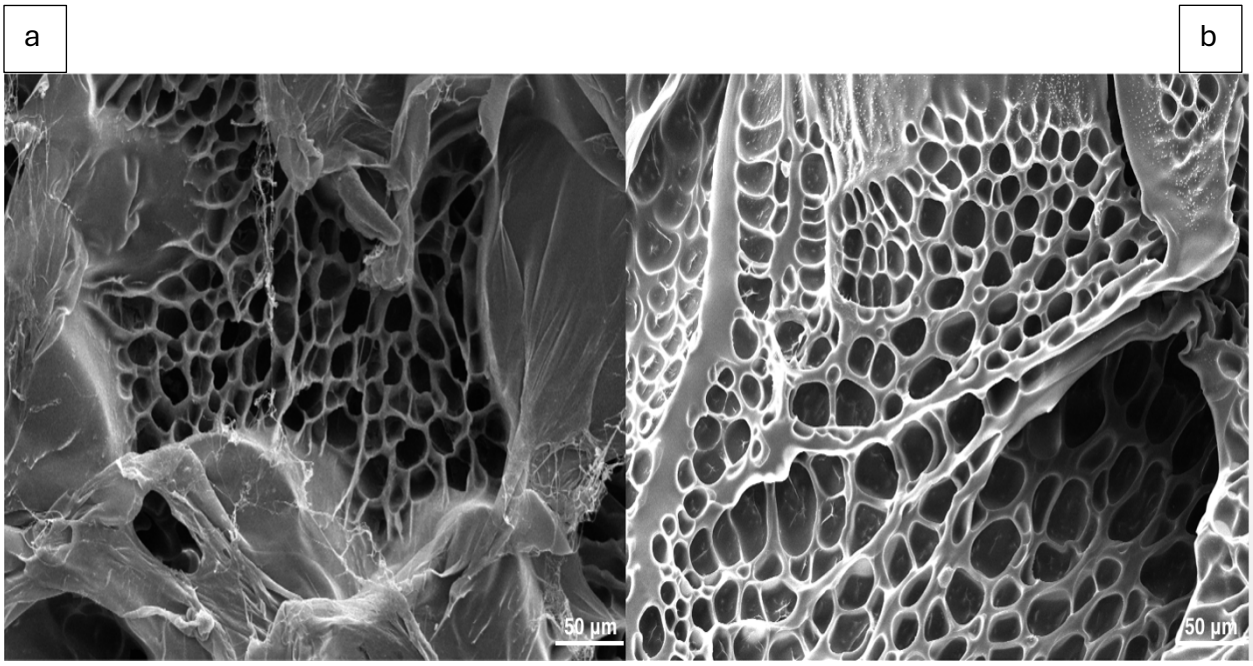

Figure 3. SEM imaging for PAM hydrogel. a) surface view with 1000x magnification, b) cross-sectional view with 1000x magnification.

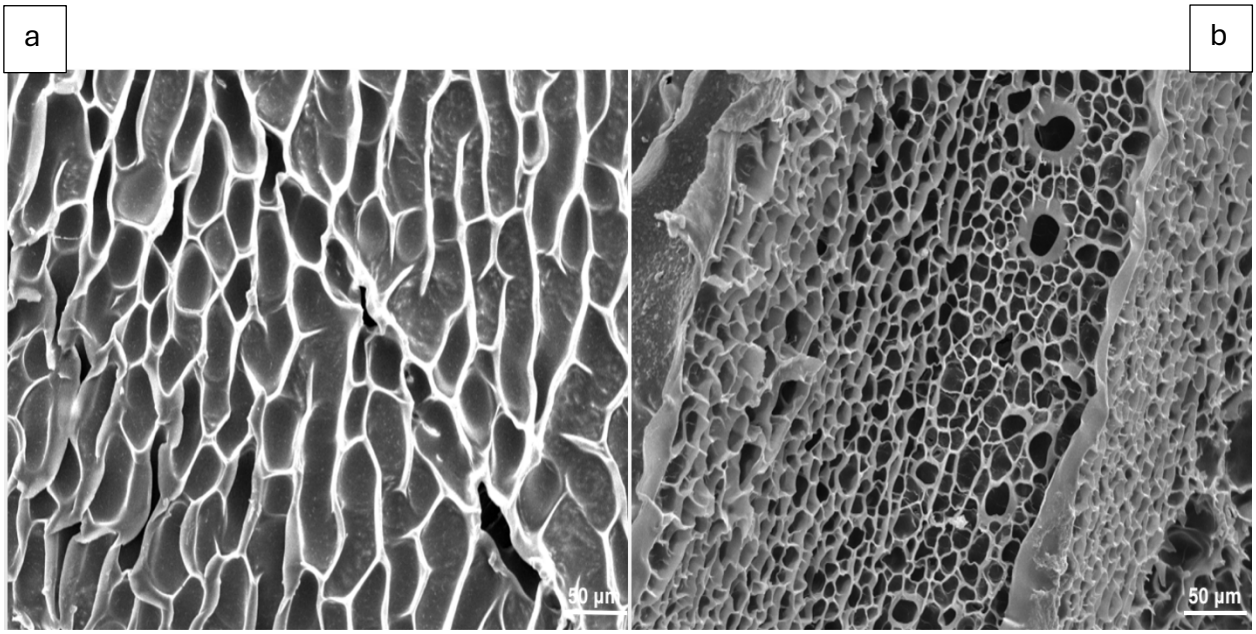

Figure 4. SEM imaging for SA-PAM hydrogel with 10wt% $CaCl_2$. a) surface view with 1000x magnification, b) cross-sectional view with 1000x magnification.

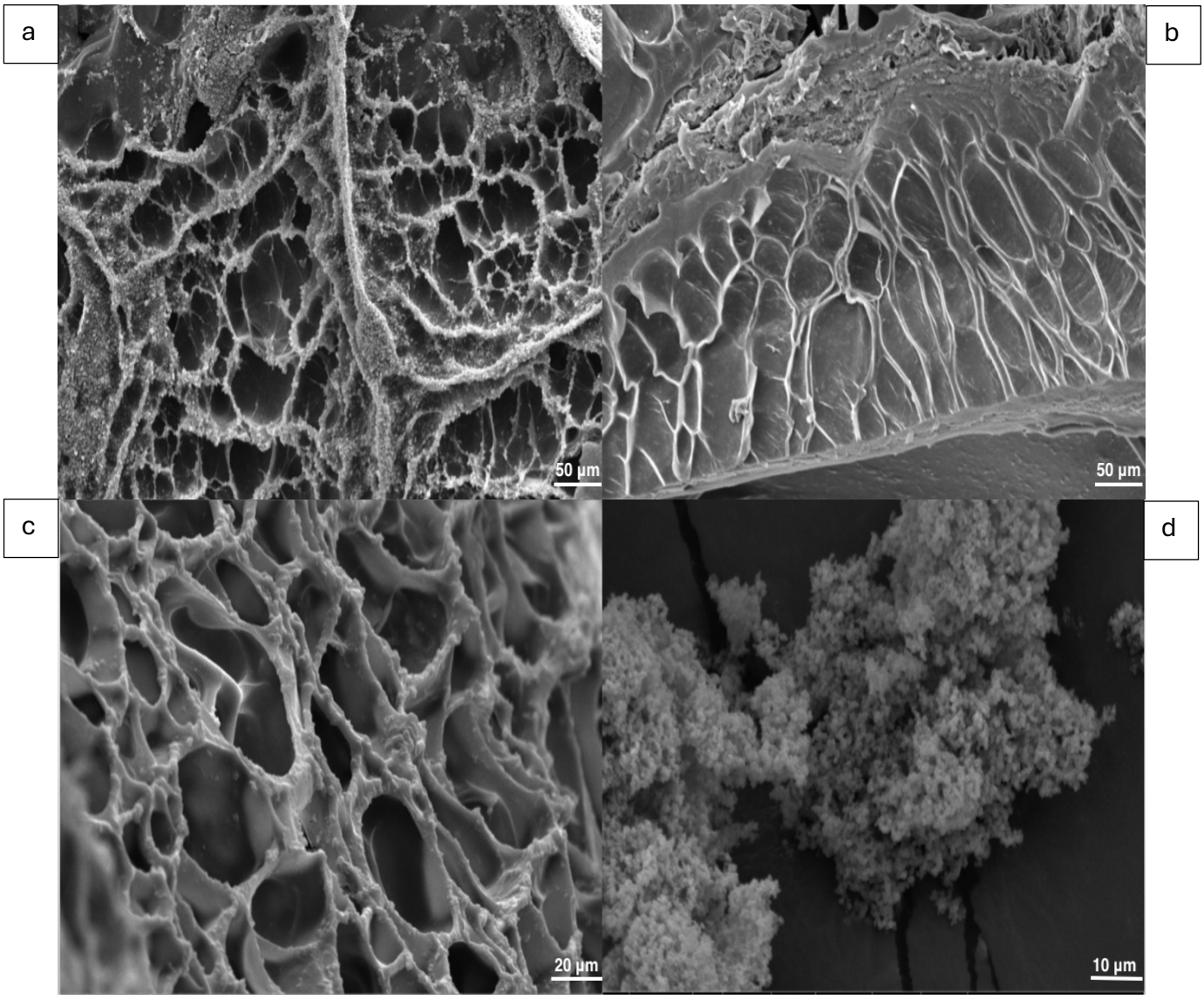

Figure 5. SEM imaging of PPY-SA-PAM hydrogel. a) surface view with 1000x magnification, b) cross sectional view with 1000x magnification, c) surface view with 2500x magnification, d) Ppy powder with 5000x magnification

4.2 Swelling Ratio Test

The analysis of swelling ratio was conducted to provide additional confirmation of the crosslinking reaction between Ca^{2+} and SA-PAM hydrogel. As portrayed in Figure 6 each polymer weight ratio of SA-PAM hydrogel, explicitly 1:10, 1:15, and 1:20, was combined with varying concentrations of $CaCl_2$ (0wt%, 10wt%, and 20wt%). In Figure 6a, the swelling ratio for the 1:10 SA-PAM hydrogel weight ratio is shown. We can observe that an increase in calcium content results in a further reduction in the swelling ratio, with the swelling behaviour at 0wt% Ca^{2+} being significantly higher than those at 10wt% and 20wt% Ca^{2+} concentration levels. Additionally, statistically significant differences (two tail T-test) were done between the swelling ratios at 0wt% vs. 10wt% Ca^{2+} and 0wt% vs. 20wt% Ca^{2+} in 24 hours, with sample size of four for all different samples. The P-values of 0.005 and 0.006 is seen for Figure 6a for compression of 0wt% vs. 10wt% Ca^{2+} and 0wt% vs. 20wt% Ca^{2+}, respectively. These findings verified the efficacy of calcium-induced crosslinking in the hydrogel structure.

Moreover, Figures 6b and 6c correspond to weight ratios 1:15 and 1:20 of SA-PAM hydrogel, respectively. Throughout statistical analysis of the diagrams, we have determined that the introduction of calcium ions into the hydrogel consistently reduces the swelling ratio significantly. Precisely, in Figure 6b, we conducted p- value of 0.002 in t-test comparison between 0wt% and 10wt% calcium concentration after 24 hours, while the comparison between 0wt% and 20wt% calcium concentration resulted in a p-value of 0.005. Furthermore, in Figure 6c, the p-values for the comparisons between 0wt% and 10wt% calcium concentration and between 0wt% and 20wt% calcium concentration in 24

hours were found to be 0.004 and 0.005, respectively. These results reaffirm our findings regarding the crosslinking of the hydrogel induced by the incorporation of calcium ions.

As, we inspected in the Figure 6, adding calcium ions (Ca^{2+}) to a sodium alginate hydrogel can decrease its swelling ratio. This occurs due to the formation of calcium alginate crosslinks within the hydrogel matrix(155,156). Sodium alginate is a linear polysaccharide composed of repeating units of β-D-mannuronic acid and α-L-guluronic acid(157). In the presence of calcium ions, sodium alginate undergoes a process called ionotropic gelation, where the calcium ions form crosslinks with the guluronic acid residues, leading to the formation of a three-dimensional network structure. This crosslinking reduces the mobility of polymer chains and restricts the uptake of water molecules, thereby decreasing the swelling capacity of the hydrogel(156,158).

The extent of decrease in swelling ratio depends on various factors such as the concentration of calcium ions, and the molecular weight of sodium alginate. Generally, higher concentrations of calcium ions or increased degrees of crosslinking result in greater reductions in swelling ratio(51,156). Controlling the swelling ratio and the crosslinking density of the $CaCl_2$ and SA-PAM hydrogel helps us open doors to various biomedical and pharmaceutical applications where controlled release of drugs or encapsulation of cells is desired.

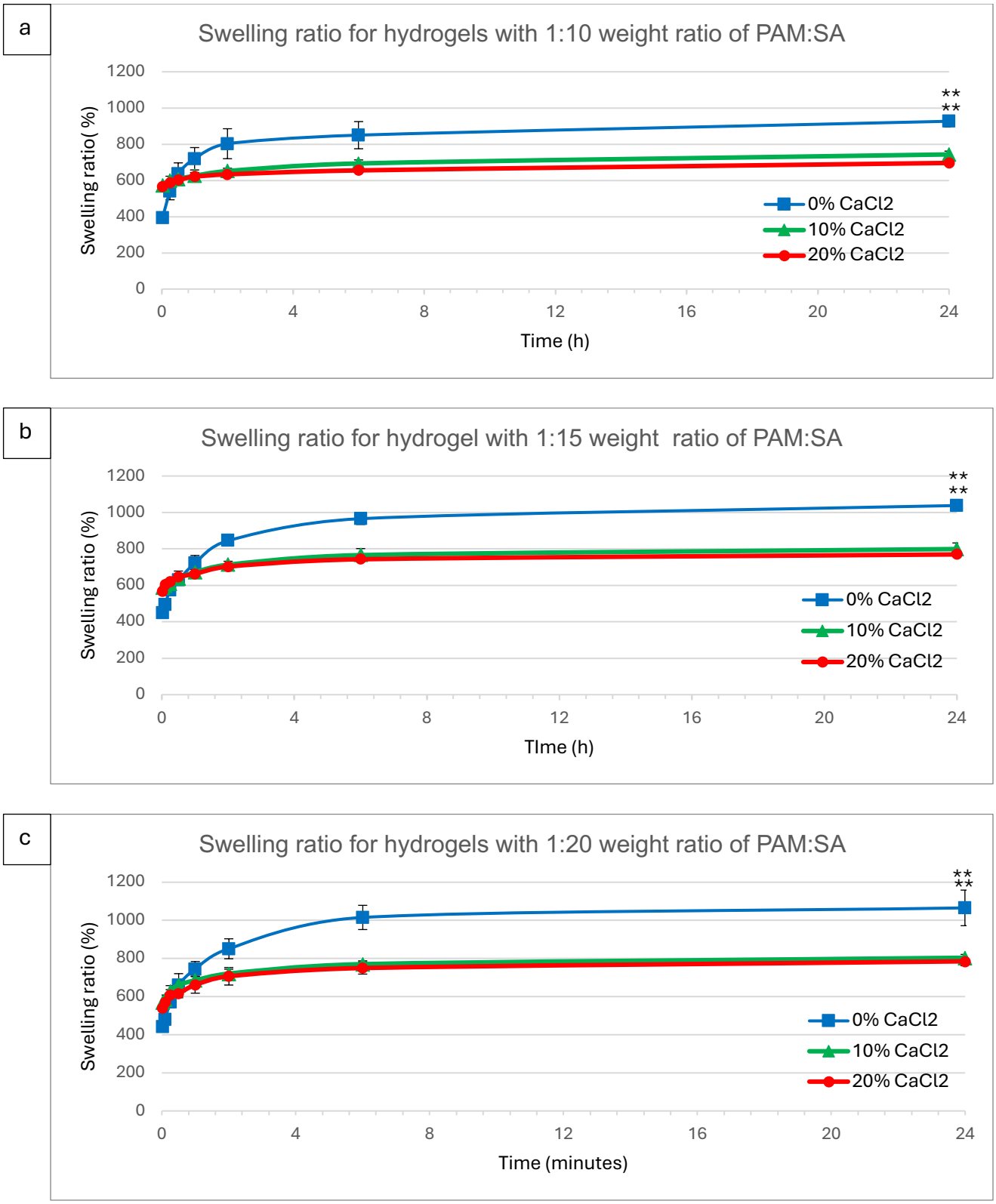

Figure 6. Swelling behaviour test for hydrogel samples with 0wt%, 10wt% and 20wt% concentration of $CaCl_2$. a) swelling ratio for hydrogels with weight ratio 1:10 of Sa-PAM hydrogel, b) swelling ratio 1:15 of SA-PAM hydrogel, c) swelling ratio 1:20 of SA-PAM hydro

4.3 Tensile Test

Tensile testing plays a pivotal role in understanding the strength and flexibility of materials, making it indispensable for developing new materials and ensuring quality. By revealing key properties like tensile strength and elasticity, this testing helps engineers and scientists predict how materials will perform under stress. This knowledge is crucial not only for maintaining high standards in material manufacturing but also for meeting regulatory requirements and ensuring the safety and reliability of structural applications across various industries.

4.3.1 Tensile test for non-conductive hydrogel samples

Analyses of the mechanical properties of SA-PAM hydrogels, influenced by different ratios of sodium acrylate (SA) to polyacrylamide (PAM) and varying concentrations of calcium chloride ($CaCl_2$), have illuminated significant understandings. The tensile tests, that we conducted across three different SA:PAM weight ratios (1:10, 1:15, and 1:20), demonstrate that the incorporation of $CaCl_2$ generally enhances the tensile strength of the hydrogels. Specifically, in Figure 7a. (1:10 SA-PAM weight ratio) the addition of 5wt% $CaCl_2$ (green curve) into the hydrogel significantly improved strength compared to the hydrogel without $CaCl_2$ (blue curve) where it changed from 32 KPa to 56KPa. Increasing the CaCl2 concentration to 10wt% (red curve) further elevated the tensile strength, while having great elasticity with almost same as the sample with 0wt% CaCl2 (0.69 mm/mm). Interestingly, the 10wt% $CaCl_2$ curve shows an initial high slope (high modulus) and extends to a high, suggesting it might be the most ductile and toughest among the 1:10 weight ratios. Although 20wt% $CaCl_2$ (black curve), the hydrogel exhibited the highest

tensile strength and modulus, yet failed abruptly at 0.36 mm/mm almost half of 10wt% concentration, showcasing a trade-off between strength and flexibility.

Moreover, In Figure 7b. the SA-PAM weight ratio of 1:15 under similar $CaCl_2$ variations similarly followed the trend observed in the first graph. The modulus of the hydrogel improves with increasing $CaCl_2$, leading to greater initial stiffness. The 10wt% CaCl2 (red curve) again offers the best balance between high stress and reasonable strain capabilities, achieving the highest peak stress at 70KPa which is almost 3 times more than the sample with no $CaCl_2$. The toughness is optimal at this concentration, which can absorb a significant amount of energy before failing, compared to the 20wt% concentration (black curve) that, despite its high modulus, exhibits pronounced brittleness and a drastic drop in toughness due to minimal elongation before breaking.

Figure 7c, showcasing an SA:PAM weight ratio of 1:20, also demonstrate similar pattern but with notable differences in strain at break and overall toughness where none of the samples could elongate more than 0.5 mm/mm. The modulus increases with $CaCl_2$ concentration, reaching its maximum at 20wt% $CaCl_2$, indicative of very high stiffness. However, the sample with 10wt% $CaCl_2$ (red curve) strikes the most favorable balance, maintaining a high modulus while still allowing for greater elongation compared to the 20wt% concentration. Therefore, across all tested SA:PAM (weight) ratios, the 10wt% $CaCl_2$ concentration is considerable noble, where the hydrogel shows not only high stress absorption but also better resistance to abrupt failure, making it suitable for applications where both strength and flexibility are required.

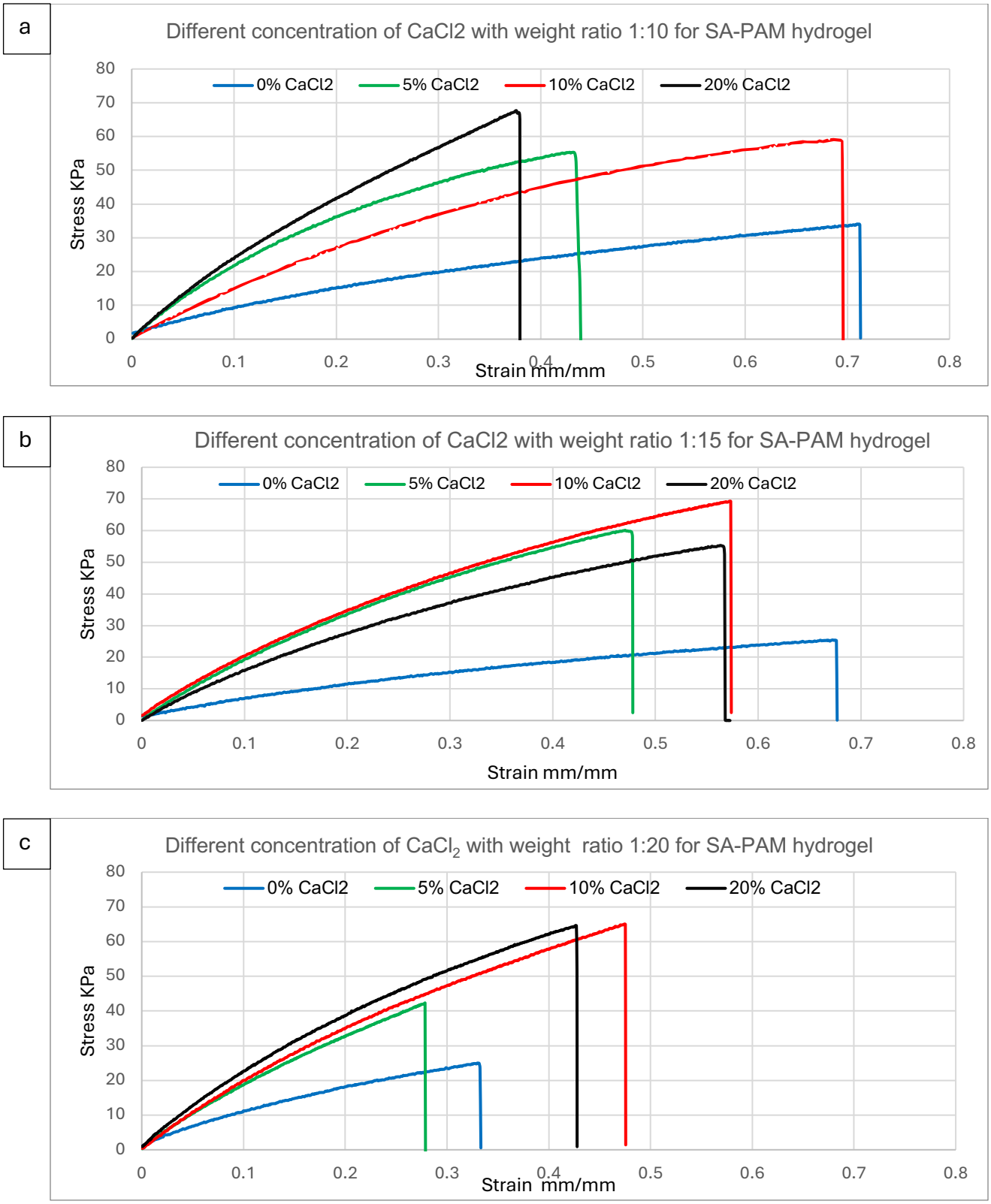

Figure 7. tensile test for hydrogel samples with various ratios with 0wt%,5wt%,10wt% and 20wt% concentration of CaCl2. a) tensile test for 1:10 weight ratio of SA-PAM hydrogel, b) tensile test for 1:15 weight ratio of SA-PAM hydrogel, c) tensile test for 1:20 weight ratio

To verify the findings in more details, each sample was tested three times, and the average is shown in Figure 8 for module, stress, strain, and toughness for our defined ratio in various concentrations of 0wt%, 5wt%, 10wt%, and 20wt% $CaCl_2$.

Examining the data more closely, Figure 8a. represents the comparison of modulus. The 1:10 weight ratio consistently exhibits the highest modulus across all $CaCl_2$ concentrations. Such ratio the modulus increases more than 4 times time from 94.8 KPa in 0wt% $CaCl_2$ to 385 KPa in 10wt% $CaCl_2$. This trend highlights a significant impact of $CaCl_2$ on hydrogel elasticity at this ratio. The 1:15 weight ratio, while showing an overall upward trend in modulus, records lower values than the 1:10 weight ratio across similar concentrations. Starting at around 110 KPa without $CaCl_2$, it reaches its peak at 317.2 KPa with 10wt% $CaCl_2$ which is significantly lower than the modulus of 1:10 weight ratio in 10wt% $CaCl_2$ with p value of 0.0039. Meanwhile, the 1:20 weight ratio presents a more variable pattern. Beginning at roughly 140 KPa at 0wt% $CaCl_2$, it peaks at 267.90 KPa with 10wt% $CaCl_2$ before and similar to 1:15 weight ratio it shows significantly lower modulus compared to 1:10 weight ratio with p value 0.001. In addition, the slight decrease of modulus to 219.20 KPa at 20wt% $CaCl_2$ concentration suggests that increasing the $CaCl_2$ concentration might not be as effective at maintaining stiffness.

The decrease in the modulus can be because of the oversaturation of $CaCl_2$ which indicates that because of the excess concentration of the Calcium chloride some of it could not effectively crosslink. In addition, the high ion concentration can result in altered hydrogel structure and cause reduction in modulus.

Figure 8b. provide analysis for stress response. The 1:10 weight ratio, which exhibits the highest stress values at all $CaCl_2$ concentrations, the stress starts at approximately 29.6 KPa when no $CaCl_2$ is present and climbs to 64 KPa at 20wt% $CaCl_2$ concentration. Although, 20wt% $CaCl_2$ shows higher stress than 62.4 KPa in 10wt%, the difference is not significant and 10wt% is still provide excellent tensile strength. Conversely, the 1:15 weight ratio, while following a similar upward trend, consistently records slightly lower stress levels compared to the 1:10 weight ratio. It begins at 21.1 KPa without $CaCl_2$ and increases to about 57.49 KPa at the highest $CaCl_2$ concentration. Moreover, the 1:20 weight ratio starts with tensile strength of 24.2 KPa at 0wt% $CaCl_2$, indicating an initial better resistance to mechanical stress possibly due to a higher proportion of the polymer. However, as $CaCl_2$ concentration increases, this ratio shows a lesser increase in stress compared to the other ratios, reaching 60.47 KPa at 20wt% $CaCl_2$. This suggests that while the initial polymer content provides inherent strength, the weight ratio becomes less effective under higher $CaCl_2$ concentrations.

Furthermore, Figure 8c. provides detailed evaluation of the strain behavior of our hydrogels samples. For the 1:10 hydrogel weight ratio, which displays the highest initial strain at 67.7% (0.677 mm/mm) with no $CaCl_2$, there is a marked decrease in strain as the $CaCl_2$ concentration increases, reaching 46% (0.46mm/mm) at 20wt% $CaCl_2$. However, it is important to mention, that while the elongation reduced by increasing $CaCl_2$, 10wt% concentration of $CaCl_2$ still represent notably high strain with 54.5% (50.545 mm/mm). This significant reduction indicates that the hydrogel becomes substantially stiffer with increased $CaCl_2$, reflecting a dense cross-linking network that limits the

material's ability to elongate. The 1:15 weight ratio starts with a strain of 49.5% (0.495 mm/mm) at 0wt% $CaCl_2$ and undergoes a modest change to 53.2% (0.532 mm/mm) at 20wt% $CaCl_2$. This behavior suggests a relatively more elastic network compared to the 1:10 weight ratio, indicating that this mixture might be preferred in applications where a balance between elasticity and stiffness is necessary. On the other hand, the 1:20 weight ratio showcases a unique trend; it starts with the lowest initial strain at 26.3% at 0wt% $CaCl_2$ but exhibits an increase to 43% at 20wt% $CaCl_2$. The almost similar strain of 40% and 43% for 10wt% and 20wt% $CaCl_2$ could suggest a threshold effect where beyond a certain point, additional $CaCl_2$ no longer contributes significantly to further cross-linking, or it might indicate a different structural rearrangement within the hydrogel matrix.

Lastly, Figure 8d, demonstrate variation in toughness of hydrogels across different ratios. For the 1:10 hydrogel weight ratio, toughness shows a marked increase from 13.3 KJ/M^3 at 0wt% $CaCl_2$ to 19.9 KJ/M^3 at 10wt% $CaCl_2$, indicating that this ratio achieves an optimal cross-linking density that allows the hydrogel to absorb substantial energy. Similarly, the 1:15 weight ratio begins at a low toughness of 6.6 KJ/M^3 at 0wt% and reaches its peak at 23.8 KJ/M^3 at 10wt% $CaCl_2$. The 1:20 weight ratio, starting with the lowest toughness of 4.4 KJ/M^3 at 0wt% $CaCl_2$, progressively increases to 17 KJ/M^3 at 10wt% $CaCl_2$. Despite improvements, it remains the least tough under all tested conditions, likely due to a less robust cross-linked network compared to the lower hydrogel to $CaCl_2$ ratios.

The analysis of Figures 7 and 8 indicates a clear trend: higher $CaCl_2$ concentrations improve the hydrogel's modulus, stress resistance, and toughness but reduce its strain

or elongation capability. This trade-off highlights the critical role of $CaCl_2$ in tailoring hydrogel properties for specific uses. The 1:10 weight ratio with 10wt% $CaCl_2$ concentration consistently offers the best overall mechanical properties, suggesting its suitability for applications requiring robust, durable materials that can withstand significant mechanical stresses.

a

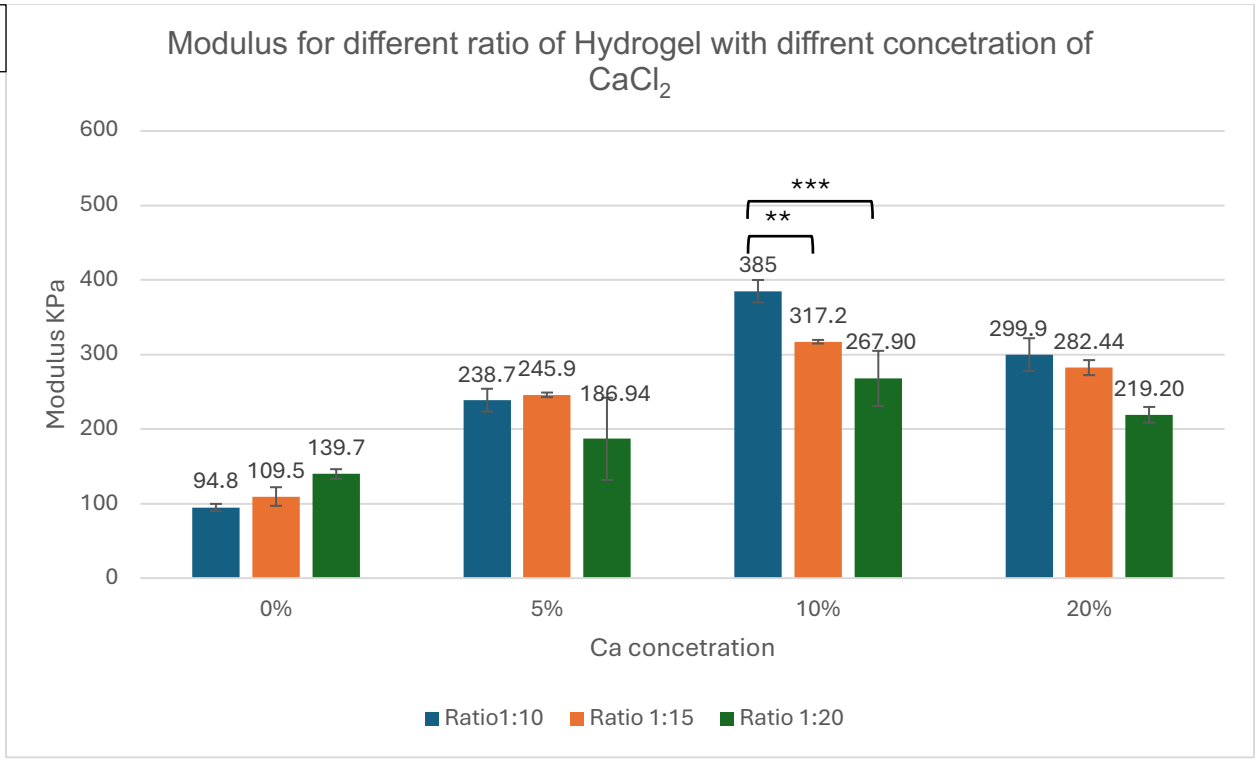
Modulus for different ratio of Hydrogel with diffrent concetration of $CaCl_2$
Modulus KPa
600
500
400
300
200
100
0
***
**
385
317.2
267.90
299.9
282.44
219.20
238.7
245.9
186.94
94.8
109.5
139.7
0%
5%
10%
20%
Ca concetration
Ratio1:10
Ratio 1:15
Ratio 1:20

b

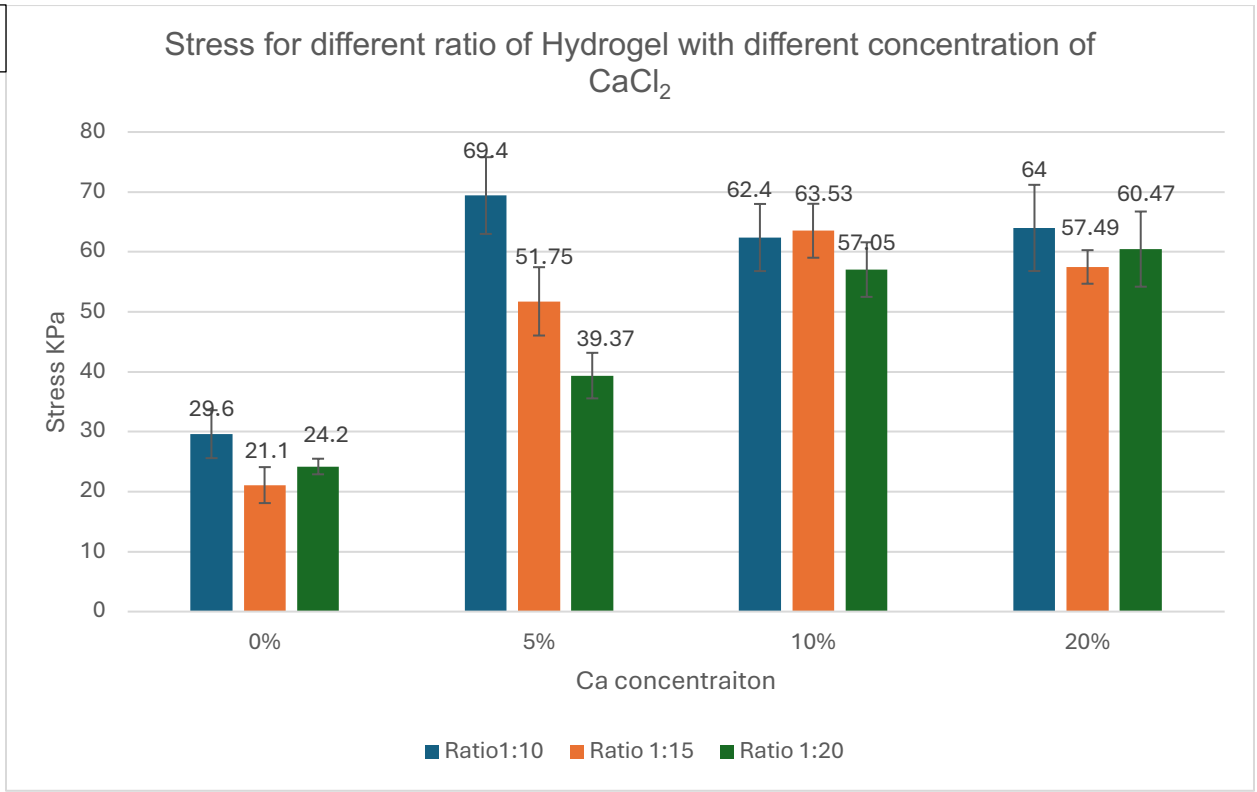
Stress for different ratio of Hydrogel with different concentration of $CaCl_2$
Stress KPa
80
70
60
50
40
30
20
10
0
69.4
51.75
39.37
62.4
63.53
57.05
64
57.49
60.47
29.6
21.1
24.2
0%
5%
10%
20%
Ca concentraiton
Ratio1:10
Ratio 1:15
Ratio 1:20

c

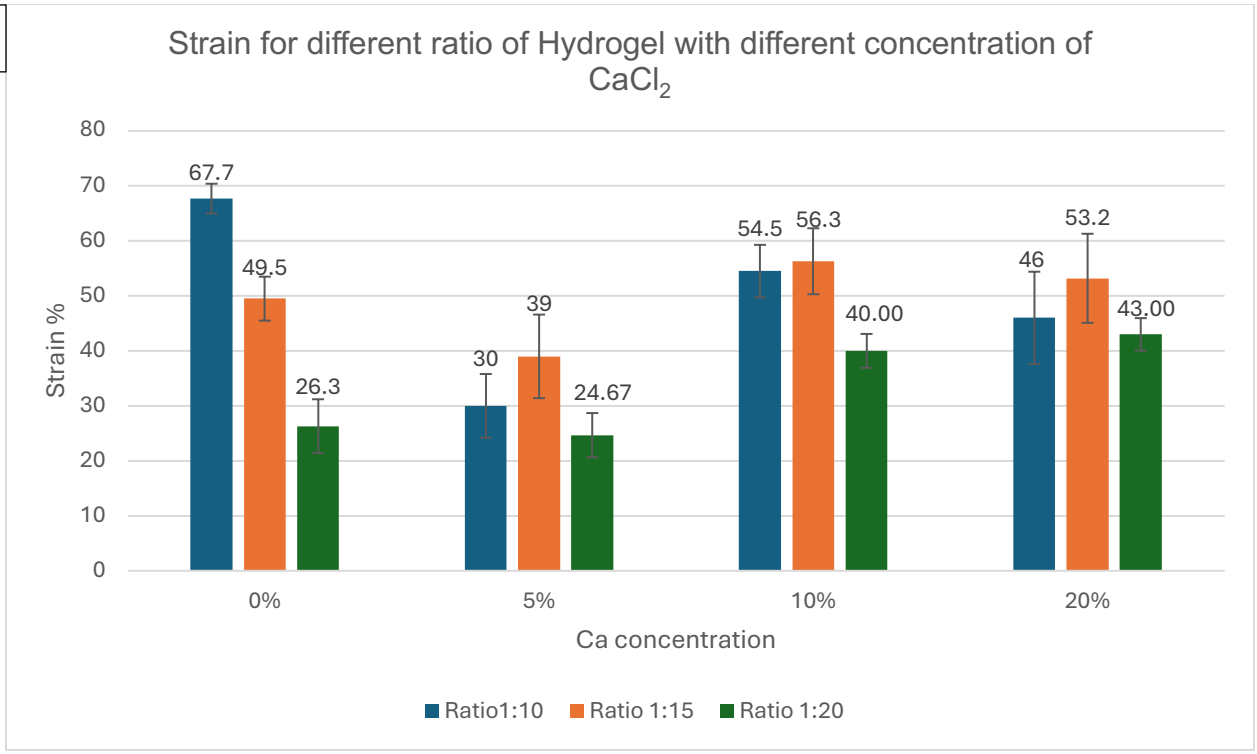

d

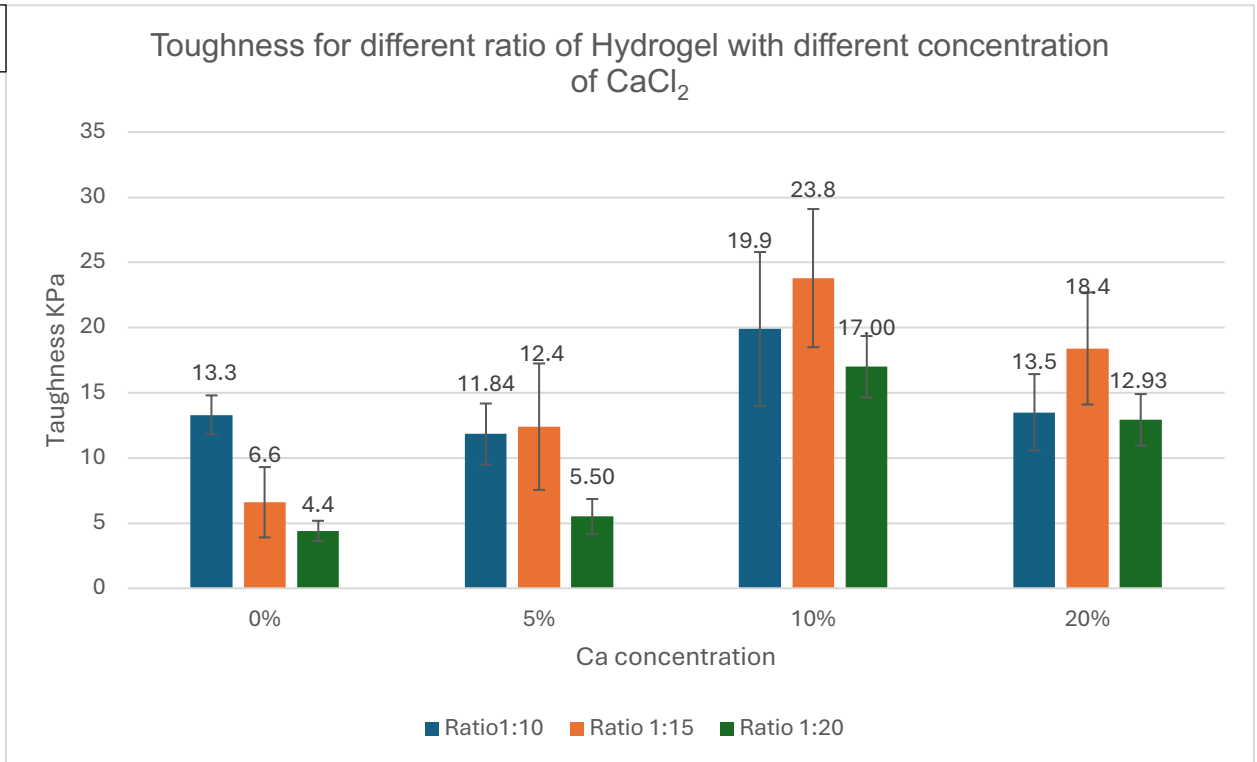

Figure 8. Bar graph of parameters of stress-strain curve for weight ratio of 1:10, 1:15, 1:20 of SA-PAM hydrogel with 0wt%, 5wt%, 10wt% and 20wt% $CaCl_2$. a) module, b) stress, c) strain, d) area under the curve (toughness). Three samples were used to test for each test.

4.3.2 Tensile test for conductive hydrogel

Conductivity is a crucial property for hydrogels used in applications such as sensors, actuators, and wearable devices. To enhance the electrical properties of SA-PAM hydrogels, we have incorporated the conductive polymer Ppy. This addition helps with hydrogels in applications requiring not only mechanical integrity but also high conductivity. The following analysis demonstrates the tensile characterization of the PPY-SA-PAM hydrogels, thereby identifying optimal formulations for specific functional requirements.

By looking at Figure 9. in the analysis of SA-PAM hydrogels enhanced with PPY, we can see those varying concentrations of $CaCl_2$ significantly influenced the mechanical properties. In Figure 9a. the hydrogel with 5wt% $CaCl_2$ (green curve) demonstrated a steady increase in stress with strain, exhibiting good elasticity and strength before a sudden drop, indicative of material failure at a relatively high strain. This suggests a balance between flexibility and mechanical strength. Additionally, the hydrogel with 10wt% $CaCl_2$ (red curve) reached the highest stress level at 67.8 KPa among the set while maintaining highest elongation, pointing to an optimal cross-linking density that provides superior strength. On the other hand, the 20wt% $CaCl_2$ sample (black curve) displayed the highest initial stiffness and the least ductility, failing at a low strain of 0.6mm/mm, which underscores the trade-offs between stiffness and breakability in hydrogel structure.

Figure 9b. is indicating hydrogels with a 1:15 SA-PAM weight ratio, revealed that the addition of 5wt% $CaCl_2$ (green curve) provides moderate stress capabilities and superior

elongation of over 100%, suggesting it is appropriate for applications requiring extended deformation. The 10wt% $CaCl_2$ (red curve), while achieving the highest stress peaks indicative of greater strength, followed a similar pattern as red curve on Figure 9a. The 20wt% $CaCl_2$ concentration (black curve) exhibited the highest initial modulus but also the most pronounced brittleness, failing at very low strains and thus, verifying that 10wt% $CaCl_2$ is optimal concentration.

Furthermore, Figure 9c. specifying the SA:PAM weight ratio of 1:20, showed unique mechanical behaviors. The hydrogel with 5wt% $CaCl_2$ (green curve) displayed less dramatic stress development but maintained a gradual failure process, indicating a balance that may favor applications requiring both strength and flexibility. The 10wt% $CaCl_2$ (red curve) exhibited a robust stress profile, achieving high peaks that suggest an optimal mix of cross-linking for mechanical strength by having highest elongation of 0.72 mm/mm. Conversely, the 20wt% $CaCl_2$ (black curve) demonstrated extreme stiffness by having tensile strength of 56 KPa, but very low strain of 0.59 mm/mm, reaffirming the heightened brittleness associated with high $CaCl_2$ concentrations. Therefore, across all SA:PAM ratios tested with addition of Ppy conductive material, The 10wt% $CaCl_2$ concentration provided the best compromise, showing enhanced tensile strength while still maintaining sufficient ductility and toughness.

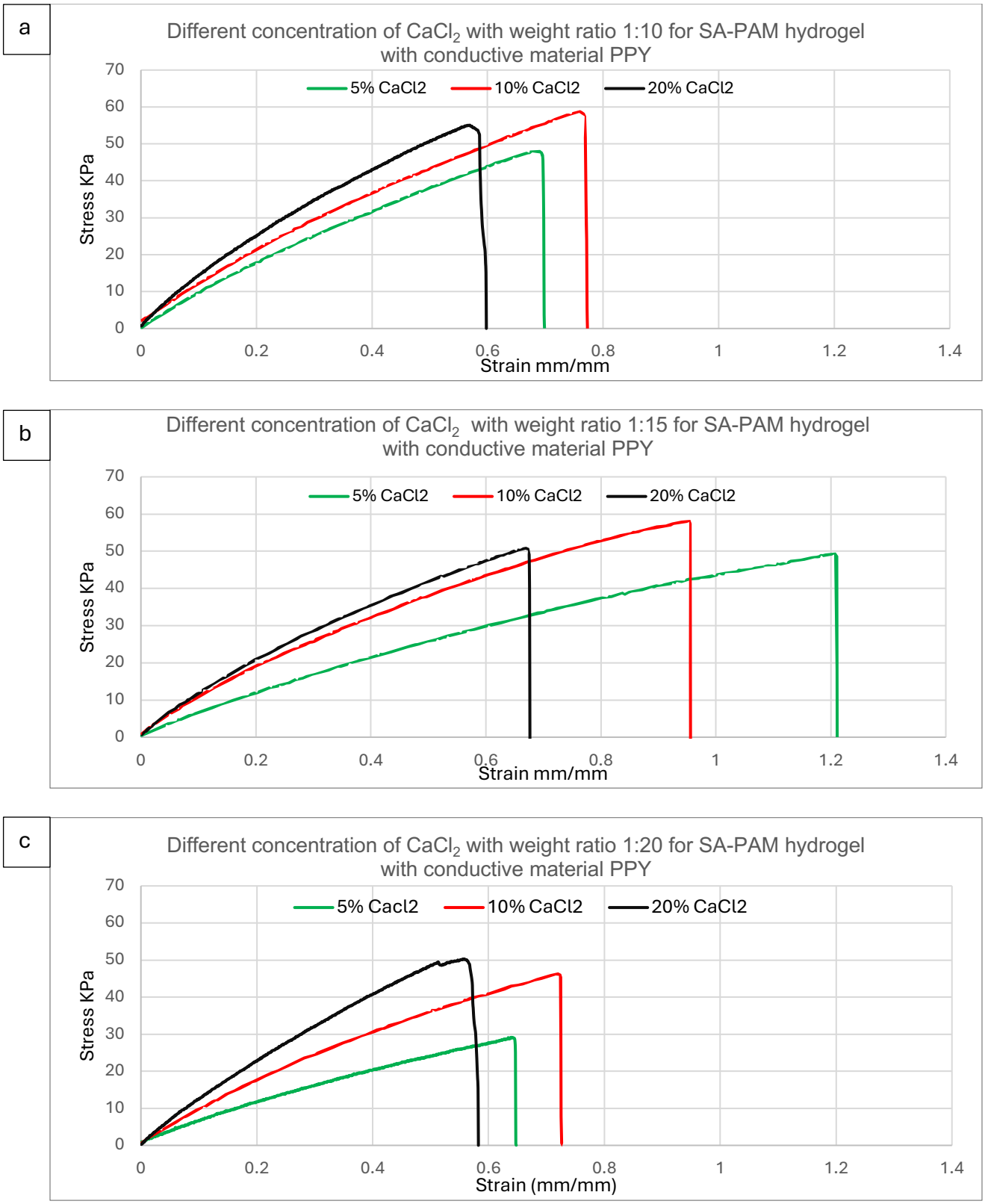

Figure 9. tensile test for conductive hydrogel samples with various ratios with ,5wt%,10wt% and 20wt% concentration of $CaCl_2$. a) tensile test for 1:10 ratio of PPY-SA-PAM hydrogel, b) tensile test for 1:15 ratio of PPY-SA-PAM hydrogel, c) tensile test for 1:20 ratio of PPY-SA-PAM hydrogel

Similar to non-conductive hydrogels, to provide a more detailed validation of the results, each sample underwent at least three separate tests. The mean values of these tests are presented in Figure 10, which shows the modulus, stress, strain, and toughness of samples with predetermined ratios across varying $CaCl_2$ concentrations of 0wt%, 5wt%, 10wt%, and 20wt% for PPY-SA-PAM hydrogel.

In Figure 10a. notably, the modulus reaches its highest peak at a 10wt% $CaCl_2$ concentration for the 1:10 hydrogel weight ratio, achieving a high of 385.3 KPa. This peak is significantly higher than 1:10 weight ratio with 20wt% $CaCl_2$ with p value of 0.004. Additionally, this suggests an optimal cross-linking density at this concentration, which is essential for maximizing stiffness without compromising the structural integrity of the hydrogel. However, a subsequent decrease in modulus at 20wt% $CaCl_2$, falling to 284.9 KPa, points to potential over-saturation or structural imbalances within the hydrogel network at higher concentrations. Moreover, the 1:15 and 1:20 weight ratios follow a similar pattern of initial increases followed by a plateau or slight reduction in modulus as $CaCl_2$ concentration increases. For instance, the 1:15 weight ratio rises to 337.2 KPa at 10wt% $CaCl_2$ and slightly decreases to 295 KPa at 20wt% $CaCl_2$. Similarly, the 1:20 weight ratio climbs to 280.5 KPa at 10wt% from 149.6 KPa in 5wt%, but then falls to 201.3 KPa at 20wt%. These trends suggest a diminishing return in cross-linking efficiency at higher $CaCl_2$ concentrations, possibly due to the hydrogel reaching its cross-linking capacity, which could lead to less effective structural reinforcement or even degradation.

The data in Figure 10b illustrate the result for stress. the 1:10 weight ratio shows an increase in tensile strength from 48.1 KPa at 5wt% $CaCl_2$ to a peak of 61.5 KPa at 10wt% $CaCl_2$, before slightly decreasing to 55.5 KPa at 20wt% $CaCl_2$. This pattern suggests a robust enhancement at 10wt% $CaCl_2$, which is likely due to optimal cross-linking density that reduces at higher concentrations. Similarly, the 1:15, and 1:20 weight ratios start at lower stress level of 50.1 KPa and 32.6 KPa respectively 5wt% $CaCl_2$, then peak at 57.4 KPa and 52.4 KPa respectively for 10wt% $CaCl_2$ before slightly decreasing at 20wt% $CaCl_2$. These behaviour reveals a general trend for all ratios where stress resistance tends to increase with the $CaCl_2$ concentration from 5wt% to 10wt% following a decrease in 20wt%. This suggests an over-crosslinking in hydrogel structures in 20wt% $CaCl_2$ concentration where the hydrogel becomes rigid and lead to a structure that is brittle, reducing its overall effectiveness under stress Therefore, a robust enhancement at 1:10 weight ratio with 10wt% $CaCl_2$, suggest a near optimal cross-linking density.

Furthermore, Figure 10c. illustrates insights into the flexibility and elasticity of our samples where we can see a similar trend of Figure 10b 1:10 and 1:15 weight ratios. 1:10 and 1:15 weight ratios start with 65.4% (0.645mm/mm) and 85.6% (0.85 mm/mm) in 5 wt% $CaCl_2$ respectively and increase to highest elongation of 88% (0.88 mm/mm) and 86.4% (0.864 mm/mm) at 10wt%, follow with around 20% decrease in 20wt% $CaCl_2$ concentration. This trend shows that the 10wt% $CaCl_2$ is an optimal concentration for the Ppy hydrogel to maintain good amount of elongation. In the contrast, the 1:20 weight ratio shows decreasing trend from 63.1% (0.631 mm/mm in 5wt% to 39.6% (0.396 mm/mm) in 20wt% $CaCl_2$, verifying that an increase in $CaCl_2$ decrease the elasticity.

Lastly, Figure 10d. showcases the toughness of our hydrogel samples containing Ppy. The 1:10 weight ratio (blue bars) peaks at 34.1 KJ/M^3 at 10wt% $CaCl_2$, indicating optimal cross-linking at this concentration, but experiences a slight decrease at 20wt% $CaCl_2$. the 1:15 weight ratio starts with the highest toughness at 24.1 KJ/M^3 at 5wt% $CaCl_2$, up to 30.8 KJ/M^3 at 10wt% $CaCl_2$ and then drop to 22.5 KJ/M^3 at 20wt% $CaCl_2$. Conversely, the 1:20 weight ratio (green bars) shows a less pronounced increase in toughness with higher $CaCl_2$, starting at 14.7 KJ/M^3 at 5wt% and peaking only slightly higher at 18.8 KPa at 10wt%, then dropping to 15.5 KJ/M^3 at 20wt% $CaCl_2$, and further to 22.5 KJ/M^3 at 20wt% $CaCl_2$. This shows that the 10wt% $CaCl_2$ is the optimal concentration for our samples with 1:10 (weight ratio) being the highest. Subsequently across the different hydrogel (weight) ratios, the trend in toughness does not change significantly with increasing $CaCl_2$ concentrations, indicating complex interactions between the polymer network and the cross-linking agent, where the optimal cross-linking density, which maximizes toughness, is influenced by both the concentration of $CaCl_2$ and the specific hydrogel ratio.

The analysis of figure10, showed the mechanical properties of conductive hydrogels infused with Ppy across various $CaCl_2$ concentrations, key findings demonstrate the complex interaction between hydrogel composition and $CaCl_2$ in optimizing our samples. These findings highlight the critical need for precise adjustment of cross-linker concentrations to modify hydrogels for specific applications, balancing between enhancing mechanical strength and maintaining necessary flexibility. Ultimately, we saw that the 1:10 weight ratio with 10wt% $CaCl_2$ concentration provides the most optimal composition.

a

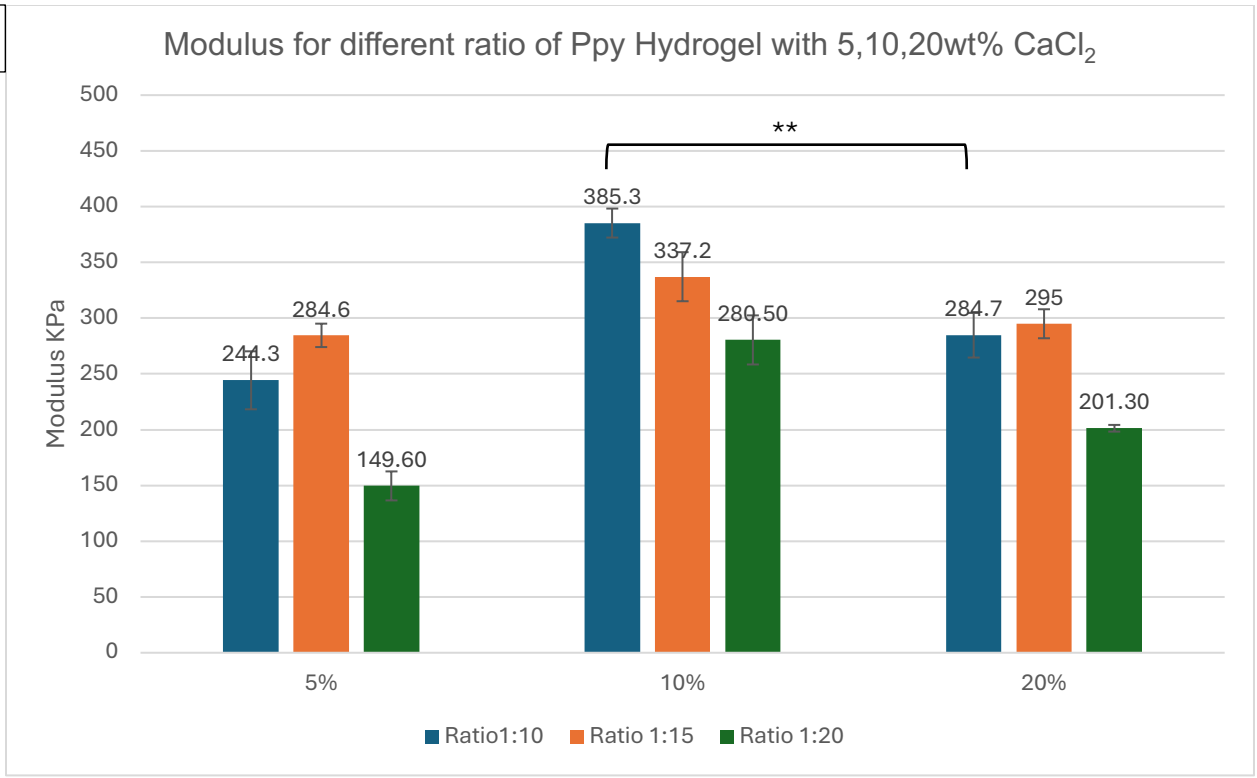
Modulus for different ratio of Ppy Hydrogel with 5,10,20wt% $CaCl_2$
Modulus KPa
500
450
400
350
300
250
200
150
100
50
0
**
385.3
337.2
280.50
284.7
295
201.30
284.6
244.3
149.60
5%
10%
20%
Ratio1:10
Ratio 1:15
Ratio 1:20

b

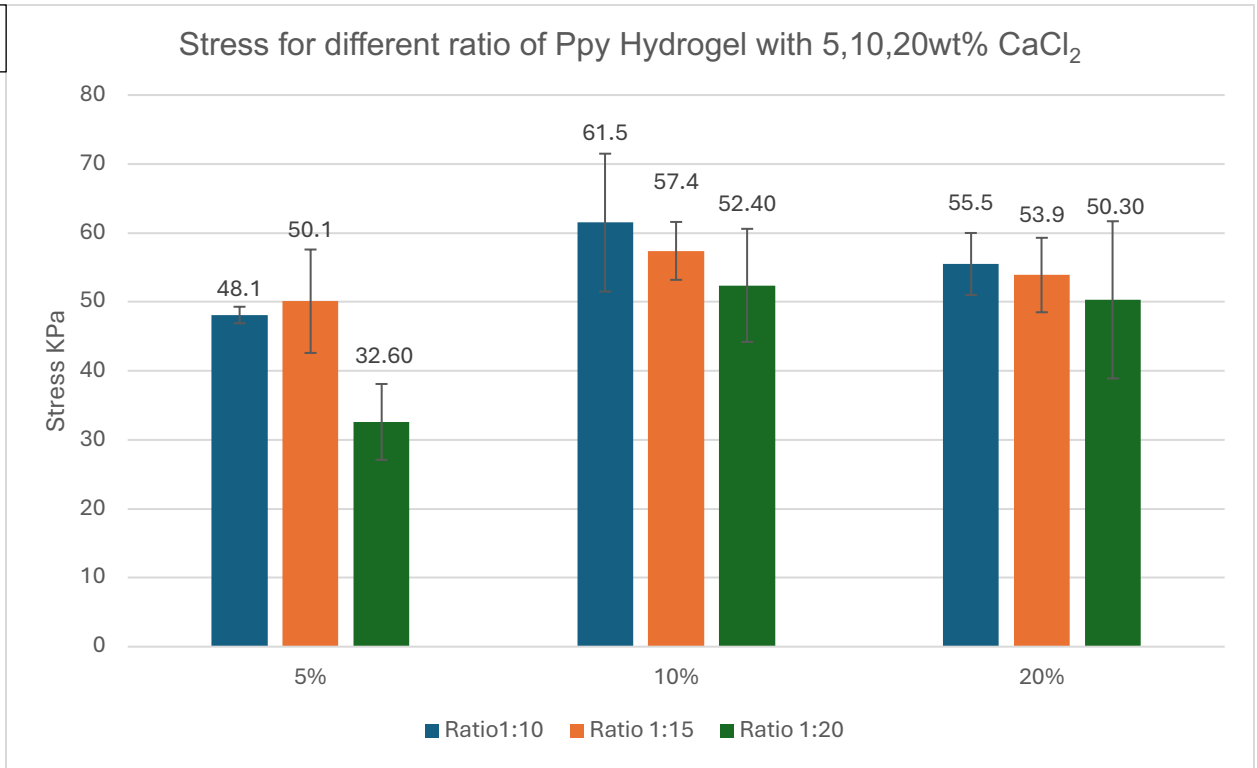
Stress for different ratio of Ppy Hydrogel with 5,10,20wt% $CaCl_2$
Stress KPa
80
70
60
50
40
30
20
10
0
61.5
57.4
52.40
55.5
53.9
50.30
50.1
48.1
32.60
5%
10%
20%
Ratio1:10
Ratio 1:15
Ratio 1:20

c

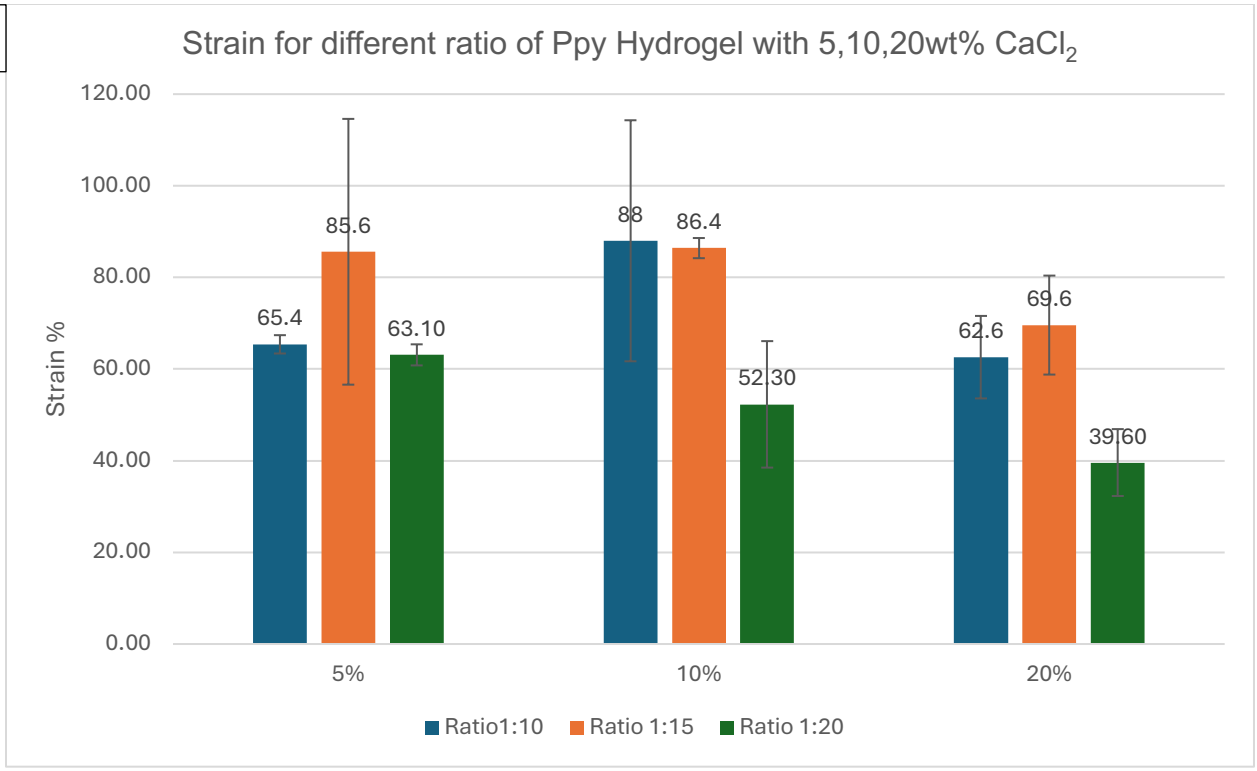

d

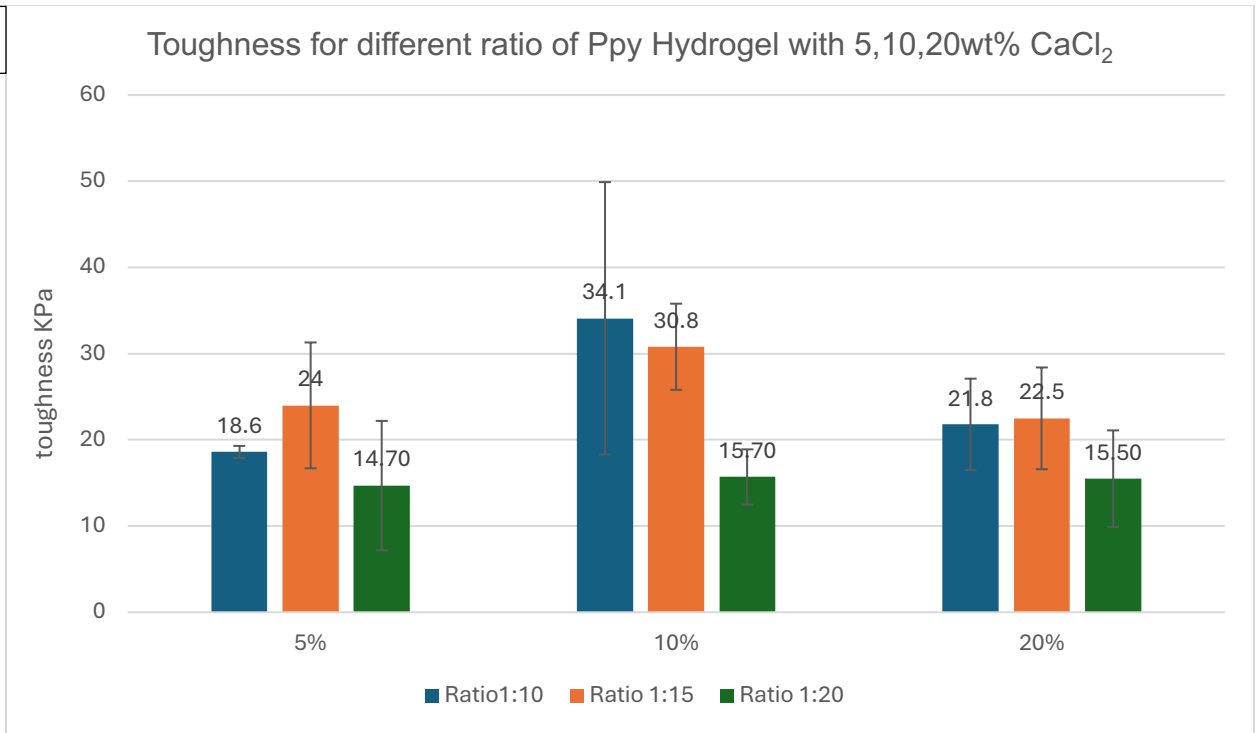

Figure 10. Bar graph of parameters of stress-strain curve for conductive hydrogels with Ppy, weight ratios of 1:10, 1:15, 1:20 of SA-PAM with 0wt%, 5wt%, 10wt% and 20wt% $CaCl_2$. a) module, b) stress, c) strain, d) area under the curve (toughness). Three samples were used to test for each experiment (n=3).

4.3.3 Comparison of tensile test between conductive and non-conductive samples

One of the most important differences between conductive and non- conductive was the absence of 0wt% $CaCl_2$ samples in experiments involving conductive polymers polypyrrole. This variance highlights importance of $CaCl_2$ as a cross-linking agent in stabilizing the hydrogel structure. In these hydrogels, $CaCl_2$ facilitates the formation of ionic bonds between polymer chains, which is essential for forming a coherent and stable gel matrix(155). The introduction of Ppy, known for its conductive properties and potential disruptive interactions with polymer chains, necessitates the presence of $CaCl_2$ to counterbalance these effects. Without $CaCl_2$, the polymer chains may fail to cross-link adequately, particularly due to the hydrophobic and rigid nature of Ppy, which can interfere with gel formation(159). Thus, we can conclude that $CaCl_2$ is important in ensuring that the conductive hydrogels not only form correctly but also maintain their structural integrity and functional properties, highlighting its pivotal role in the successful integration of conductive materials like Ppy into hydrogel systems.

When analyzing the mechanical properties of non-conductive hydrogels (Figure 8) and comparing them with conductive hydrogels containing Ppy (Figure 10), several distinct patterns and differences emerge, which are crucial for understanding the effect of Ppy on hydrogel behavior. Both types of hydrogels exhibit increased modulus and stress resistance with higher $CaCl_2$ concentrations. However, non-conductive hydrogels display less pronounced increases, suggesting the impact of Ppy on cross-linking and stiffness. In contrast, conductive hydrogels with Ppy show moderated increases especially at higher $CaCl_2$ concentration. Additionally, regarding the stress the conductive hydrogels have

lower tensile strength. These differences likely due to Ppy affecting the cross-linking efficiency and interfere with formation the ultimate stress resistance.

Furthermore, non-conductive hydrogels experience reduced strain with increasing $CaCl_2$ concentration. Whereas conductive hydrogels maintain higher initial strain levels across all concentrations, suggesting that Ppy provides enhanced elasticity, though this reduces with higher $CaCl_2$ concentrations. For toughness, non-conductive hydrogels exhibited improvement consistently with increase in $CaCl_2$ concentration, while conductive hydrogels exhibit fewer uniform enhancements. Through this analyzation we saw that the 1:10 weight ratio of PAM-SA hydrogel with 10wt% $CaCl_2$ provides the best formation.

4.4 Compression Test

Compression tests are performed to evaluate the mechanical properties of materials under compressive load, which is critical for understanding how they behave under forces that reduce their size. This information is essential for applications where the material will experience compressive stress, as it helps determine its strength, stiffness, and durability, ensuring it can withstand real-world conditions without failing.

4.4.1 Compression Test for Non-conductive Samples

Figure 11. represent the results of compression tests on SA-PAM hydrogel samples with varying concentrations of $CaCl_2$ and different weight polymer ratios. They illustrate the stress-strain behavior of each sample, providing insights into how different formulations affect the mechanical properties of our samples.

Figure 11a. illustrates the stress-strain behavior and mechanical properties of SA-PAM hydrogel with a 1:10 weight polymer ratio. The blue curve, representing 0wt% $CaCl_2$, shows a gradual increase in stress with strain, peaking at approximately 300 KPa at a strain of around 0.55 mm/mm. The initial slope of this curve indicates a lower modulus, suggesting that the hydrogel is less stiff. The green curve for 5wt% $CaCl_2$ demonstrates a more rapid increase in stress, achieving a peak of around 400 KPa at a strain of 0.6 mm/mm. This curve's steeper initial slope implies a higher modulus, meaning increased stiffness. Additionally, the red curve, corresponding to 10wt% $CaCl_2$, exhibits a significantly steeper rise, with stress of around 3 times more than 5wt% sample, peaking at approximately 1300 KPa at a strain of 0.75 mm/mm. This indicates the highest modulus and the greatest stiffness among the curves. The large area under the red curve denotes the highest toughness, indicating considerable energy absorption before failure. The black curve for 20wt% $CaCl_2$ shows a substantial initial increase in stress, peaking at about 800 KPa at a strain of around 0.6 mm/mm. Despite having a high modulus, the peak stress is lower than the red curve, indicating reduced toughness compared to the 10wt% $CaCl_2$ hydrogel.

Moreover, in Figure 11b. the samples with 1:15 weight polymer ratio follows same trend as Figure 11a. with an exception that none of the samples show mechanical strength of more than 500 KPa. With this said, the blue curve for 0wt% $CaCl_2$ reveals a slow initial stress increase, peaking at around 330 KPa at a strain of 0.7 mm/mm. This gentle initial slope suggests a lower modulus and stiffness, while the area under the curve indicates moderate toughness. The green curve for 5wt% $CaCl_2$ shows a more pronounced stress

increase, peaking at about 440 KPa at a strain of 0.55 mm/mm. The steeper initial slope compared to the blue curve suggests a higher modulus and increased stiffness, and the larger area under the curve reflects higher toughness. The red curve for 10wt% $CaCl_2$ indicates the steepest rise, with stress peaking at approximately 500 KPa at a strain of 0.5 mm/mm. This curve demonstrates the highest modulus and stiffness among the four, with substantial toughness due to the large area under the curve. The black curve for 20wt% $CaCl_2$, while showing a slightly lower peak stress than the red curve, maintains a high modulus due to its initial slope. The peak stress is around 470 KPa at a strain of 0.6 mm/mm, which is lower but not significantly than 10wt% ratio. The observed trend shows slightly different but overall close mechanical strength for samples with 10wt% and 20wt% $CaCl_2$, showing that increasing the ratio doesn't necessarily increase the strength of the hydrogel.

Figure 11c. illustrates the stress-strain behavior and mechanical properties for SA-PAM hydrogels with a 1:20 weight polymer ratio. The blue curve for 0wt% $CaCl_2$ shows a gradual stress increase, peaking at around 610 KPa at a strain of 0.78 mm/mm. The moderate initial slope suggests a higher modulus and stiffness compared to previous ratios. The green curve for 5wt% $CaCl_2$ demonstrates a less steep initial slope than the blue curve, peaking at approximately 430 KPa at a strain of 0.72 mm/mm, suggesting a slightly lower modulus and stiffness. However, the toughness remains greater due to addition of $CaCl_2$. Similar to Figure 11a. the red curve shows the highest modulus and stiffness as well as highest stress level of about 1230 KPa at a strain of 0.62 mm/mm. the sharp increase provides the largest area under the curve denoting the highest toughness

and energy absorption before failure. On the other hand, the black curve for 20wt% $CaCl_2$, despite its high modulus due to the initial slope, shows a peak stress of around 450 KPa at a strain of 0.55 mm/mm, which is less than 50% of the peak stress for the 10wt% $CaCl_2$ sample.

Across all three weight ratio samples of PAM-SA (1:10, 1:15, and 1:20), increasing the concentration of $CaCl_2$ consistently results in higher compressive stress tolerance, higher modulus, and increased toughness, although the relationship is not strictly linear for the 20wt% $CaCl_2$ concentration. The hydrogels' stiffness improves with higher $CaCl_2$ concentrations, enabling them to withstand greater compressive forces. However, the strain at which peak stress occurs tends to vary, indicating a complex interaction between the hydrogel composition and its mechanical properties. These observations underscore the significant influence of both $CaCl_2$ concentration and polymer ratio on the mechanical properties of SA-PAM hydrogels, with 10wt% $CaCl_2$ concentration generally showing enhanced stiffness and peak stress while also increasing the energy absorption capacity, reflecting better toughness.

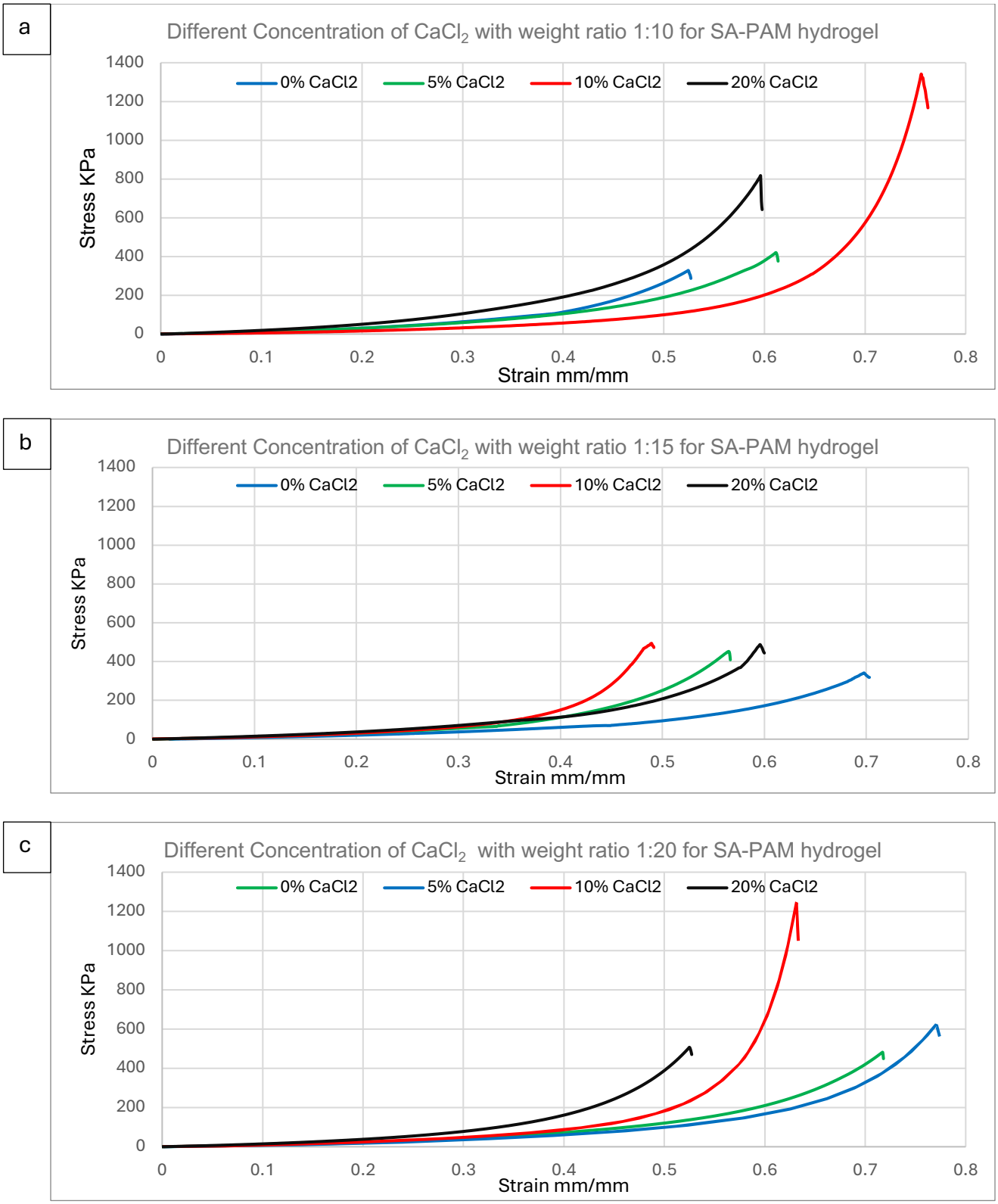

Figure 11. compression mechanical test for non-conductive hydrogel samples with various ratios with ,5wt%,10wt% and 20wt% concentration of $CaCl_2$. a) tensile test for 1:10 weight ratio of SA-PAM hydrogel, b) tensile test for 1:15 weight ratio of SA-PAM hydrogel, c) tensile test for 1:20 weight ratio of SA-PAM hydrogel.

Similar to the tensile test, we ran compression tests three times for each sample and the result of the average is shown on Figure 12, providing deeper insight into the mean value of each parameter of hydrogels with different weight polymer ratios (1:10, 1:15, and 1:20) across four concentrations of calcium chloride: 0wt%, 5wt%, 10wt%, and 20wt% to determine the applications for our samples.

Figure 12a. shows represent the modulus for our compression test comparison. At a 0wt% $CaCl_2$ concentration, the modulus values show a gradual increase with higher polymer ratios, going from 67 KPa for the 1:10 weight ratio to 78.5 KPa for the 1:20 ratio. This suggests that higher polymer concentrations without $CaCl_2$ slightly enhance stiffness, likely due to a denser polymer network that provides more resistance to deformation. Although the introduction of 5wt% $CaCl_2$ increases the stiffness, the significant difference is observed at 10wt% $CaCl_2$ concentration where 1:10 weight ratio is almost 3 times more than its 0wt% $CaCl_2$. Additionally, the peak of 178.9 KPa in 1:10 shows optimal stiffness compared to 134.1 KPa and 126.9 KPa for the 1:15 and 1:20 weight ratios, respectively. Notably, Statistical analysis also shows a significant difference for this ratio compared to the 1:15 weight ratio, with a p-value of 0.005. In contrast, when the $CaCl_2$ concentration is increased to 20wt%, the modulus values decrease compared to the 10wt% concentration. Specifically, the modulus is 106.5 KPa for the 1:10 ratio, 134.6 KPa for the 1:15 weight ratio, and 95.4 KPa for the 1:20 weight ratio. This suggests that an excessive amount of $CaCl_2$ may lead to over-crosslinking, reducing the hydrogel's stiffness.

Figure 12b. is responsible for visualization of stress responses for our samples. At 0wt% $CaCl_2$, the stress values increase moderately with higher polymer ratios. The stress is 361 KPa for the 1:10 ratio, 329.6 KPa for the 1:15 ratio, and peaks at 456.1 KPa for the 1:20 weight ratio. Moreover, the same pattern is showing in 5wt% $CaCl_2$ compared to 0wt% while being moderately higher than 0wt% $CaCl_2$, with the 1:20 weight ratio again demonstrating the highest stress at 570.1 KPa. This trend suggests no significant difference between them. On the other hand, the effect of $CaCl_2$ becomes more pronounced at a 10wt% concentration. Similar to Figure 12a. the hydrogel with a 1:10 weight polymer ratio exhibits a remarkably high stress of 1514.1 KPa, almost three times greater than its counterpart at 0wt% $CaCl_2$. This intense increase highlights the fundamental role of $CaCl_2$ in optimizing the cross-link density, which significantly strengthens the hydrogel. However, at 20wt% $CaCl_2$, stress values decrease across all ratios with highest being 778.7 KPa for the 1:10 weight ratio, indicating potential over-cross linking that reduces mechanical integrity.

Figure 12.c Provides comprehensive analysis of strain percentage. At a 0wt% $CaCl_2$ concentration, there is progressive increase in values with higher polymer ratios. Specifically, the strain rises from 57.8% at the 1:10 ratio to 66.5% at the 1:20 weight ratio. This trend suggests that higher polymer concentrations enhance the hydrogel's flexibility and deformability. Furthermore, adding 5wt% $CaCl_2$ leads to a slight increase in strain values across all polymer ratios. The 1:20 weight ratio exhibits the highest strain at 64.5%, while the 1:10 and 1:15 weight ratios show 61% and 60.8%, respectively. The differences between the ratios are less pronounced than at 0wt% $CaCl_2$, indicating that the addition

of $CaCl_2$ maintains the hydrogel's flexibility while providing moderate cross-linking that enhances structural integrity. At a 10wt% $CaCl_2$ concentration, the strain values peak significantly, particularly for the 1:10 weight ratio, which reaches 75.9%. The 1:20 weight ratio also shows high strain at 71.5%, while the 1:15 ratio decreases to 57.7%. These results suggest that at 10wt% $CaCl_2$, hydrogels with the 1:10 and 1:20 weight polymer ratios achieve an optimal balance between cross-linking and flexibility. Similar to Figure 12b. increasing $CaCl_2$ to 20wt% results in a decrease in strain values compared to the 10wt% concentration. The strain values are relatively uniform across ratios, with a slight peak of 63.7% at the 1:15 weight ratio. This decline verify reduction in hydrogel's flexibility and elasticity.

The last section Figure 12d. presents the toughness for our samples. Even though, 5wt% show relatively higher value than 0wt% they are not significantly different. For example, the 1:15 weight ratio goes from 47.1 KJ/M^3 to 53.4 KJ/M^3 for 5wt% $CaCl_2$ with p value 0.38. Additionally, at a 10wt% $CaCl_2$ concentration, the toughness peaks significantly for the 1:10 weight ratio, reaching 145.8 KJ/M^3. This dramatic increase highlights the effectiveness of $CaCl_2$ in optimizing cross-link density, substantially improving the hydrogel's toughness. notably, the 1:20 ratio also shows considerable toughness at 86.6 KJ/M^3, while the 1:15 ratio decreases to 51.5 KJ/M^3. Increasing the $CaCl_2$ concentration to 20wt% results in a decrease in toughness values compared to the 10wt% concentration. The 1:10 weight ratio maintains a relatively high toughness of 95.6 KJ/M^3, while the 1:15 and 1:20 weight ratios show reduced values of 71.1 KJ/M^3 and 62.1 KJ/M^3, respectively. Similar to other 20wt% values for Figure 12a, b, and c. this decrease

suggests that excessive $CaCl_2$ may lead to over-crosslinking, which reduces the material's ability to absorb energy efficiently.

a

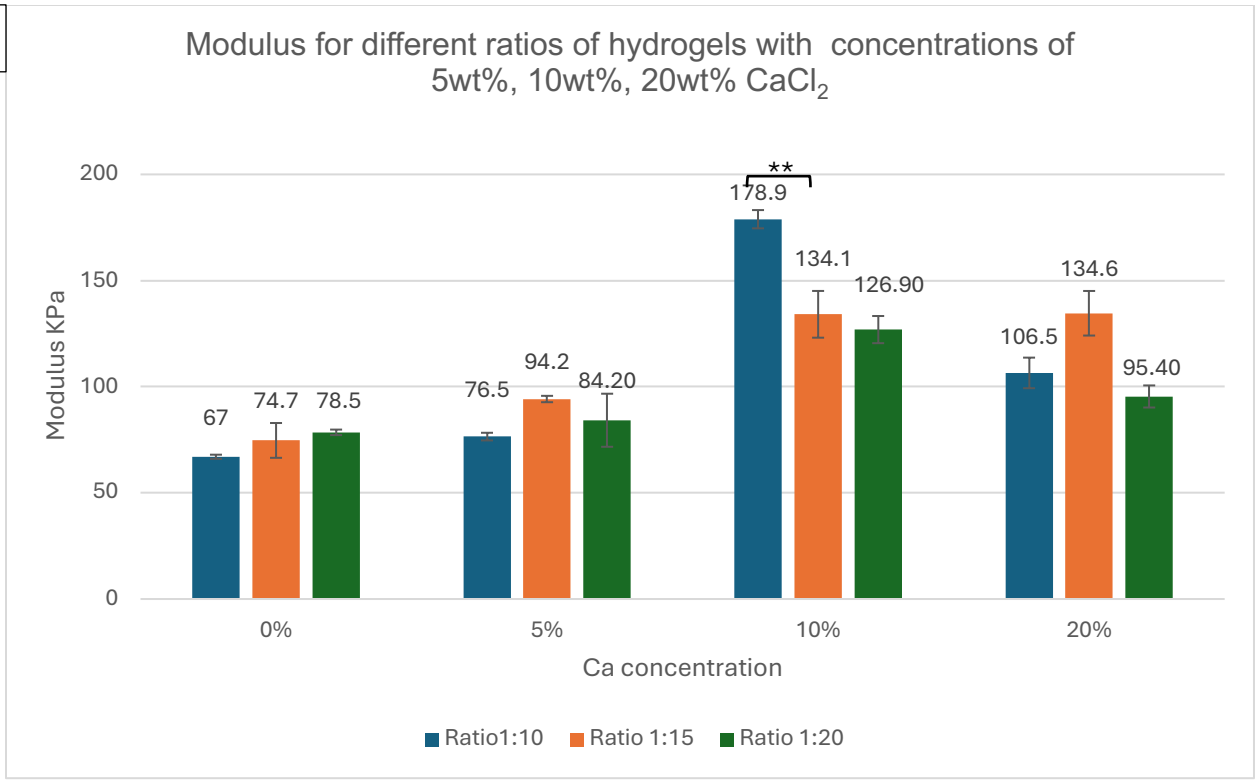
Modulus for different ratios of hydrogels with concentrations of 5wt%, 10wt%, 20wt% CaCl2
Modulus KPa
200
150
100
50
0
**
178.9
134.1
126.90
106.5
134.6
95.40
94.2
84.20
76.5
67
74.7
78.5
0%
5%
10%
20%
Ca concentration
Ratio1:10
Ratio 1:15
Ratio 1:20

b

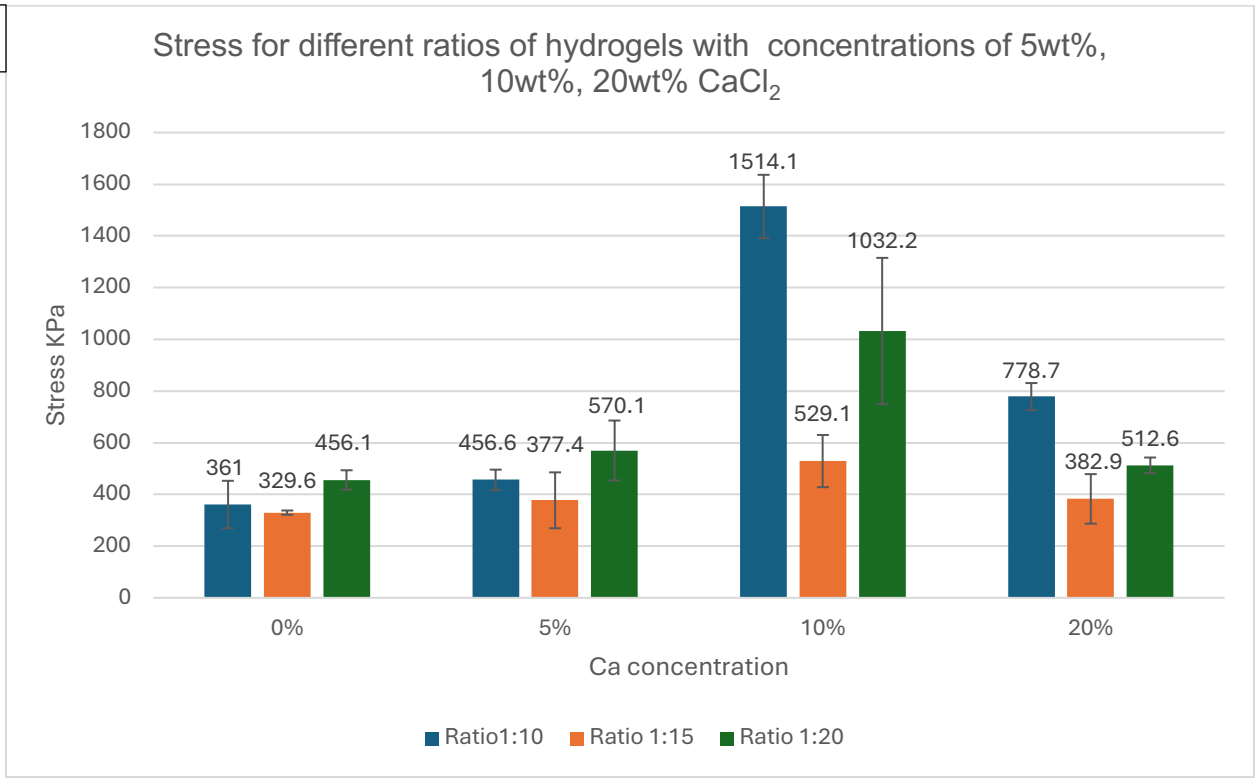
Stress for different ratios of hydrogels with concentrations of 5wt%, 10wt%, 20wt% CaCl2
Stress KPa
1800
1600
1400
1200
1000
800
600
400
200
0
1514.1
1032.2
529.1
778.7
382.9
512.6
570.1
456.6
377.4
456.1
361
329.6
0%
5%
10%
20%
Ca concentration
Ratio1:10
Ratio 1:15
Ratio 1:20

c

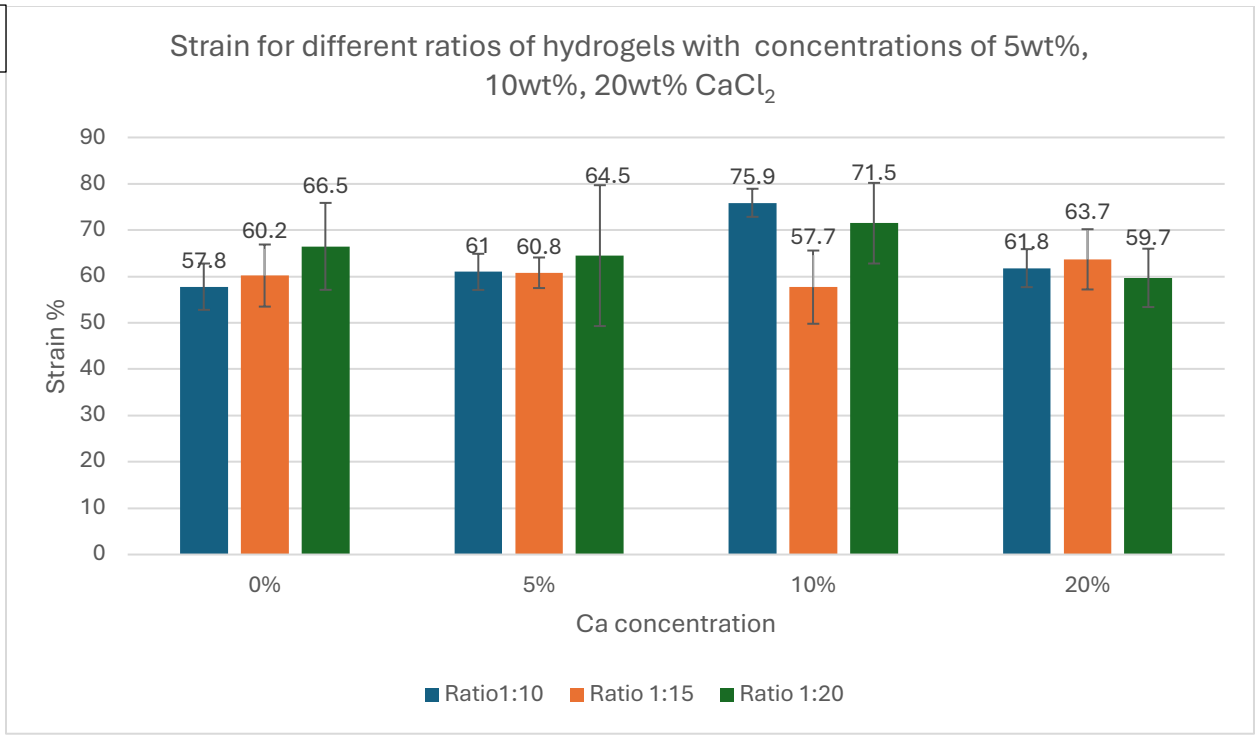

d

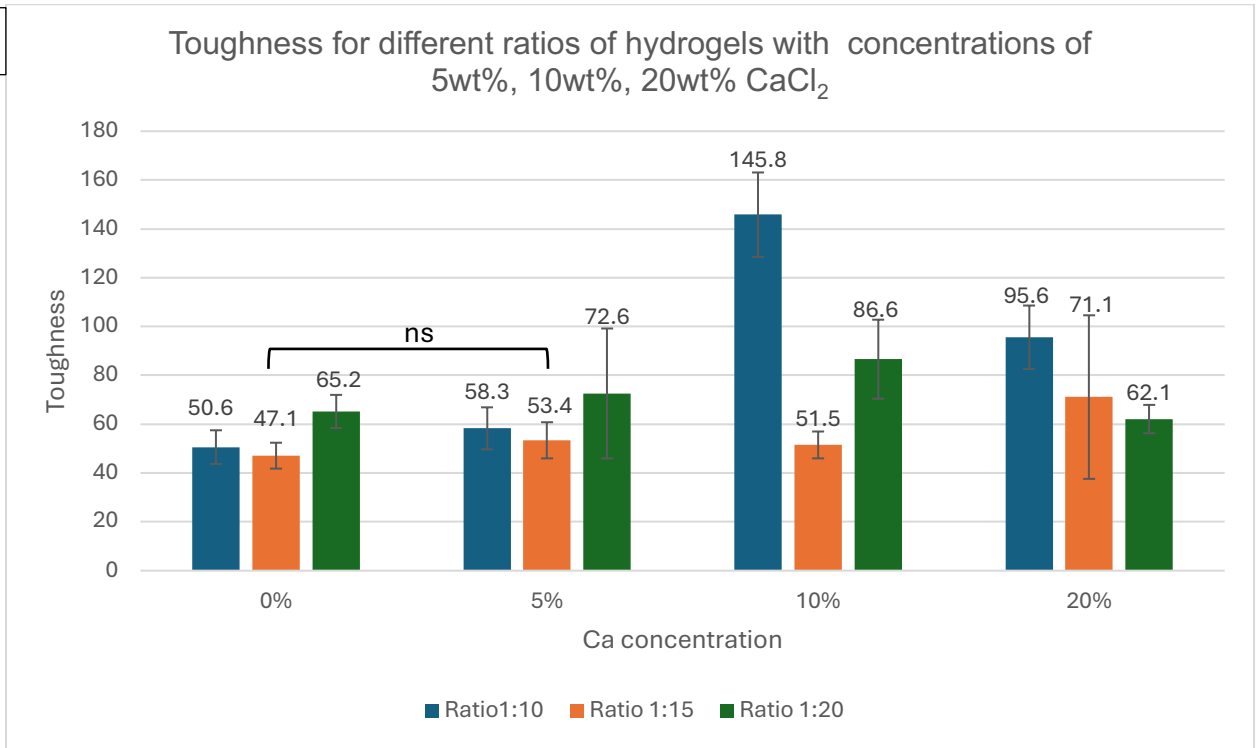

Figure 12. Bar graph of parameters of stress-strain curve for non- conductive hydrogels for compression test, weight ratios of 1:10, 1:15, 1:20 of SA-PAM with 0wt%, 5wt%, 10wt% and 20wt% $CaCl_2$. a) module, b) stress, c) strain, d) area under the curve (toughness). Three samples was used to test for each experiment (n=3).

4.4.2 Conductive hydrogels

Conductive hydrogels, such as those incorporating polypyrrole (PPY), offer a unique combination of electrical conductivity and mechanical flexibility, in this section we are looking at the conductive samples and their behaviour under 5wt%, 10wt% and 15wt% $CaCl_2$ condition with various (weight) polymer ratios.

Figure 13 illustrates the stress-strain behavior of SA-PAM hydrogels with a varying polymer ratio and conductive material Ppy at different $CaCl_2$ concentrations. Figure 13.a is responsible for conductive hydrogels with 1:10 weight polymer ratio, the 5wt% $CaCl_2$ hydrogel (green curve) shows a gradual increase in stress, peaking at 600 KPa at a strain of 0.8 mm/mm, indicating moderate modulus and toughness. In comparison, the 10wt% $CaCl_2$ hydrogel (red curve) peaks at 1050 KPa at a strain of 0.7 mm/mm, demonstrating higher modulus, stiffness, and toughness. The 20wt% $CaCl_2$ hydrogel (black curve) peaks at 950 KPa at a strain of 0.6 mm/mm, suggesting that although a higher $CaCl_2$ concentration increases stress strength, beyond a certain limit it becomes brittle and cannot withstand higher strains.

Figure 13b illustrates the stress-strain behavior of PPY-SA-PAM hydrogels with a 1:15 weight polymer ratio. The 5wt% $CaCl_2$ hydrogel reaches a peak stress of around 700 KPa at a strain of 0.8 mm/mm, indicating a moderate modulus and toughness. The 10wt% $CaCl_2$ hydrogel (red curve) and the 20wt% $CaCl_2$ hydrogel (black curve) show similar peak stresses, with the 10wt% hydrogel peaking at 700 KPa and the 20wt% hydrogel at 800 KPa. However, they occur at different strains of 0.75 mm/mm and 0.65 mm/mm,

respectively, suggesting that the 10wt% $CaCl_2$ concentration provides stiffer and tougher hydrogels. Similarly, in Figure 13c, the 10wt% $CaCl_2$ hydrogel (red curve) and the 20wt% $CaCl_2$ hydrogel (black curve) show relatively close peak stress values of around 700 KPa. However, the 10wt% $CaCl_2$ hydrogel demonstrates higher modulus and toughness, as indicated by a larger strain of 0.8 mm/mm.

The analysis of the stress-strain behavior for SA-PAM hydrogels with conductive material PPY across different $CaCl_2$ concentrations and weight polymer ratios (1:10, 1:15, and 1:20) reveals that increasing $CaCl_2$ concentration enhances the mechanical properties of the hydrogels, with the 10wt% $CaCl_2$ concentrations providing the best balance of strength and durability across different polymer ratios. These findings underscore the importance of optimizing $CaCl_2$ concentration and polymer ratio to tailor the mechanical performance of conductive hydrogels for specific applications.

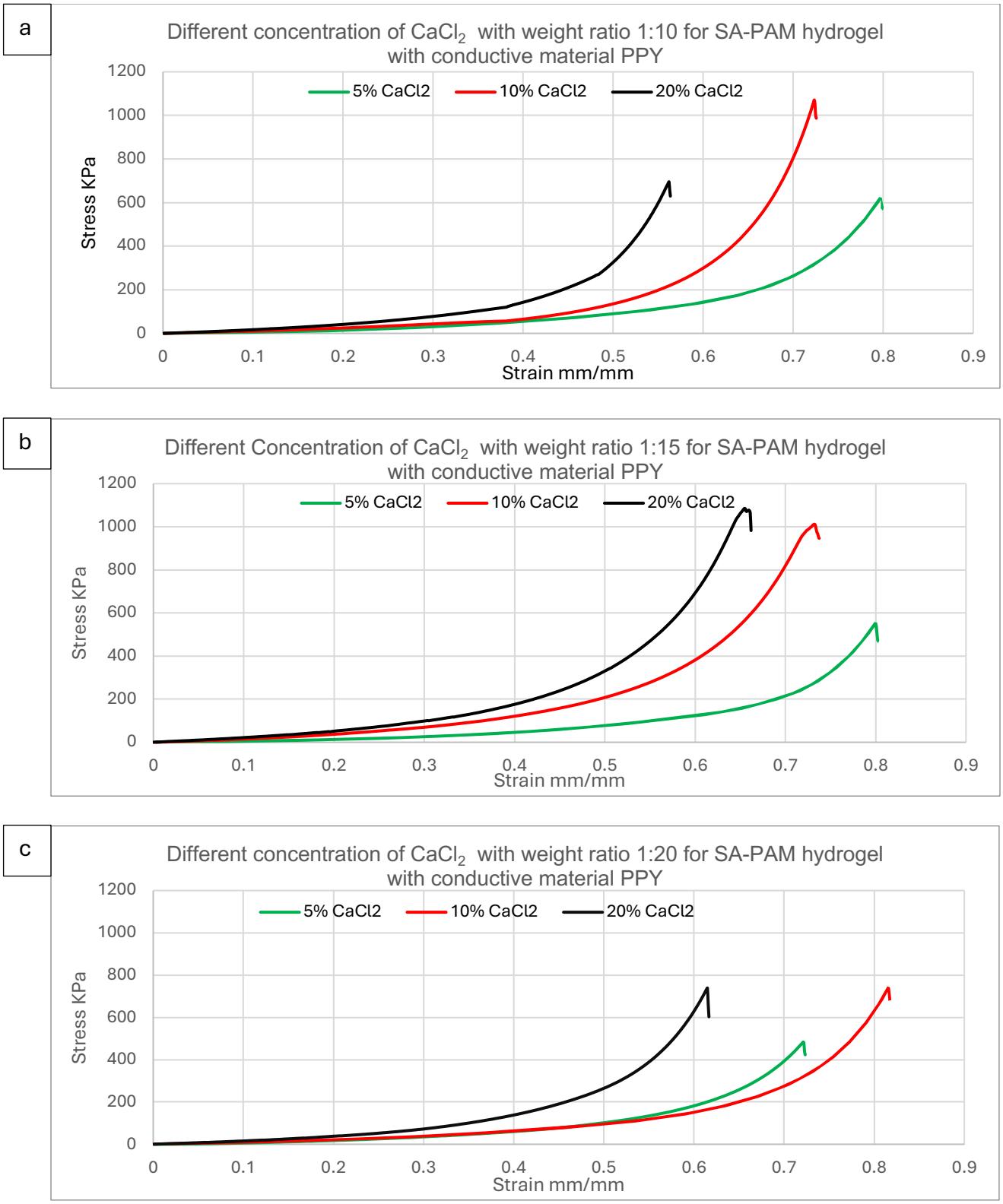

Figure 13. Compression test for conductive hydrogel samples with various ratios with ,5wt%,10wt% and 20wt% concentration of $CaCl_2$. a) tensile test for 1:10 weight ratio of PPY-SA-PAM hydrogel, b) tensile test for 1:15 weight ratio of PPY-SA-PAM hydrogel, c) tensile test for 1:20 weight ratio

Figure 14 provides insight and comparison regarding average of the modulus, stress, strain and toughness of three separate tests for our conductive Ppy hydrogels at $CaCl_2$ concentrations of 5wt%, 10wt%, and 20wt% across weight polymer ratios of 1:10, 1:15, and 1:20.

Figure 14a assesses the modulus of conductive polypyrrole (Ppy) hydrogels. At 5wt% $CaCl_2$, the modulus is highest at 120.10 KPa for the 1:10 weight ratio, suggesting effective initial cross-linking. For the 1:15 and 1:20 weight ratios, the modulus drops to 84.3 KPa and 112.20 KPa, respectively, indicating varied cross-linking efficiency at different polymer concentrations. Additionally, the 10wt% $CaCl_2$ level shows a uniform and optimal increase in modulus across all weight ratios with 234.20 KPa at 1:10, 230.1 KPa at 1:15, and 231.80 KPa at 1:20, indicating a saturated cross-linking effect on stiffness. Similarly, the pattern continues for 20wt% $CaCl_2$ where all the ratio values increased from 10wt% $CaCl_2$, while the modulus decreased 7 KPa for the 1:20 weight ratio. These changes indicate the effect of the $CaCl_2$ in the hydrogel.

Moreover, Figure 14b. represents the stress behaviour of our samples. Similar to Figure 14a, at 5wt% $CaCl_2$, stress is highest for the 1:10 weight ratio at 576.10 KPa. This peak suggests that lower polymer ratios optimize $CaCl_2$ utilization for cross-linking, thereby enhancing strength. Stress decreases with increasing polymer content, with the 1:20 weight ratio recording the lowest at 500.70 KPa, indicating a potential reduced cross-linking efficiency. Furthermore, a significant increase in stress values is observed at 10wt% $CaCl_2$, peaking at 1092.30 KPa for the 1:10 weight ratio. This indicates that a

moderate level of $CaCl_2$ maximizes cross-link density and mechanical strength. However, stress values decline progressively in higher polymer ratios, with the 1:15 and 1:20 weight ratio showing 882.9 and 824.30 KPa respectively. suggesting less effective use of 10wt% $CaCl_2$ in denser hydrogel networks. Interestingly, at 20wt% $CaCl_2$, there is a reduction in stress across all ratios compared to 10wt% $CaCl_2$, with the 1:15 weight ratio highest at 837.8 KPa. However, the p – value of 0.2 verifies no significant difference between 1:10 and 1:15 weight ratio in here. Overall, similar to other 20wt% graphs this decrease may reflect over-crosslinking, which can lead to brittleness and diminished ability to sustain high stress.

Figure 14c. analyzes the strain responses of conductive polypyrrole (Ppy) hydrogels. The 5wt% $CaCl_2$ concentration shows the highest strain observed in the 1:15 weight ratio at 79.1%, suggesting an optimal balance of polymer concentration and cross-linking that enhances flexibility. The 1:10 and 1:20 weight ratios also, exhibit lower strains at 73.33% and 71.30%, respectively. With a 10wt% $CaCl_2$ concentration, there is a noticeable decrease in strain across all ratios, for example, the 1:10 weight ratio decreased from 73.33% in 5 wt% CaCl2 to 69.50% in here. This reduction suggests that increasing $CaCl_2$ concentration enhances stiffness, thereby marginally reducing hydrogel flexibility. Similar trend can be observed for 20wt% $CaCl_2$, where strain values across the ratios become more uniform but generally lower compared to 5wt% $CaCl_2$ concentrations, highlighting the effects of over-cross-linking which sacrifice the flexibility for stiffness. Notably, there is no significant difference across all the concentrations in our samples with no p- value

smaller than 0.05, showing the effect of the Ppy with $CaCl_2$ maintaining relatively adequate strain for our samples.

Figure 14d examines the toughness of our samples. At a 5wt% $CaCl_2$ concentration, the toughness is highest for the 1:10 weight ratio at 81.96 KJ/M^3, indicating effective utilization of $CaCl_2$ for cross-linking at lower polymer ratios. As the polymer ratio increases, there is a decline in toughness, with the 1:20 weight ratio showing 69.50 KJ/M^3, suggesting reduced cross-linking efficiency with increased polymer content. When the $CaCl_2$ concentration increases to 10wt%, the toughness values shift, with the 1:15 weight ratio now showing the highest toughness at 127.4 KJ/M^3, surpassing the 1:10 weight ratio which registers at 111.6 KJ/M^3, and the 1:20 weight ratio at 103.8 KJ/M^3. However, this increase is still not significant as the statistical data provide the p- value of 0.32. Increasing the $CaCl_2$ concentration further to 20wt% leads to a general decrease in toughness for the 1:10 weight ratio being significantly lower than 10wt% $CaCl_2$, now at 69.7 KJ/M^3, with p value of 0.01. this sharp decrease denotes potential over-cross linking that may compromise the material's ability to absorb energy. On the other hand, the 1:15 and 1:20 weight ratios show higher toughness values at 116.7 KJ/M^3 and 91.7 KJ/M^3, respectively, suggesting that higher weight polymer ratios may mitigate the brittleness associated with excessive cross-linking at this concentration.

Overall, conductive polypyrrole (Ppy) hydrogels show optimal mechanical properties at a 10wt% $CaCl_2$ concentration, balancing strength and flexibility. Decreasing $CaCl_2$

concentration to 5wt% or increasing to 20wt% leads to variable properties underscoring the need for careful calibration of $CaCl_2$ levels in hydrogel design.

a

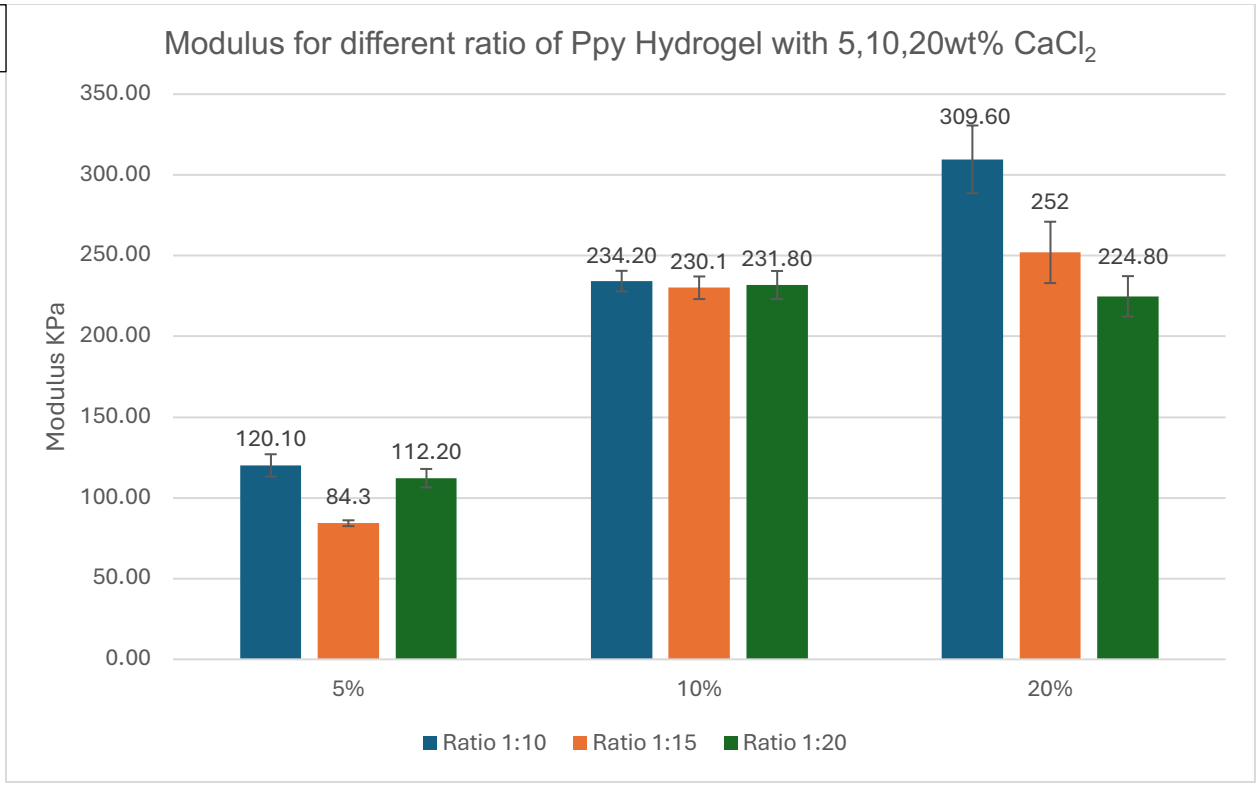
Modulus for different ratio of Ppy Hydrogel with 5,10,20wt% $CaCl_2$
Modulus KPa
350.00
300.00
250.00
200.00
150.00
100.00
50.00
0.00
120.10
84.3
112.20
234.20
230.1
231.80
309.60
252
224.80
5%
10%
20%
Ratio 1:10
Ratio 1:15
Ratio 1:20

b

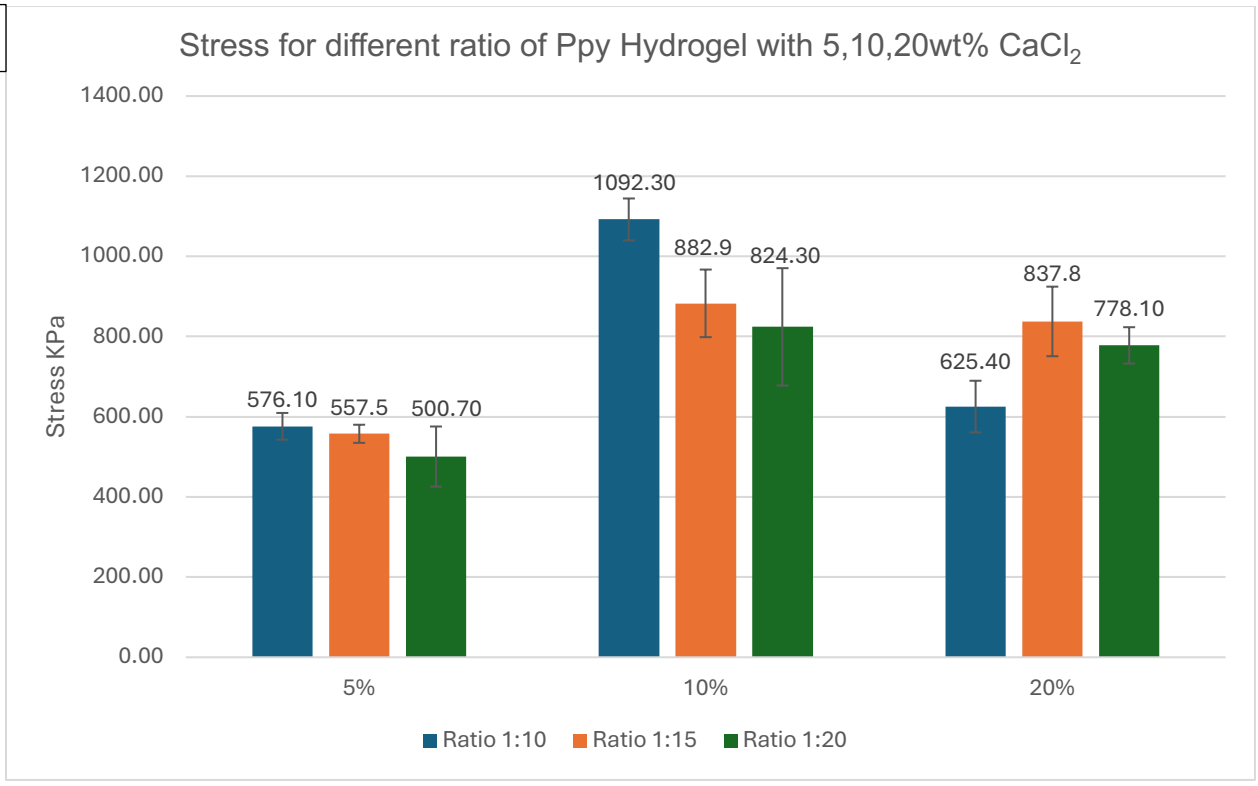
Stress for different ratio of Ppy Hydrogel with 5,10,20wt% $CaCl_2$
Stress KPa
1400.00
1200.00
1000.00
800.00
600.00
400.00
200.00
0.00
576.10
557.5
500.70
1092.30
882.9
824.30
625.40
837.8
778.10
5%
10%
20%
Ratio 1:10
Ratio 1:15
Ratio 1:20

c

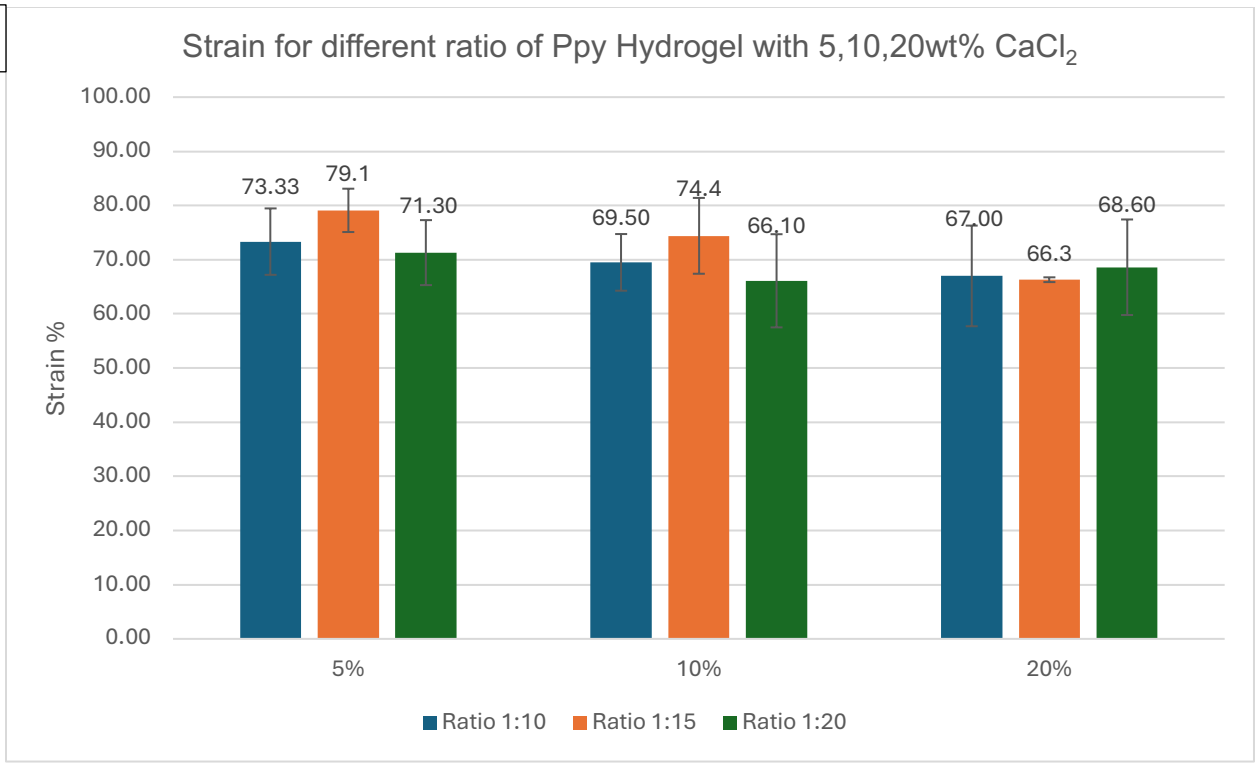

d

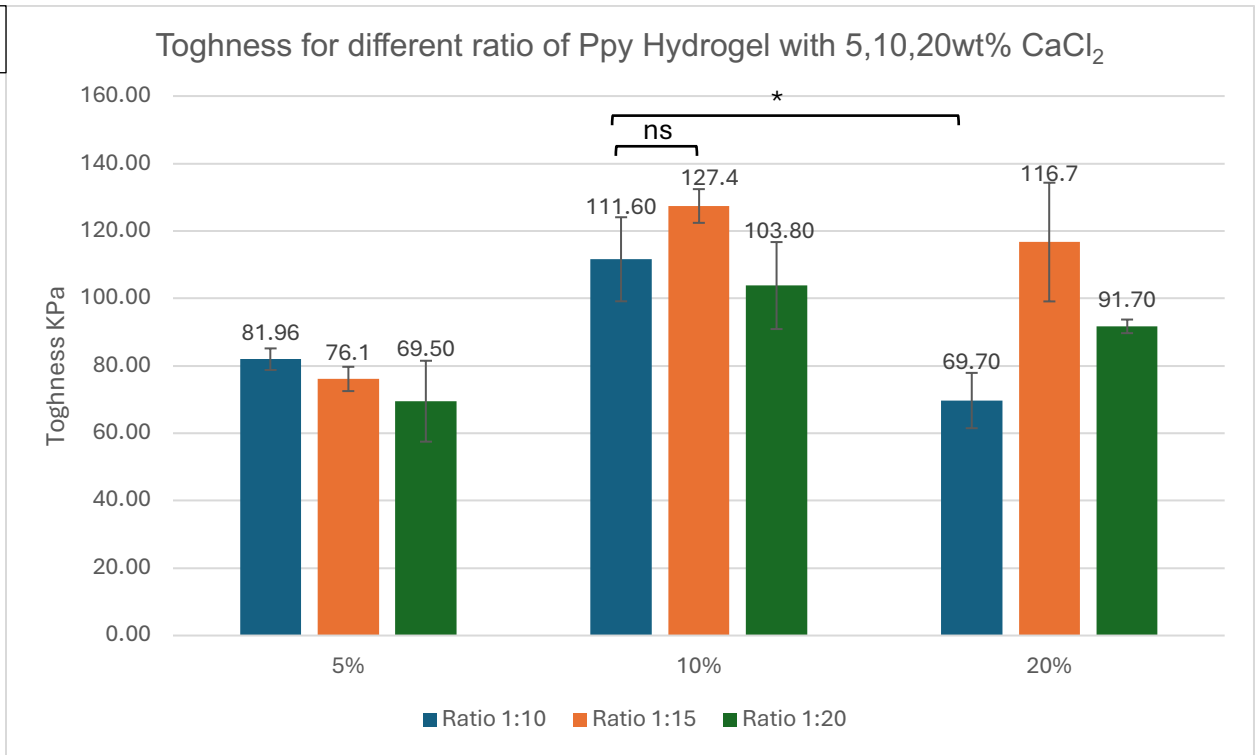

Figure 14. Bar graph for compression test of parameters of stress-strain curve for conductive hydrogels with Ppy, weight ratios of 1:10, 1:15, 1:20 of SA-PAM with 0wt%, 5wt%, 10wt% and 20wt% $CaCl_2$. a) module, b) stress, c) strain, d) area under the curve (toughness). Three samples were used to test for each experiment (n=3).

4.4.3 Comparison of compression test between conductive and non-conductive samples

The analysis of Figures 12 and 14 reveals distinct mechanical behaviors between non-conductive hydrogels (Figure 12) and their conductive counterparts (Figure 14) across a range of weight polymer ratios and $CaCl_2$ concentrations. This comparative study highlights the impact of conductivity on the material properties of hydrogels, underscoring the role of polymer composition in defining hydrogel functionality.

By observing modulus, conductive hydrogels tend to exhibit higher moduli at equivalent concentrations and ratios, suggesting that the incorporation of Ppy contributes to a stiffer matrix. This can be attributed to the inherent properties of Ppy, which might foster denser cross-linking networks or introduce additional physical interactions between polymer chains. Non-conductive hydrogels, while versatile, generally show lower modulus values, indicating potentially fewer rigid networks which could be advantageous in applications requiring higher flexibility. Moreover, while conductive hydrogels demonstrate enhanced modulus, the stress resistance comparison between Figures 12b and 14b reveals a more complex interaction. For example, at 10wt% $CaCl_2$, the 1:10 weight ratio in both non-conductive and conductive hydrogels exhibit exceptionally high stress values. This indicates the optimalization of this hydrogel in achieving comparable or superior stress resistance under certain conditions, verifying the notion that conductivity uniformly enhances mechanical strength as well.

Strain analysis presents a more nuanced picture. Conductive hydrogels display a varied strain profile, with some formulations showing comparable or slightly reduced elasticity compared to non-conductive hydrogels. This can be interpreted as a trade-off between enhanced mechanical properties (such as increased toughness and stress capacity) and the flexibility to extend without breaking. Non-conductive hydrogels generally maintain higher or more consistent strain percentages, beneficial for applications necessitating extensive material deformation. Furthermore, in terms of toughness, Figures 12d and 14d show that non-conductive hydrogels occasionally outperform conductive ones, particularly in higher polymer ratios at certain $CaCl_2$ concentrations. This could suggest that while conductivity generally enhances structural integrity, the specific formulation and cross-linking density crucially influence the overall energy absorption capacity without a straightforward advantage conferred by conductivity.

In summary, the introduction of conductivity into hydrogel formulations notably enhances certain mechanical properties like modulus, stress capacity, and toughness but may slightly compromise elasticity. This comparative insight is crucial for tailoring hydrogel properties to specific applications, where the choice between conductive and non-conductive materials must align with the operational demands of the end-use scenario, balancing between strength, stiffness, and flexibility. It is also noteworthy to mention, the 1:10 weight polymer ratio with 10wt% $CaCl_2$ concentration emerges as the best-performing sample, demonstrating an optimal balance of mechanical properties in both tensile and compression analyses, which highlights its potential as a superior choice for applications requiring robust strength and durability in hydrogel formulations.

4.5 Rheology characterization

Rheology test was performed to analyze the properties our hydrogels, confirming their successful synthesis and determining their suitability for specific applications. This testing helps in understanding how these materials behave under stress and strain, crucial for ensuring their performance in real-world conditions. Figure 15 presents rheological data for non-conductive PAM-SA hydrogels under various concentrations of $CaCl_2$, Figure 15a, b and c are responsible for 1:10, 1:15 and 1:20 weight polymer ratio respectively. Similarly Figure 16 illustrates the rheological behaviour for conductive PPY-PAM-SA hydrogels where Figure 16a, b and c are responsible for 1:10, 1:15 and 1:20 weight ratios of PAM and SA.

Rheological analysis demonstrated that both types of hydrogels exhibit stable storage (G') and loss (G") moduli across various frequencies, with the storage modulus consistently higher than the loss modulus. This stability indicates robust hydrogel formation capable of maintaining structural integrity under dynamic mechanical stresses. Notably, increasing concentrations of $CaCl_2$ led to enhanced G' and G", suggesting stronger ionic cross-linking within the hydrogel networks. The conductive hydrogels showed more pronounced improvements, likely due to the structural augmentation from the polypyrrole (PPY. To be more specific, the 1:10 weight polymer ratio consistently showed the highest values of G' and G", reflecting an optimal polymer and filler distribution that maximizes the mechanical and electrical properties of the hydrogel. Overall, these results confirm the efficacy of the mechanical properties observed in testing, underscoring the hydrogels' potential for tailored applications.

a

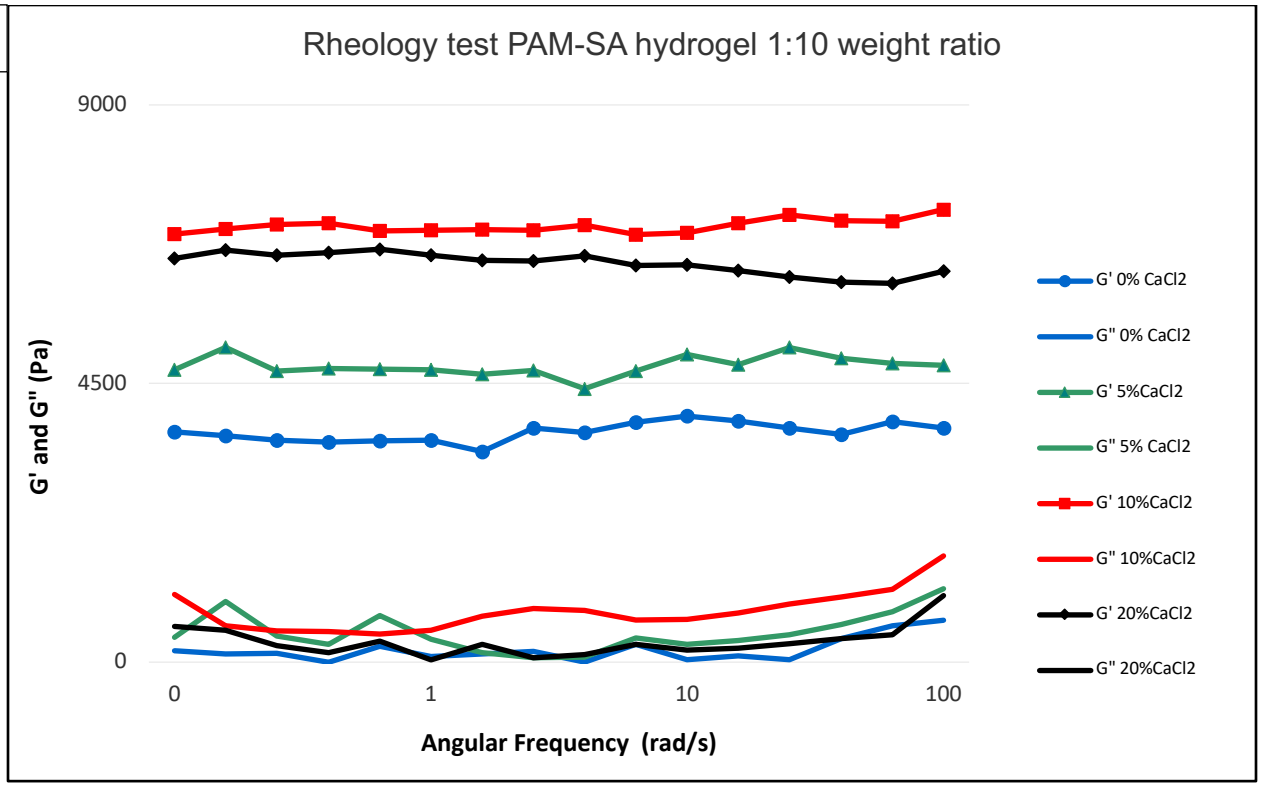
Rheology test PAM-SA hydrogel 1:10 weight ratio
9000
4500
0
G' and G" (Pa)
0
1
10
100
Angular Frequency (rad/s)
G' 0% CaCl2
G" 0% CaCl2
G' 5%CaCl2
G" 5% CaCl2
G' 10%CaCl2
G" 10%CaCl2
G' 20%CaCl2
G" 20%CaCl2

b

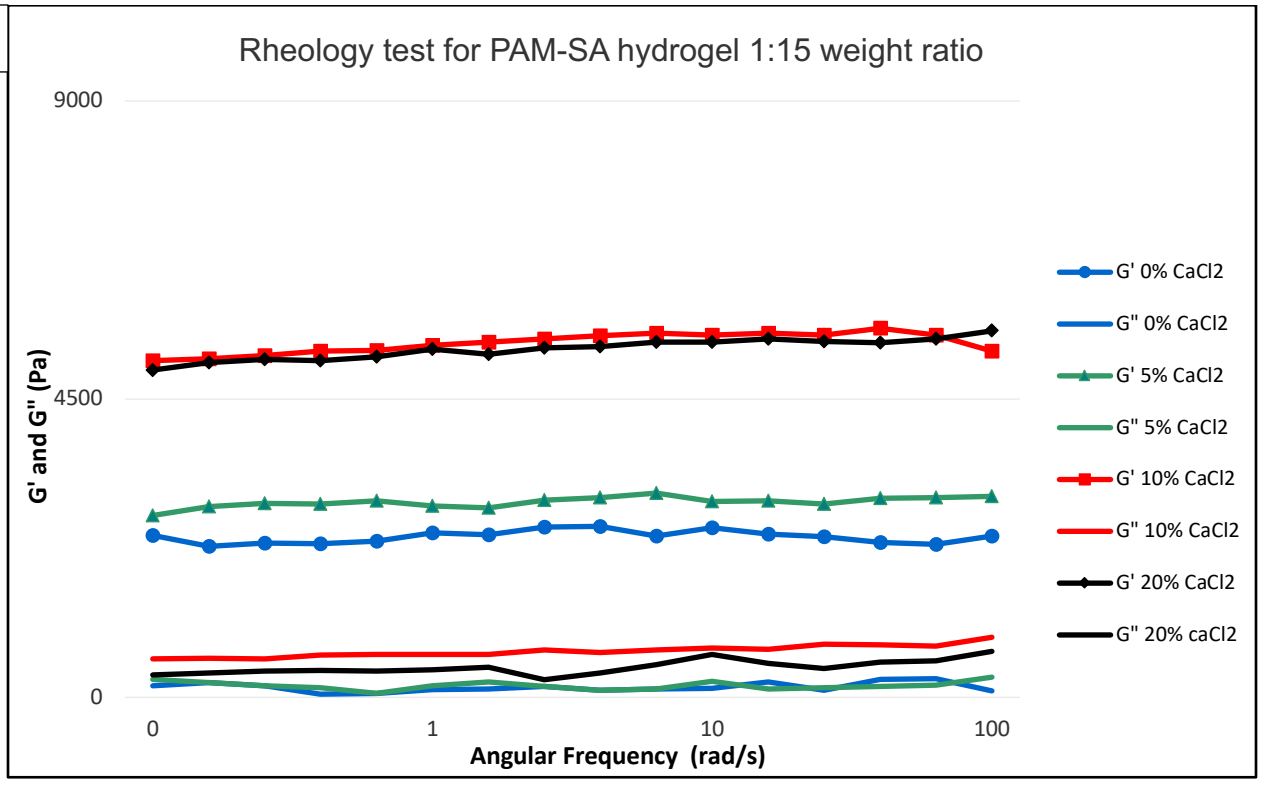
Rheology test for PAM-SA hydrogel 1:15 weight ratio
9000
4500
0
G' and G" (Pa)
0
1
10
100
Angular Frequency (rad/s)
G' 0% CaCl2
G" 0% CaCl2
G' 5% CaCl2
G" 5% CaCl2
G' 10% CaCl2
G" 10% CaCl2
G' 20% CaCl2
G" 20% caCl2

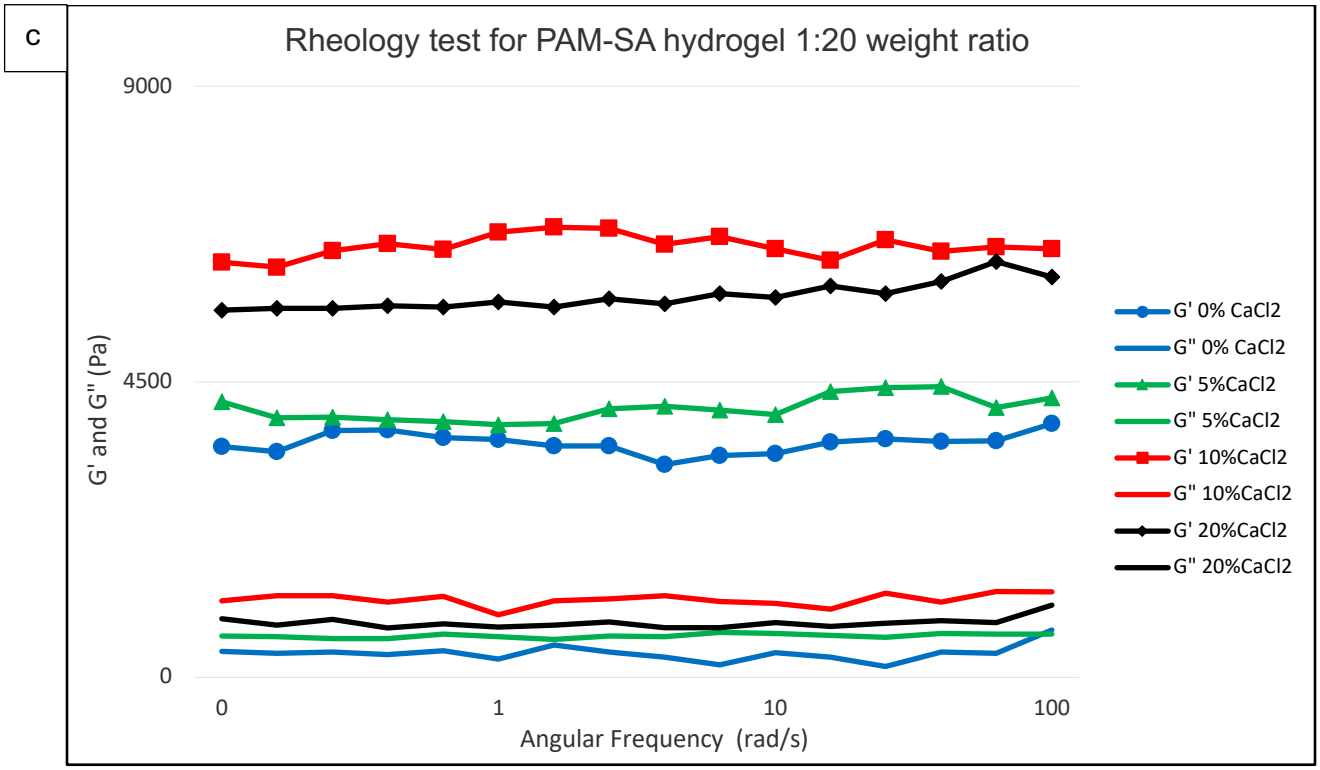

Figure 15. rheology performance test for non-conductive samples under 0wt%, 5wt%, 10wt% and 20wt% $CaCl_2$. a) 1:10 SA-PAM polymer ratio, b) 1:15 SA-PAM polymer ratio, c) 1:20 SA-PAM polymer ratio.

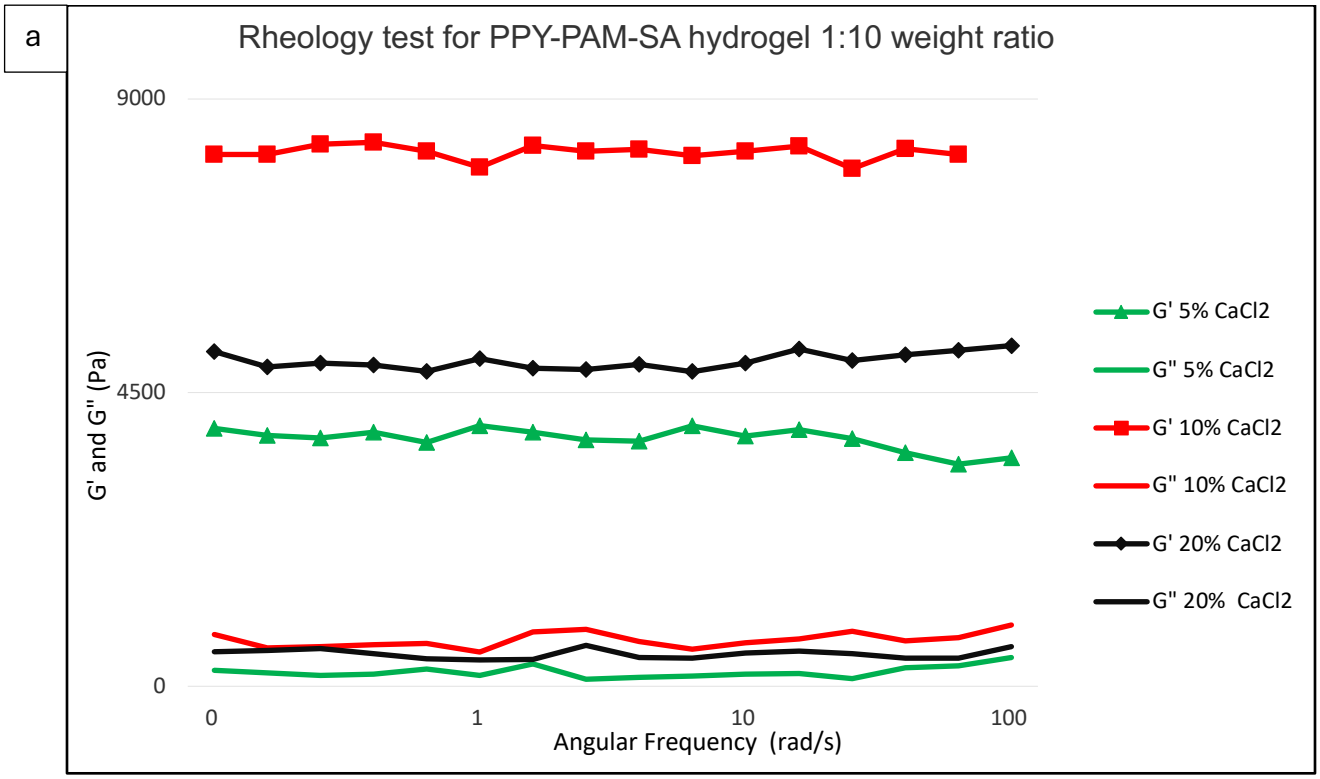

b

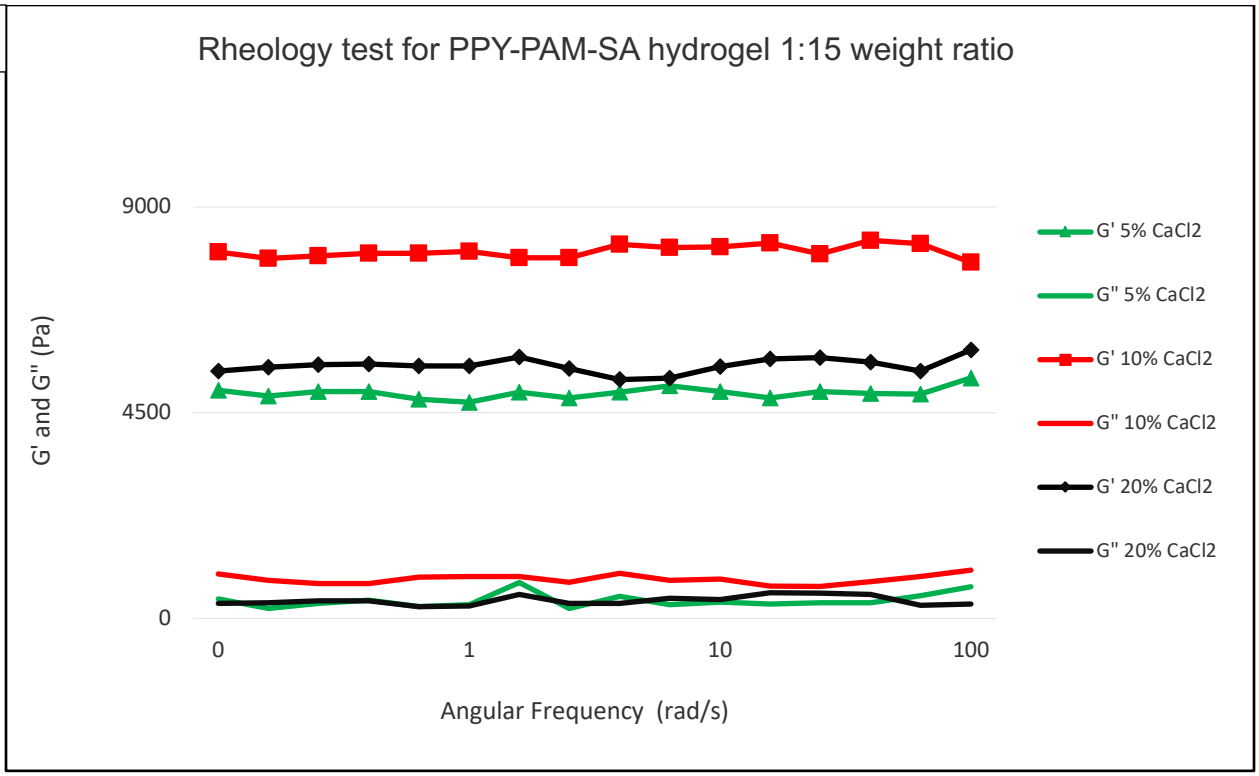

c

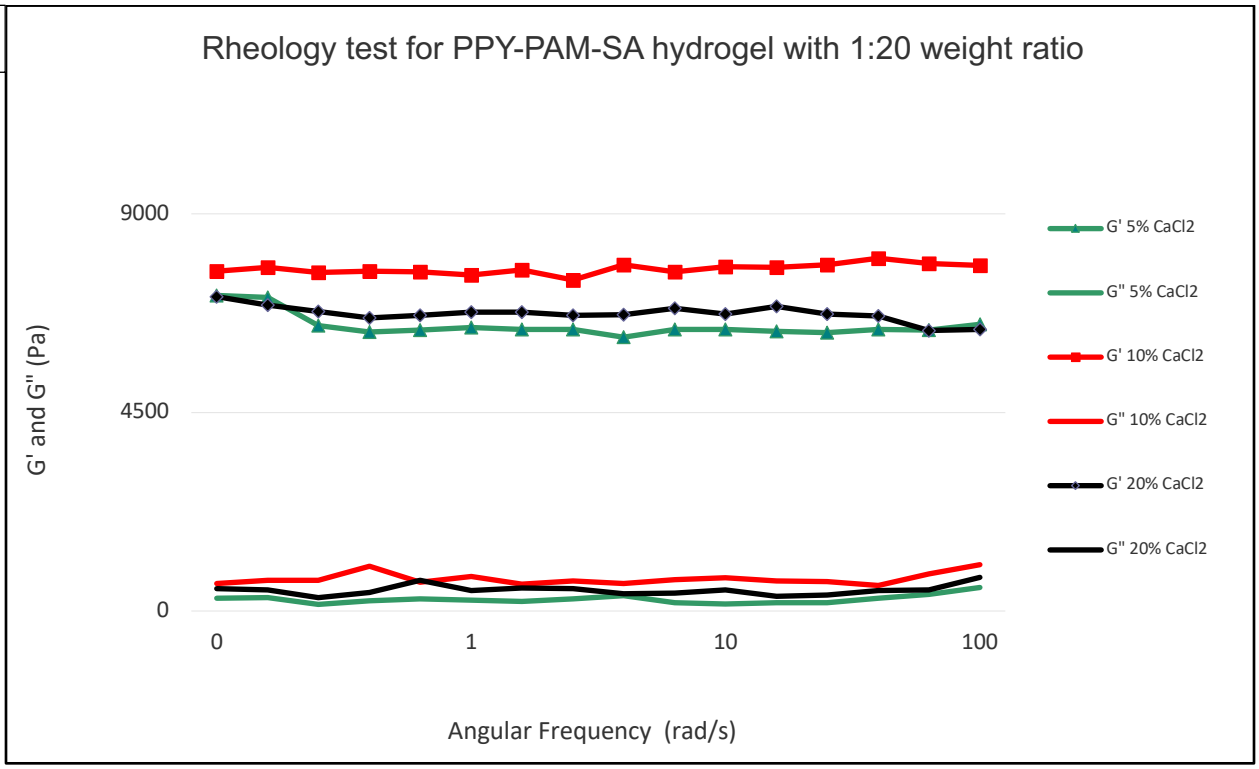

Figure 16. rheology performance test for conductive (PPY) samples under 0wt%, 5wt%, 10wt% and 20wt% $CaCl_2$. a) 1:10 SA-PAM weight polymer ratio, b) 1:15 SA-PAM weight polymer ratio, c) 1:20 SA-PAM weight polymer ratio.

4.6 Conductivity

Conductivity is a fundamental property that describes a material's ability to transmit electricity. To be more specific, it refers to the ease with which electrons can flow through a material, making it critical for applications in electronics and energy management(160). This property varies widely among different materials, ranging from highly conductive metals and polymers to insulating polymers, and is essential for designing devices that control and utilize electric currents effectively (161). Conductive hydrogels are used in various applications, including biosensors, tissue engineering, drug delivery systems, and wearable electronics. Their unique properties enable them to mimic natural tissue mechanics while conducting electrical signals(162).

Moreover, the conductivity assay was conducted to evaluate the efficacy of the polypyrrole (Ppy) materials incorporated into the hydrogel precursor. The hydrogels were segmented into sections measuring 4 cm in length, 2 cm in width, and 1 mm in thickness. Figure 16 a and b outline the conductivity results of positive current for non-conductive and conductive hydrogels, respectively. Each test was done three times for each weight polymer ratio and the average has been used in the tables here. The results indicate that the conductive samples exhibit significantly higher conductivity than the non-conductive samples. Specifically in Figure 16a, at 5wt% $CaCl_2$ concentration, the conductivity ranges from 0.0079 S/cm for the 1:10 weight ratio to 0.0076 S/cm for the 1:15 weight ratio. This trend amplifies at 10wt% $CaCl_2$, where conductivity escalates to 0.0082 S/cm for the 1:10 weight ratio and peaks at 0.0090 S/cm for the 1:20 weight ratio, illustrating a clear correlation between higher $CaCl_2$ levels and increased ionic conductivity across all ratios.

Contrastingly, in the Ppy-PAM-SA hydrogels (Figure 16b), although overall conductivity values are substantially higher, the pattern varies. At 5wt% $CaCl_2$, conductivity begins at 0.2267 S/cm for the 1:10 weight ratio and decreases to 0.1143 S/cm for the 1:15 weight ratio. Remarkably, at 10wt% $CaCl_2$, conductivity peaks at 0.2847 S/cm for the 1:10 weight ratio, demonstrating the optimal interaction between Ppy and the ionic network at this concentration. The significant difference between our samples with 10wt% $CaCl_2$ further verified our findings by the p value of 0.027 for 1:10 VS 1:15 and P value of 0.018 for 1:10 VS 1:20. However, at 20wt% $CaCl_2$, there is a notable decrease to 0.1993 S/cm for the 1:10 weight ratio, suggesting that excessive $CaCl_2$ may disrupt the conductive pathways formed by Ppy, possibly due to over-crosslinking or ion screening effects which impede effective charge transport. This comparison clearly delineates how Ppy integration significantly enhances conductivity but also introduces sensitivity to higher ionic concentrations which can adversely affect the conductivity at higher $CaCl_2$ levels. These observations are crucial for designing hydrogel-based applications where specific conductivity levels are requisite, necessitating a balanced approach in hydrogel formulation.

a

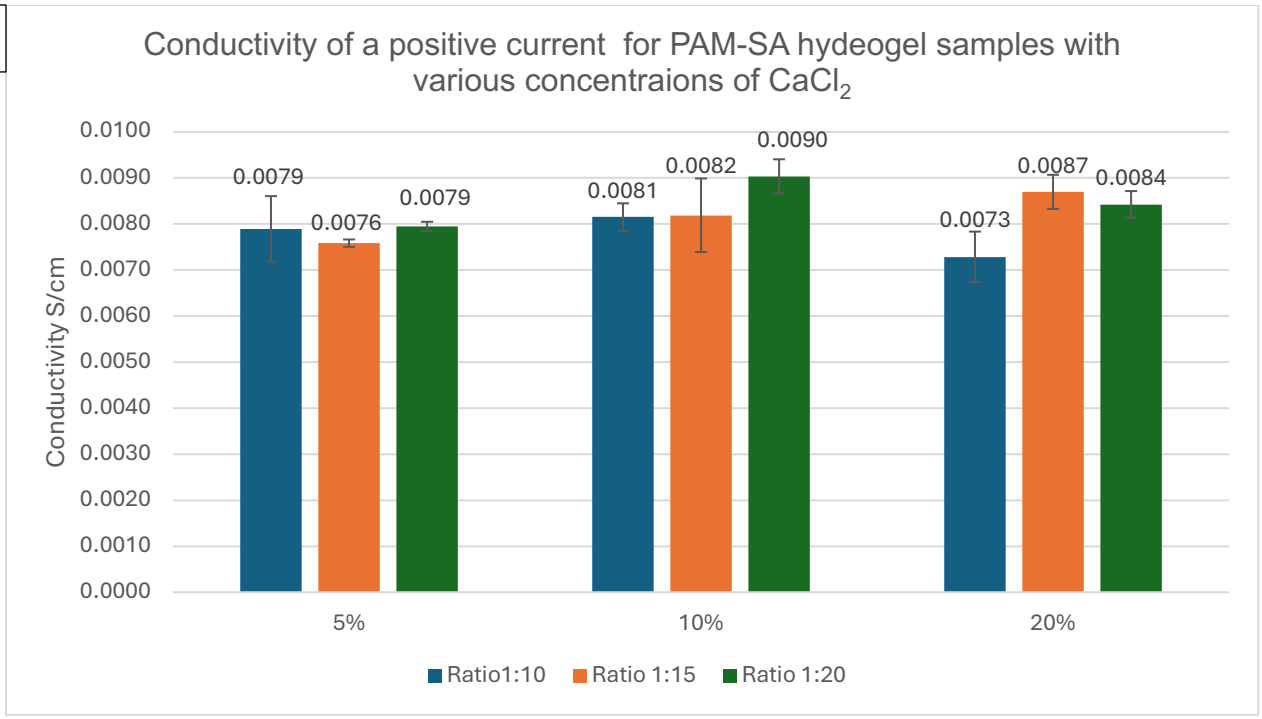

b

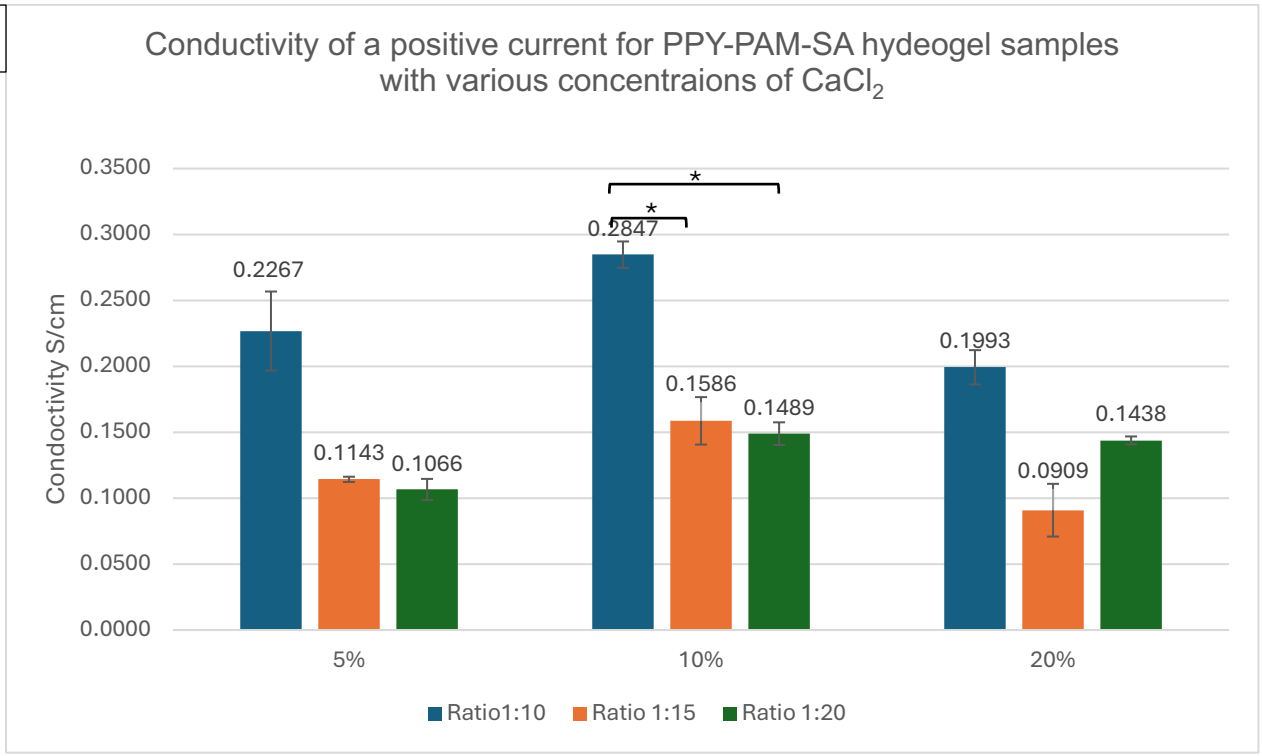

Figure 17. Conductivity test result for our samples. a) the conductivity of positive current graph for non-conductive hydrogels. b) the conductivity figure for hydrogels with conductive material Ppy. Our sample size is 3 for this experiment.

Similar to positive current graphs, Figure 18a shows conductivity of negative current data for PAM-SA hydrogel samples at three different weight ratios (1:10, 1:15, and 1:20) with varying concentrations of $CaCl_2$ (5wt%, 10wt%, 20wt%). The conductivity values are relatively low, reflecting the non-conductive nature of the PAM-SA hydrogel matrix. The values across the different conditions are consistent, typically ranging from approximately 0.0073 S/cm to 0.0089 S/cm. the peak value of 0.089 S/cm is observed for 1:20 weight ratio with 10wt% $CaCl_2$. No consistent trend is observed with increases in $CaCl_2$ concentration or changes in the ratio, indicating that the conductivity of PAM-SA hydrogels may be relatively insensitive to these parameters within the tested ranges.

On the other hand, figure 18b. demonstrates significantly higher conductivity values compared to the PAM-SA hydrogels, which is expected due to the conductive properties of Ppy. The highest conductivity is observed at the lowest hydrogel weight ratio (1:10) and a $CaCl_2$ concentration of 10wt%, reaching up to 0.2748 S/cm which is significantly higher than 1:15 weight ratio with p value of 0.049. the same trend is observed with 1:20 weight ratio with p value of 0.034. This suggests that lower hydrogel ratios and moderate $CaCl_2$ concentrations favor conductivity in Ppy-incorporated hydrogels. Conductivity tends to decrease with increasing hydrogel ratios reaching 0.1094 S/cm, 0.1099 S/cm and 0.1151 S/cm for 1:10,1:15 and 1:20 weight ratios, respectively. This decline is possibly due to a dilution effect or reduced interaction between conductive pathways within the hydrogel structure. The range of conductivity values across different conditions spans from about 0.0921 S/cm to 0.2748 S/cm, highlighting the impact of both the hydrogel composition and the $CaCl_2$ concentration on the electrical properties of the hydrogels.

Moreover, as we saw in Figure 16 b and 18b. increasing concentrations of $CaCl_2$ in PAM-SA hydrogels embedded with Ppy lead to decreased conductivity, predominantly due to enhanced ionic strength and the resultant ion screening effect, which obstructs charge mobility. Additionally, higher $CaCl_2$ levels promote a denser hydrogel network through more extensive crosslinking, potentially restricting the mobility of Ppy chains and disrupting their ability to form effective conductive pathways. The structural densification could also reduce the hydrogel's water content, further diminishing the medium necessary for ionic conduction. These factors combined contribute to the observed reduction in conductivity with higher concentrations of $CaCl_2$. It is also important to note that the observed lower conductivity might be attributed to errors in the complete formation of the hydrogels or inconsistencies in their homogeneity. (163,164).

a

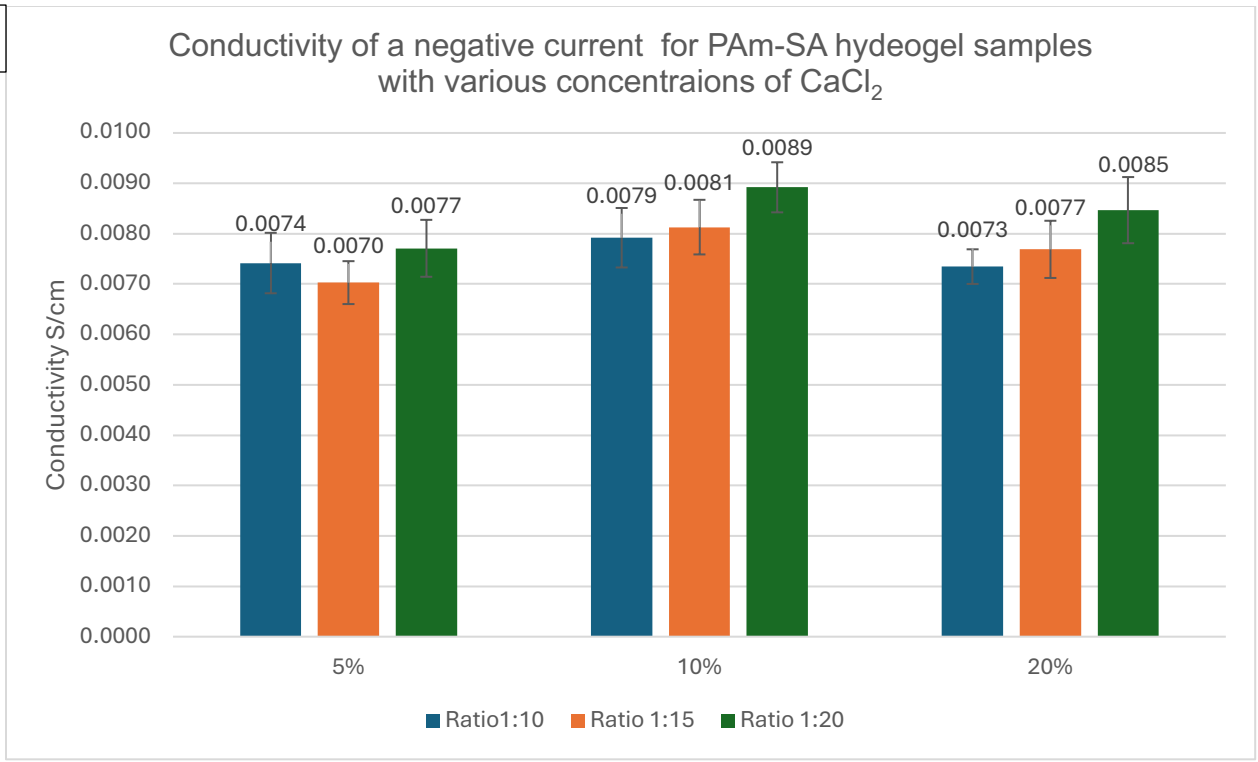

b

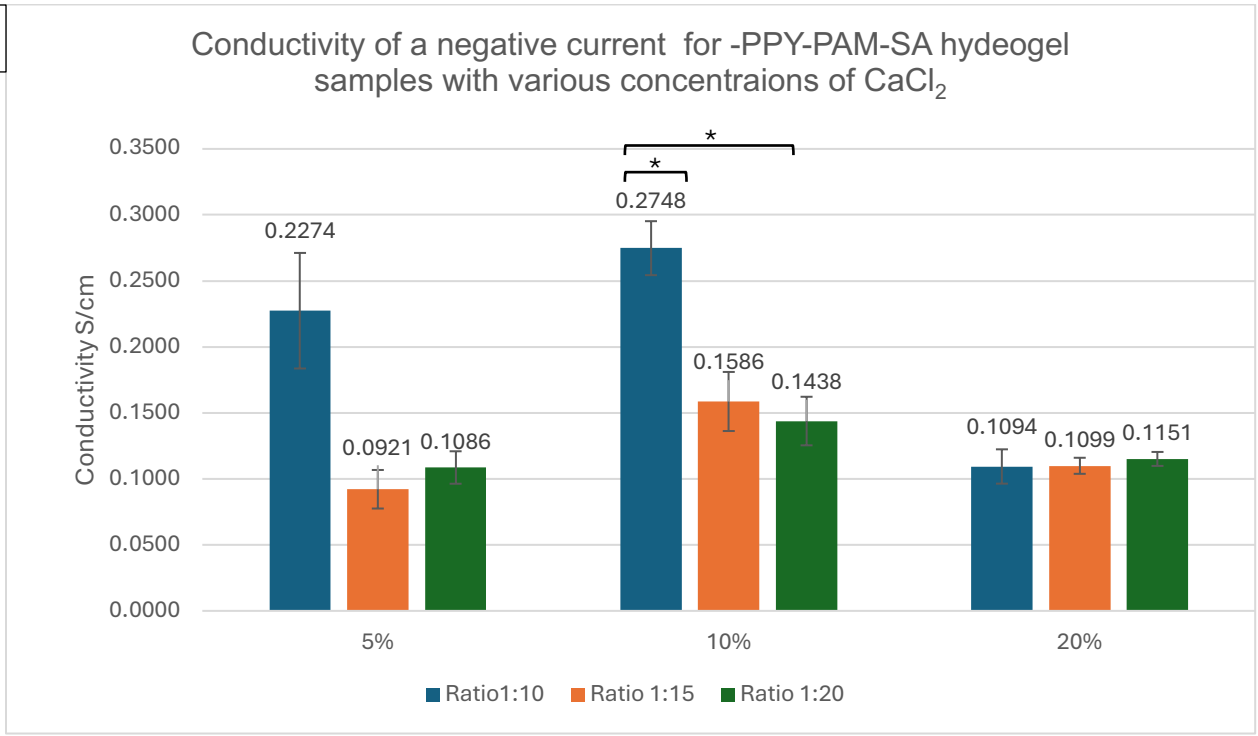

Figure 18. Conductivity test result for our samples. a) the conductivity graph of negative current for non-conductive hydrogels. b) the conductivity figure for hydrogels with conductive material Ppy. Our sample size is 3 for this experiment.

4.7 Microneedle

Hydrogel microneedles are an innovative advancement in transdermal drug delivery, merging hydrogel technology with minimally invasive microneedles. Made from biocompatible, water-soluble polymers, these devices enable controlled, sustained release of drugs through painless penetration of the skin's upper layer(131). Ideal for enhancing drug bioavailability and patient compliance, hydrogel microneedles are promising for chronic disease management, vaccinations, and cosmetic applications, revolutionizing approaches in medicine and dermatology(165). The description can be further enhanced with some additional scientific details and precise terminology to better suit an academic context. The microneedle device was engineered using a precision mold with dimensions of 10 cm in length and 5 cm in width, featuring needles that are 2 cm in height. The matrix was composed using a polymer blend at a weight ratio of 1:10 of sodium alginate (SA) to polyacrylamide (PAM), supplemented with a 10wt% concentration of calcium chloride. As depicted in Figure 19, the microneedles have been constructed to ensure optimal sharpness, allowing for effective penetration of the dermis. This structural design is crucial for the targeted delivery of therapeutics across the skin barrier, enabling applications in transdermal drug delivery and other biomedical fields.

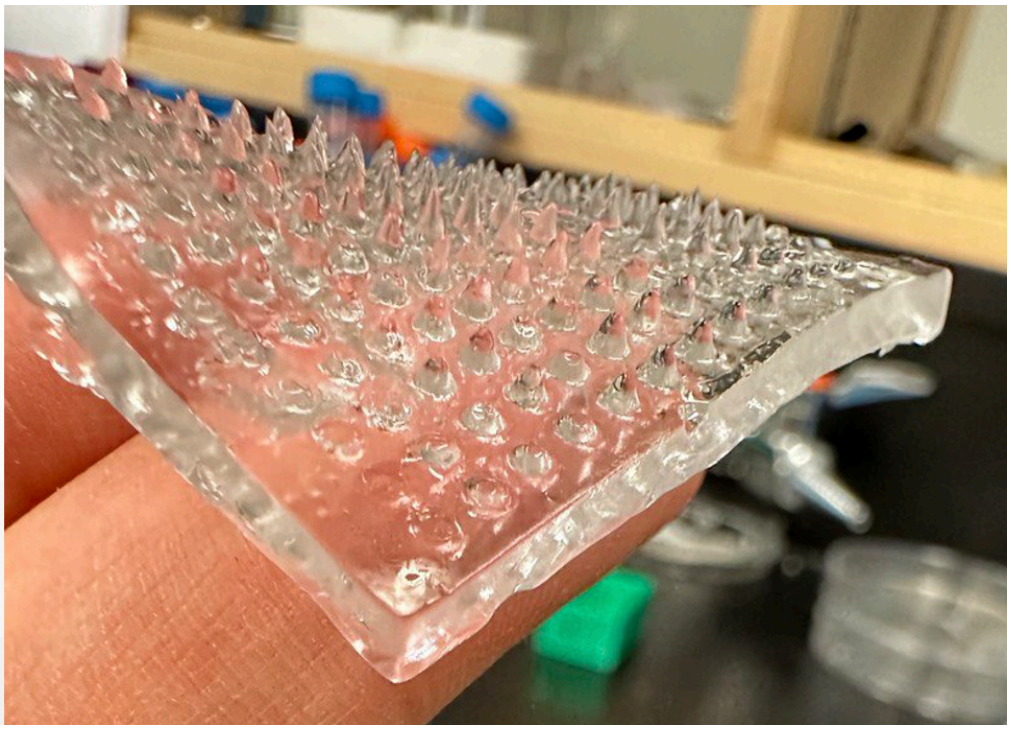

Figure 19. Picture of hydrogel microneedle that is made by 1:10 polymer weight ratio and 10wt% $CaCl_2$

Chapter V: Conclusion

The comprehensive study presented in this work demonstrates the successful development of conductive hydrogels based on Sodium Alginate (SA), Polyacrylamide (PAM), and Polypyrrole (Ppy). The inclusion of $CaCl_2$ significantly enhanced the mechanical properties and functionality of these hydrogels. The incorporation of Ppy into the SA-PAM matrix was a pivotal enhancement, significantly boosting the conductivity of the hydrogels to impressive levels without compromising their intrinsic flexibility. Fourier Transform Infrared Spectroscopy (FTIR) and Scanning Electron Microscopy (SEM) were employed to further characterize these hydrogels. FTIR spectra confirmed the presence of key functional groups, ensuring the integrity of the crosslinked network within the hydrogels. The observed peaks at specific wavelengths substantiated the formation of amide and carboxylic bonds essential for the hydrogels' robust structure. SEM analysis provided visual evidence of the dense, uniform network structure, with images displaying well-defined cross-sectional views that highlight the even distribution and stability of the crosslinked matrix.

Mechanical testing revealed that these hydrogels demonstrated optimal properties at a specific formulation of a 1:10 SA-PAM ratio with a 10wt% $CaCl_2$ concentration. At this composition, the hydrogels exhibited peak tensile strengths and an improved modulus of elasticity, crucial for applications requiring durable, reliable performance under physical stress. For instance, the compression test results showed that conductive hydrogel with this optimal formulation achieved a stress of 1092 KPa at a strain of 70%, indicating substantial mechanical robustness. The tensile and compression tests across various

ratios and concentrations highlighted the critical role of $CaCl_2$ in enhancing the hydrogels' structural properties, demonstrating a substantial increase in stress tolerance and energy absorption capabilities. Furthermore, swelling ratio tests affirmed the effectiveness of $CaCl_2$ in modulating the hydrogels' ability to swell, which is essential for drug release applications. The reduction in swelling ratios with increased $CaCl_2$ concentrations pointed to denser crosslinking within the hydrogel matrix.

The enhanced mechanical and conductive properties of these hydrogels suggest promising applications in biosensors and microneedle-based transdermal drug delivery systems. Their ability to mold to complex biological geometries while maintaining functionality introduces new possibilities for the development of non-invasive medical devices that combine efficacy with patient comfort. To be more specific, the enhanced understanding of the interaction between polymer composition, crosslinker concentration, and hydrogel properties opens new avenues for the future design of hydrogels with tailored mechanical and functional characteristics.

Future research should aim to refine these hydrogel formulations further, optimizing their physical and chemical properties to tailor them more precisely for specific medical applications. Long-term studies focusing on biocompatibility, degradation, and clinical efficacy are necessary to transition these hydrogels from laboratory prototypes to clinically approved devices. This foundational work sets the stage for future innovations that could significantly enhance the utility of hydrogel-based systems in medical

technology, promising to revolutionize the field with materials that are both robust and versatile.

Chapter VI: References

1. Chai Q, Jiao Y, Yu X. Hydrogels for Biomedical Applications: Their Characteristics and the Mechanisms behind Them. Gels. 2017 Jan 24;3(1):6.
2. Ahmed EM. Hydrogel: Preparation, characterization, and applications: A review. J Adv Res. 2015 Mar;6(2):105–21.
3. Fan Z, Liu B, Wang J, Zhang S, Lin Q, Gong P, et al. A Novel Wound Dressing Based on Ag/Graphene Polymer Hydrogel: Effectively Kill Bacteria and Accelerate Wound Healing. Adv Funct Mater. 2014 Jul 17;24(25):3933–43.
4. Jiang Y, Chen J, Deng C, Suuronen EJ, Zhong Z. Click hydrogels, microgels and nanogels: Emerging platforms for drug delivery and tissue engineering. Biomaterials. 2014 Jun;35(18):4969–85.
5. Emileh A, Vasheghani-Farahani E, Imani M. Swelling behavior, mechanical properties and network parameters of pH- and temperature-sensitive hydrogels of poly((2-dimethyl amino) ethyl methacrylate-co-butyl methacrylate). Eur Polym J. 2007 May;43(5):1986–95.
6. Quinn CAP, Connor RE, Heller A. Biocompatible, glucose-permeable hydrogel for in situ coating of implantable biosensors. Biomaterials. 1997 Dec;18(24):1665–70.
7. Holzer R, Bloch W, Brinkmann C. Continuous Glucose Monitoring in Healthy Adults—Possible Applications in Health Care, Wellness, and Sports. Sensors. 2022 Mar 5;22(5):2030.
8. Boland CS, Khan U, Backes C, O'Neill A, McCauley J, Duane S, et al. Sensitive, High-Strain, High-Rate Bodily Motion Sensors Based on Graphene–Rubber Composites. ACS Nano. 2014 Sep 23;8(9):8819–30.
9. Mattmann C, Clemens F, Tröster G. Sensor for Measuring Strain in Textile. Sensors. 2008 Jun 3;8(6):3719–32.
10. Chitrakar C, Hedrick E, Adegoke L, Ecker M. Flexible and Stretchable Bioelectronics. Materials. 2022 Feb 23;15(5):1664.
11. Yamada T, Hayamizu Y, Yamamoto Y, Yomogida Y, Izadi-Najafabadi A, Futaba DN, et al. A stretchable carbon nanotube strain sensor for human-motion detection. Nat Nanotechnol. 2011 May 27;6(5):296–301.
12. Pyarasani RD, Jayaramudu T, John A. Polyaniline-based conducting hydrogels. J Mater Sci. 2019 Jan 4;54(2):974–96.
13. Bai H, Sheng K, Zhang P, Li C, Shi G. Graphene oxide/conducting polymer composite hydrogels. J Mater Chem. 2011;21(46):18653.
14. Zhu F, She X, Huang H, Zhang Z, Ji J, Li L. Fabrication of multifunctional polypyrrole hydrogel enhanced by polyvinyl alcohol. Polymer Bulletin. 2024 Apr 7;81(5):4107–21.
15. Chen Q, Zhu L, Chen H, Yan H, Huang L, Yang J, et al. A Novel Design Strategy for Fully Physically Linked Double Network Hydrogels with Tough, Fatigue Resistant, and Self-Healing Properties. Adv Funct Mater. 2015 Mar 3;25(10):1598–607.
16. Cui S, Yang F, Yu D, Shi C, Zhao D, Chen L, et al. Double Network Physical Crosslinked Hydrogel for Healing Skin Wounds: New Formulation Based on Polysaccharides and Zn2+. Int J Mol Sci. 2023 Aug 22;24(17):13042.

17. Xin H. Double-Network Tough Hydrogels: A Brief Review on Achievements and Challenges. Gels. 2022 Apr 18;8(4):247.
18. Zeng S, Chen H, Cai F, Kang Y, Chen M, Li Q. Electrochemical fabrication of carbon nanotube/polyaniline hydrogel film for all-solid-state flexible supercapacitor with high areal capacitance. J Mater Chem A Mater. 2015;3(47):23864–70.
19. Wang X, Li X, Zhao L, Li M, Li Y, Yang W, et al. Polypyrrole-doped conductive self-healing multifunctional composite hydrogels with a dual crosslinked network. Soft Matter. 2021;17(36):8363–72.
20. Li J, Wu C, Chu PK, Gelinsky M. 3D printing of hydrogels: Rational design strategies and emerging biomedical applications. Materials Science and Engineering: R: Reports. 2020 Apr;140:100543.
21. Turner JG, White LR, Estrela P, Leese HS. Hydrogel-Forming Microneedles: Current Advancements and Future Trends. Macromol Biosci. 2021 Feb 26;21(2).
22. Sun W, Araci Z, Inayathullah M, Manickam S, Zhang X, Bruce MA, et al. Polyvinylpyrrolidone microneedles enable delivery of intact proteins for diagnostic and therapeutic applications. Acta Biomater. 2013 Aug;9(8):7767–74.
23. Dragan ES. Advances in interpenetrating polymer network hydrogels and their applications. Pure and Applied Chemistry. 2014 Nov 1;86(11):1707–21.
24. bt Ibrahim SF, Mohd Azam NAN, Mat Amin KA. Sodium alginate film: the effect of crosslinker on physical and mechanical properties. IOP Conf Ser Mater Sci Eng. 2019 May 3;509:012063.
25. Calvo PA, Rodríguez J, Grande H, Mecerreyes D, Pomposo JA. Chemical oxidative polymerization of pyrrole in the presence of m-hydroxybenzoic acid- and m-hydroxycinnamic acid-related compounds. Synth Met. 2002 Jan;126(1):111–6.
26. Fu J, in het Panhuis M. Hydrogel properties and applications. J Mater Chem B. 2019;7(10):1523–5.
27. Yoo EH, Lee SY. Glucose Biosensors: An Overview of Use in Clinical Practice. Sensors. 2010 May 4;10(5):4558–76.
28. Bauer JA, Zámocká M, Majtán J, Bauerová-Hlinková V. Glucose Oxidase, an Enzyme “Ferrari”: Its Structure, Function, Production and Properties in the Light of Various Industrial and Biotechnological Applications. Biomolecules. 2022 Mar 19;12(3):472.
29. Batool R, Rhouati A, Nawaz MH, Hayat A, Marty JL. A Review of the Construction of Nano-Hybrids for Electrochemical Biosensing of Glucose. Biosensors (Basel). 2019 Mar 25;9(1):46.
30. Zhao X, Wu H, Guo B, Dong R, Qiu Y, Ma PX. Antibacterial anti-oxidant electroactive injectable hydrogel as self-healing wound dressing with hemostasis and adhesiveness for cutaneous wound healing. Biomaterials. 2017 Apr;122:34–47.
31. Maulvi FA, Lakdawala DH, Shaikh AA, Desai AR, Choksi HH, Vaidya RJ, et al. In vitro and in vivo evaluation of novel implantation technology in hydrogel contact lenses for controlled drug delivery. Journal of Controlled Release. 2016 Mar;226:47–56.
32. Hsu KH, Lazon de la Jara P, Ariyavidana A, Watling J, Holden B, Garrett Q, et al. Release of Betaine and Dexpanthenol from Vitamin E Modified Silicone-Hydrogel Contact Lenses. Curr Eye Res. 2015 Mar 4;40(3):267–73.

33. Filho D, Guerrero M, Pariguana M, Marican A, Durán-Lara EF. Hydrogel-Based Microneedle as a Drug Delivery System. Pharmaceutics. 2023 Oct 10;15(10):2444.
34. Ullah F, Othman MBH, Javed F, Ahmad Z, Akil HMd. Classification, processing and application of hydrogels: A review. Materials Science and Engineering: C. 2015 Dec;57:414–33.
35. Kean T, Thanou M. Biodegradation, biodistribution and toxicity of chitosan. Adv Drug Deliv Rev. 2010 Jan;62(1):3–11.
36. Aranaz I, Alcántara AR, Civera MC, Arias C, Elorza B, Heras Caballero A, et al. Chitosan: An Overview of Its Properties and Applications. Polymers (Basel). 2021 Sep 24;13(19):3256.
37. Shariatinia Z. Pharmaceutical applications of chitosan. Adv Colloid Interface Sci. 2019 Jan;263:131–94.
38. Giri TK, Thakur A, Alexander A, Ajazuddin, Badwaik H, Tripathi DK. Modified chitosan hydrogels as drug delivery and tissue engineering systems: present status and applications. Acta Pharm Sin B. 2012 Oct;2(5):439–49.
39. Ravi Kumar MNV. A review of chitin and chitosan applications. React Funct Polym. 2000 Nov;46(1):1–27.
40. Mu M, Li X, Tong A, Guo G. Multi-functional chitosan-based smart hydrogels mediated biomedical application. Expert Opin Drug Deliv. 2019 Mar 4;16(3):239–50.
41. Moon RJ, Martini A, Nairn J, Simonsen J, Youngblood J. Cellulose nanomaterials review: structure, properties and nanocomposites. Chem Soc Rev. 2011;40(7):3941.
42. Curvello R, Raghuwanshi VS, Garnier G. Engineering nanocellulose hydrogels for biomedical applications. Adv Colloid Interface Sci. 2019 May;267:47–61.
43. Zainal SH, Mohd NH, Suhaili N, Anuar FH, Lazim AM, Othaman R. Preparation of cellulose-based hydrogel: a review. Journal of Materials Research and Technology. 2021 Jan;10:935–52.
44. Chang C, Zhang L. Cellulose-based hydrogels: Present status and application prospects. Carbohydr Polym. 2011 Feb;84(1):40–53.
45. Kamel S, A. Khattab T. Recent Advances in Cellulose-Based Biosensors for Medical Diagnosis. Biosensors (Basel). 2020 Jun 17;10(6):67.
46. Ge S, Zhang L, Zhang Y, Lan F, Yan M, Yu J. Nanomaterials-modified cellulose paper as a platform for biosensing applications. Nanoscale. 2017;9(13):4366–82.
47. Sankhala D, Sardesai AU, Pali M, Lin KC, Jagannath B, Muthukumar S, et al. A machine learning-based on-demand sweat glucose reporting platform. Sci Rep. 2022 Feb 14;12(1):2442.
48. Aziz T, Farid A, Haq F, Kiran M, Ullah A, Zhang K, et al. A Review on the Modification of Cellulose and Its Applications. Polymers (Basel). 2022 Aug 5;14(15):3206.
49. Ratajczak K, Stobiecka M. High-performance modified cellulose paper-based biosensors for medical diagnostics and early cancer screening: A concise review. Carbohydr Polym. 2020 Feb;229:115463.
50. Ferri S, Kojima K, Sode K. Review of Glucose Oxidases and Glucose Dehydrogenases: A Bird's Eye View of Glucose Sensing Enzymes. J Diabetes Sci Technol. 2011 Sep 1;5(5):1068–76.

51. Lee KY, Mooney DJ. Alginate: Properties and biomedical applications. Prog Polym Sci. 2012 Jan;37(1):106–26.
52. Rhim JW. Physical and mechanical properties of water resistant sodium alginate films. LWT - Food Science and Technology. 2004 May;37(3):323–30.
53. Gao C, Liu M, Chen J, Zhang X. Preparation and controlled degradation of oxidized sodium alginate hydrogel. Polym Degrad Stab. 2009 Sep;94(9):1405–10.
54. Thakur S, Sharma B, Verma A, Chaudhary J, Tamulevicius S, Thakur VK. Recent progress in sodium alginate based sustainable hydrogels for environmental applications. J Clean Prod. 2018 Oct;198:143–59.
55. Han E, Li X, Cai JR, Cui HY, Zhang XA. Development of Highly Sensitive Amperometric Biosensor for Glucose Using Carbon Nanosphere/Sodium Alginate Composite Matrix for Enzyme Immobilization. Analytical Sciences. 2014 Sep 10;30(9):897–902.
56. Roquero DM, Katz E. “Smart” alginate hydrogels in biosensing, bioactuation and biocomputing: State-of-the-art and perspectives. Sensors and Actuators Reports. 2022 Nov;4:100095.
57. Zhao Z, Jiang H. Enzyme-based Electrochemical Biosensors. In: Biosensors. InTech; 2010.
58. Kausar A. Poly(acrylic acid) nanocomposites: Design of advanced materials. Journal of Plastic Film & Sheeting. 2021 Oct 22;37(4):409–28.
59. Sennakesavan G, Mostakhdemin M, Dkhar LK, Seyfoddin A, Fatihhi SJ. Acrylic acid/acrylamide based hydrogels and its properties - A review. Polym Degrad Stab. 2020 Oct;180:109308.
60. Calixto G, Yoshii AC, Rocha e Silva H, Stringhetti Ferreira Cury B, Chorilli M. Polyacrylic acid polymers hydrogels intended to topical drug delivery: preparation and characterization. Pharm Dev Technol. 2015 May 19;20(4):490–6.
61. Gao X, He C, Xiao C, Zhuang X, Chen X. Biodegradable pH-responsive polyacrylic acid derivative hydrogels with tunable swelling behavior for oral delivery of insulin. Polymer (Guildf). 2013 Mar;54(7):1786–93.
62. Arkaban H, Barani M, Akbarizadeh MR, Pal Singh Chauhan N, Jadoun S, Dehghani Soltani M, et al. Polyacrylic Acid Nanoplatforms: Antimicrobial, Tissue Engineering, and Cancer Theranostic Applications. Polymers (Basel). 2022 Mar 21;14(6):1259.
63. Philippova OE, Hourdet D, Audebert R, Khokhlov AR. Interaction of Hydrophobically Modified Poly(acrylic acid) Hydrogels with Ionic Surfactants. Macromolecules. 1996 Jan 1;29(8):2822–30.
64. Jiang S, Liu S, Feng W. PVA hydrogel properties for biomedical application. J Mech Behav Biomed Mater. 2011 Oct;4(7):1228–33.
65. Bursali EA, Coskun S, Kizil M, Yurdakoc M. Synthesis, characterization and in vitro antimicrobial activities of boron/starch/polyvinyl alcohol hydrogels. Carbohydr Polym. 2011 Jan 30;83(3):1377–83.
66. Wang T, Gunasekaran S. State of water in chitosan–PVA hydrogel. J Appl Polym Sci. 2006 Sep 5;101(5):3227–32.
67. Chen Y, Li J, Lu J, Ding M, Chen Y. Synthesis and properties of Poly(vinyl alcohol) hydrogels with high strength and toughness. Polym Test. 2022 Apr;108:107516.

68. Chakravarty S, Dutta P, Kalita S, Sen Sarma N. PVA-based nanobiosensor for ultrasensitive detection of folic acid by fluorescence quenching. Sens Actuators B Chem. 2016 Sep;232:243–50.
69. Kamoun EA, Kenawy ERS, Chen X. A review on polymeric hydrogel membranes for wound dressing applications: PVA-based hydrogel dressings. J Adv Res. 2017 May;8(3):217–33.
70. Kulicke WM, Kniewske R, Klein J. Preparation, characterization, solution properties and rheological behaviour of polyacrylamide. Prog Polym Sci. 1982 Jan;8(4):373–468.
71. Choi S, Choi Y jin, Jang M, Lee JH, Jeong JH, Kim J. Supertough Hybrid Hydrogels Consisting of a Polymer Double-Network and Mesoporous Silica Microrods for Mechanically Stimulated On-Demand Drug Delivery. Adv Funct Mater. 2017 Nov 4;27(42).
72. Saeidi M, Chenani H, Orouji M, Adel Rastkhiz M, Bolghanabadi N, Vakili S, et al. Electrochemical Wearable Biosensors and Bioelectronic Devices Based on Hydrogels: Mechanical Properties and Electrochemical Behavior. Biosensors (Basel). 2023 Aug 15;13(8):823.
73. Gamboa J, Paulo-Mirasol S, Estrany F, Torras J. Recent Progress in Biomedical Sensors Based on Conducting Polymer Hydrogels. ACS Appl Bio Mater. 2023 May 15;6(5):1720–41.
74. Kim S, Kim C, Lee K. Hydrogels as filler materials. In: Hydrogels for Tissue Engineering and Regenerative Medicine. Elsevier; 2024. p. 413–32.
75. Wang Y, Li D. Creating Complex Polyacrylamide Hydrogel Structures Using 3D Printing with Applications to Mechanobiology. Macromol Biosci. 2020 Jul 17;20(7).
76. Kontou E, Spathis G, Niaounakis M, Kefalas V. Physical and chemical cross-linking effects in polyurethane elastomers. Colloid Polym Sci. 1990 Jul;268(7):636–44.
77. Hennink WE, van Nostrum CF. Novel crosslinking methods to design hydrogels. Adv Drug Deliv Rev. 2012 Dec;64:223–36.
78. Wang K, Zhang X, Li C, Sun X, Meng Q, Ma Y, et al. Chemically Crosslinked Hydrogel Film Leads to Integrated Flexible Supercapacitors with Superior Performance. Advanced Materials. 2015 Dec 15;27(45):7451–7.
79. Hu W, Wang Z, Xiao Y, Zhang S, Wang J. Advances in crosslinking strategies of biomedical hydrogels. Biomater Sci. 2019;7(3):843–55.
80. Huang X, Li J, Luo J, Gao Q, Mao A, Li J. Research progress on double-network hydrogels. Mater Today Commun. 2021 Dec;29:102757.
81. Xu C, Lee W, Dai G, Hong Y. Highly Elastic Biodegradable Single-Network Hydrogel for Cell Printing. ACS Appl Mater Interfaces. 2018 Mar 28;10(12):9969–79.
82. Gong JP. Why are double network hydrogels so tough? Soft Matter. 2010;6(12):2583.
83. Chen H, Yang F, Hu R, Zhang M, Ren B, Gong X, et al. A comparative study of the mechanical properties of hybrid double-network hydrogels in swollen and as-prepared states. J Mater Chem B. 2016;4(35):5814–24.
84. Huang Y, Jayathilaka PB, Islam MS, Tanaka CB, Silberstein MN, Kilian KA, et al. Structural aspects controlling the mechanical and biological properties of tough, double network hydrogels. Acta Biomater. 2022 Jan;138:301–12.

85. Hong S, Sycks D, Chan HF, Lin S, Lopez GP, Guilak F, et al. 3D Printing of Highly Stretchable and Tough Hydrogels into Complex, Cellularized Structures. Advanced Materials. 2015 Jul;27(27):4035–40.
86. Darabi MA, Khosrozadeh A, Wang Q, Xing M. Gum Sensor: A Stretchable, Wearable, and Foldable Sensor Based on Carbon Nanotube/Chewing Gum Membrane. ACS Appl Mater Interfaces. 2015 Dec 2;7(47):26195–205.
87. Yi J, Choe G, Park J, Lee JY. Graphene oxide-incorporated hydrogels for biomedical applications. Polym J. 2020 Aug 8;52(8):823–37.
88. Shin M, Lim J, Park Y, Lee JY, Yoon J, Choi JW. Carbon-based nanocomposites for biomedical applications. RSC Adv. 2024;14(10):7142–56.
89. Xu Y, Lin Z, Huang X, Liu Y, Huang Y, Duan X. Flexible Solid-State Supercapacitors Based on Three-Dimensional Graphene Hydrogel Films. ACS Nano. 2013 May 28;7(5):4042–9.
90. Peng H, Lv Y, Wei G, Zhou J, Gao X, Sun K, et al. A flexible and self-healing hydrogel electrolyte for smart supercapacitor. J Power Sources. 2019 Aug;431:210–9.
91. Feng X, Chen W, Yan L. Reduced graphene oxide hydrogel film with a continuous ion transport network for supercapacitors. Nanoscale. 2015;7(8):3712–8.
92. Min J, Patel M, Koh WG. Incorporation of Conductive Materials into Hydrogels for Tissue Engineering Applications. Polymers (Basel). 2018 Sep 28;10(10):1078.
93. Bhadra S, Khastgir D, Singha NK, Lee JH. Progress in preparation, processing and applications of polyaniline. Prog Polym Sci. 2009 Aug;34(8):783–810.
94. Pagar SB, Ghorude TN, Nikolova MP, SenthilKannan K. Synthesis, physical, chemical, biological, mechanical and electronic studies of polypyrrole (PPy) of versatile scales for electro-mechano, pharmaceutical utilities. Heliyon. 2023 Sep;9(9):e20086.
95. Brahim S, Narinesingh D, Guiseppi-Elie A. Polypyrrole-hydrogel composites for the construction of clinically important biosensors. Biosens Bioelectron. 2002 Jan;17(1–2):53–9.
96. Shi Y, Pan L, Liu B, Wang Y, Cui Y, Bao Z, et al. Nanostructured conductive polypyrrole hydrogels as high-performance, flexible supercapacitor electrodes. J Mater Chem A. 2014;2(17):6086–91.
97. Pyarasani RD, Jayaramudu T, John A. Polyaniline-based conducting hydrogels. J Mater Sci. 2019 Jan 4;54(2):974–96.
98. Zamiri G, Haseeb ASMA. Recent Trends and Developments in Graphene/Conducting Polymer Nanocomposites Chemiresistive Sensors. Materials. 2020 Jul 24;13(15):3311.
99. Bianco A, Kostarelos K, Prato M. Applications of carbon nanotubes in drug delivery. Curr Opin Chem Biol. 2005 Dec;9(6):674–9.
100. Xia H qi, Tang H, Zhou B, Li Y, Zhang X, Shi Z, et al. Mediator-free electron-transfer on patternable hierarchical meso/macro porous bienzyme interface for highly-sensitive sweat glucose and surface electromyography monitoring. Sens Actuators B Chem. 2020 Jun;312:127962.
101. Taylor DL, in het Panhuis M. Self-Healing Hydrogels. Advanced Materials. 2016 Nov 4;28(41):9060–93.

102. Imato K, Otsuka H. Self-healing Polymers through Dynamic Covalent Chemistry. In: Dynamic Covalent Chemistry. Wiley; 2017. p. 359–87.
103. Kilic R, Sanyal A. Self-Healing Hydrogels Based on Reversible Covalent Linkages: A Survey of Dynamic Chemical Bonds in Network Formation. In 2020. p. 243–94.
104. Quan L, Xin Y, Wu X, Ao Q. Mechanism of Self-Healing Hydrogels and Application in Tissue Engineering. Polymers (Basel). 2022 May 27;14(11):2184.
105. Rumon MdMH, Akib AA, Sultana F, Moniruzzaman Md, Niloy MS, Shakil MS, et al. Self-Healing Hydrogels: Development, Biomedical Applications, and Challenges. Polymers (Basel). 2022 Oct 26;14(21):4539.
106. Darabi MA, Khosrozadeh A, Mbeleck R, Liu Y, Chang Q, Jiang J, et al. Skin-Inspired Multifunctional Autonomic-Intrinsic Conductive Self-Healing Hydrogels with Pressure Sensitivity, Stretchability, and 3D Printability. Advanced Materials. 2017 Aug 22;29(31).
107. Berger J, Reist M, Mayer JM, Felt O, Peppas NA, Gurny R. Structure and interactions in covalently and ionically crosslinked chitosan hydrogels for biomedical applications. European Journal of Pharmaceutics and Biopharmaceutics. 2004 Jan;57(1):19–34.
108. Li Y, Wang X, Wei Y, Tao L. Chitosan-based self-healing hydrogel for bioapplications. Chinese Chemical Letters. 2017 Nov;28(11):2053–7.
109. Park J, Oh Y, Jeong S, Song HW, Choi E, Kim H. Biobased Stimuli-Responsive Hydrogels That Comprise Supramolecular Interpenetrating Networks and Exhibit Programmed Behaviors. Chemistry of Materials. 2021 Oct 26;33(20):8124–32.
110. Liang Z, Zhang J, Wu C, Hu X, Lu Y, Wang G, et al. Flexible and self-healing electrochemical hydrogel sensor with high efficiency toward glucose monitoring. Biosens Bioelectron. 2020 May;155:112105.
111. Narwal V, Deswal R, Batra B, Kalra V, Hooda R, Sharma M, et al. Cholesterol biosensors: A review. Steroids. 2019 Mar;143:6–17.
112. Tavakoli J, Tang Y. Hydrogel Based Sensors for Biomedical Applications: An Updated Review. Polymers (Basel). 2017 Aug 16;9(12):364.
113. Bhatia D, Paul S, Acharjee T, Ramachairy SS. Biosensors and their widespread impact on human health. Sensors International. 2024;5:100257.
114. Chang Q, He Y, Liu Y, Zhong W, Wang Q, Lu F, et al. Transparent Protein Hydrogels: Protein Gel Phase Transition: Toward Superiorly Transparent and Hysteresis-Free Wearable Electronics (Adv. Funct. Mater. 27/2020). Adv Funct Mater. 2020 Jul 2;30(27).
115. Hsu HH, Zhang X, Xu K, Wang Y, Wang Q, Luo G, et al. Self-powered and plant-wearable hydrogel as LED power supply and sensor for promoting and monitoring plant growth in smart farming. Chemical Engineering Journal. 2021 Oct;422:129499.
116. Shi Y, Wang W, Lei Z, Wang W, Yu D. A transparent, anti-fatigue, flexible multifunctional hydrogel with self-adhesion and conductivity for biosensors. Polymer (Guildf). 2023 Jul;281:126121.
117. Rahsepar M, Foroughi F, Kim H. A new enzyme-free biosensor based on nitrogen-doped graphene with high sensing performance for electrochemical detection of glucose at biological pH value. Sens Actuators B Chem. 2019 Mar;282:322–30.

118. Yan C, Hua Y, Guo J, Miao P. Programmable DNA hydrogels construction with functional regulations for biosensing applications. TrAC Trends in Analytical Chemistry. 2024 Apr;173:117628.
119. KanoKPaka P, Chang YH, Chang CC, Rinawati M, Wang PC, Chang LY, et al. Enabling glucose adaptive self-healing hydrogel based triboelectric biosensor for tracking a human perspiration. Nano Energy. 2023 Jul;112:108513.
120. Won P, Kim KK, Kim H, Park JJ, Ha I, Shin J, et al. Transparent Soft Actuators/Sensors and Camouflage Skins for Imperceptible Soft Robotics. Advanced Materials. 2021 May 21;33(19).
121. Li G, Hao J, Li W, Ma F, Ma T, Gao W, et al. Integrating Highly Porous and Flexible Au Hydrogels with Soft-MEMS Technologies for High-Performance Wearable Biosensing. Anal Chem. 2021 Oct 26;93(42):14068–75.
122. Lin PH, Sheu SC, Chen CW, Huang SC, Li BR. Wearable hydrogel patch with noninvasive, electrochemical glucose sensor for natural sweat detection. Talanta. 2022 May;241:123187.
123. Johnston L, Wang G, Hu K, Qian C, Liu G. Advances in Biosensors for Continuous Glucose Monitoring Towards Wearables. Front Bioeng Biotechnol. 2021 Aug 19;9.
124. Tirone TA, Brunicardi FC. Overview of Glucose Regulation. World J Surg. 2001 Apr 20;25(4):461–7.
125. Zhai D, Liu B, Shi Y, Pan L, Wang Y, Li W, et al. Highly Sensitive Glucose Sensor Based on Pt Nanoparticle/Polyaniline Hydrogel Heterostructures. ACS Nano. 2013 Apr 23;7(4):3540–6.
126. Völlmecke K, Afroz R, Bierbach S, Brenker LJ, Frücht S, Glass A, et al. Hydrogel-Based Biosensors. Gels. 2022 Nov 25;8(12):768.
127. Naikoo GA, Salim H, Hassan IU, Awan T, Arshad F, Pedram MZ, et al. Recent Advances in Non-Enzymatic Glucose Sensors Based on Metal and Metal Oxide Nanostructures for Diabetes Management- A Review. Front Chem. 2021 Sep 22;9.
128. Adeel M, Rahman MdM, Caligiuri I, Canzonieri V, Rizzolio F, Daniele S. Recent advances of electrochemical and optical enzyme-free glucose sensors operating at physiological conditions. Biosens Bioelectron. 2020 Oct;165:112331.
129. Hassan MH, Vyas C, Grieve B, Bartolo P. Recent Advances in Enzymatic and Non-Enzymatic Electrochemical Glucose Sensing. Sensors. 2021 Jul 8;21(14):4672.
130. Prausnitz MR. Microneedles for transdermal drug delivery. Adv Drug Deliv Rev. 2004 Mar;56(5):581–7.
131. Birchall JC, Clemo R, Anstey A, John DN. Microneedles in Clinical Practice–An Exploratory Study Into the Opinions of Healthcare Professionals and the Public. Pharm Res. 2011 Jan 18;28(1):95–106.
132. HWA C, BAUER EA, COHEN DE. Skin biology. Dermatol Ther. 2011 Sep;24(5):464–70.
133. Mooney K, McElnay JC, Donnelly RF. Children&s views on microneedle use as an alternative to blood sampling for patient monitoring. International Journal of Pharmacy Practice. 2014 Sep 1;22(5):335–44.
134. Takeuchi K, Kim B. Functionalized microneedles for continuous glucose monitoring. Nano Converg. 2018 Dec 24;5(1):28.
135. Kim YC, Park JH, Prausnitz MR. Microneedles for drug and vaccine delivery. Adv Drug Deliv Rev. 2012 Nov;64(14):1547–68.

136. Tariq N, Ashraf MW, Tayyaba S. A Review on Solid Microneedles for Biomedical Applications. J Pharm Innov. 2022 Dec 13;17(4):1464–83.
137. Cárcamo-Martínez Á, Mallon B, Domínguez-Robles J, Vora LK, Anjani QK, Donnelly RF. Hollow microneedles: A perspective in biomedical applications. Int J Pharm. 2021 Apr;599:120455.
138. Martanto W, Moore JS, Couse T, Prausnitz MR. Mechanism of fluid infusion during microneedle insertion and retraction. Journal of Controlled Release. 2006 May;112(3):357–61.
139. Larrañeta E, Lutton REM, Woolfson AD, Donnelly RF. Microneedle arrays as transdermal and intradermal drug delivery systems: Materials science, manufacture and commercial development. Materials Science and Engineering: R: Reports. 2016 Jun;104:1–32.
140. McAllister D V., Wang PM, Davis SP, Park JH, Canatella PJ, Allen MG, et al. Microfabricated needles for transdermal delivery of macromolecules and nanoparticles: Fabrication methods and transport studies. Proceedings of the National Academy of Sciences. 2003 Nov 25;100(24):13755–60.
141. Avcil M, Çelik A. Microneedles in Drug Delivery: Progress and Challenges. Micromachines (Basel). 2021 Oct 28;12(11):1321.
142. Peña-Juárez MaC, Guadarrama-Escobar OR, Escobar-Chávez JJ. Transdermal Delivery Systems for Biomolecules. J Pharm Innov. 2022 Jun 6;17(2):319–32.
143. Dang N, Liu TY, Prow TW. Nano- and Microtechnology in Skin Delivery of Vaccines. In: Micro and Nanotechnology in Vaccine Development. Elsevier; 2017. p. 327–41.
144. Ita K. Dissolving microneedles for transdermal drug delivery: Advances and challenges. Biomedicine & Pharmacotherapy. 2017 Sep;93:1116–27.
145. Zhan H, Ma F, Huang Y, Zhang J, Jiang X, Qian Y. Application of composite dissolving microneedles with high drug loading ratio for rapid local anesthesia. European Journal of Pharmaceutical Sciences. 2018 Aug;121:330–7.
146. Juhász L, Moldován K, Gurikov P, Liebner F, Fábián I, Kalmár J, et al. False Morphology of Aerogels Caused by Gold Coating for SEM Imaging. Polymers (Basel). 2021 Feb 16;13(4):588.
147. Heu R, Shahbazmohamadi S, Yorston J, Capeder P. Target Material Selection for Sputter Coating of SEM Samples. Micros Today. 2019 Jul 8;27(4):32–6.
148. Feira JMC da, Klein JM, Forte MM de C. Ultrasound-assisted synthesis of polyacrylamide-grafted sodium alginate and its application in dye removal. Polímeros. 2018 May 21;28(2):139–46.
149. Cao Z, Zhang Y, Luo K, Wu Y, Gao H, Cheng J, et al. Preparation and Properties of Polyacrylamide/Sodium Alginate Hydrogel and the Effect of Fe Adsorption on Its Mechanical Performance. J Renew Mater. 2021;9(8):1447–62.
150. LibreTexts Chemistry. https://chem.libretexts.org/Ancillary_Materials/Reference/Reference_Tables/Spectroscopic_Reference_Tables/Infrared_Spectroscopy_Absorption_Table. 2020. Infrared Spectroscopy Absorption Table.
151. Pereira R, Tojeira A, Vaz DC, Mendes A, Bártolo P. Preparation and Characterization of Films Based on Alginate and Aloe Vera. International Journal of Polymer Analysis and Characterization. 2011 Oct;16(7):449–64.

152. Asadi S, Eris S, Azizian S. Alginate-Based Hydrogel Beads as a Biocompatible and Efficient Adsorbent for Dye Removal from Aqueous Solutions. ACS Omega. 2018 Nov 30;3(11):15140–8.
153. Ahmad Z, Choudhary MA, Mehmood A, Wakeel R, Akhtar T, Rafiq MA. Synthesis of polypyrrole nano/microspheres using cobalt(III) as an oxidizing agent and its ammonia sensing behavior. Macromol Res. 2016 Jul 1;24(7):596–601.
154. Annabi N, Nichol JW, Zhong X, Ji C, Koshy S, Khademhosseini A, et al. Controlling the Porosity and Microarchitecture of Hydrogels for Tissue Engineering. Tissue Eng Part B Rev. 2010 Aug;16(4):371–83.
155. Li J, Wu Y, He J, Huang Y. A new insight to the effect of calcium concentration on gelation process and physical properties of alginate films. J Mater Sci. 2016 Jun 8;51(12):5791–801.
156. Kumar A, Kothari A, Kumar P, Singh A, Tripathi K, Gairolla J, et al. Introduction to Alginate: Biocompatible, Biodegradable, Antimicrobial Nature and Various Applications. In 2023.
157. Stender EGP, Dybdahl Andersen C, Fredslund F, Holck J, Solberg A, Teze D, et al. Structural and functional aspects of mannuronic acid–specific PL6 alginate lyase from the human gut microbe Bacteroides cellulosilyticus. Journal of Biological Chemistry. 2019 Nov;294(47):17915–30.
158. Gadziński P, Froelich A, Jadach B, Wojtyłko M, Tatarek A, Białek A, et al. Ionotropic Gelation and Chemical Crosslinking as Methods for Fabrication of Modified-Release Gellan Gum-Based Drug Delivery Systems. Pharmaceutics. 2022 Dec 28;15(1):108.
159. Cui S, Mao J, Rouabhia M, Elkoun S, Zhang Z. A biocompatible polypyrrole membrane for biomedical applications. RSC Adv. 2021;11(28):16996–7006.
160. Zhu T, Ni Y, Biesold GM, Cheng Y, Ge M, Li H, et al. Recent advances in conductive hydrogels: classifications, properties, and applications. Chem Soc Rev. 2023;52(2):473–509.
161. Hummel RE. Electrical Properties of Polymers, Ceramics, Dielectrics, and Amorphous Materials. In: Electronic Properties of Materials. Berlin, Heidelberg: Springer Berlin Heidelberg; 2001. p. 166–93.
162. Liu K, Wei S, Song L, Liu H, Wang T. Conductive Hydrogels—A Novel Material: Recent Advances and Future Perspectives. J Agric Food Chem. 2020 Jul 15;68(28):7269–80.
163. Ding H, Liu J, Shen X, Li H. Advances in the Preparation of Tough Conductive Hydrogels for Flexible Sensors. Polymers (Basel). 2023 Oct 5;15(19):4001.
164. Zhang Y, Li S, Gao Z, Bi D, Qu N, Huang S, et al. Highly conductive and tough polyacrylamide/sodium alginate hydrogel with uniformly distributed polypyrrole nanospheres for wearable strain sensors. Carbohydr Polym. 2023 Sep;315:120953.
165. Faraji Rad Z, Prewett PD, Davies GJ. An overview of microneedle applications, materials, and fabrication methods. Beilstein Journal of Nanotechnology. 2021 Sep 13;12:1034–46.